ABSTRACT

Many contaminants of concern in the subsurface are volatile. This fact has been exploited of late in the application of vapor-phase extraction methods for aquifer rehabilitation. The design of vapor-phase extraction systems may be aided by use of mathematical models to simulate the restoration process. Because many common contamination problems are multiphase problems, these simulations often require the use of compositional multiphase models. A common assumption made in compositional multiphase models is that individual solute species are in equilibrium for all phases present in a system: solid, aqueous, immiscible fluid, and vapor. This work reports on an investigation to characterize the rate of mass transfer between the aqueous and vapor phases.

A rectangular cross-section experimental apparatus was designed and built to investigate the rate of mass transfer at the interface between the unsaturated and saturated zone. Aqueous solutions with the solute toluene were circulated through a porous media, while depth-averaged aqueous- and vapor-phase concentrations were measured at the inlet and outlet. Experimental control variables included the aqueous-phase velocity, vapor-phase velocity, influent solute concentration, and media size. Data reduction required determination of longitudinal and transverse dispersivity, which was accomplished using a fluoride tracer method along with a two-dimensional finite element model.

In addition, a numerical code was developed to model the transport of VOC's in the subsurface, and the code was used in conjunction with the lab data to simulate toluene transport under ambient conditions. Results from the simulations indicate that the aqueous and vapor phases may not be in equilibrium at the unsaturated-saturated zone interface throughout much of the area of a contaminant plume.

ACKNOWLEDGMENTS

I would like to thank my advisor, Dr C. T. Miller, for his positive outlook throughout this project. By providing a rare combination of advice and latitude, he helped make this project a challenging and rewarding experience. I would also like to thank Randy Goodman for his valuable assistance in developing the apparatus and in designing the endcaps for the square column. Finally, thanks to Kris for enduring the crazy schedule that kept me in the lab and at the computer for too many nights and weekends. This project was funded solely by a grant from the U.S. Army research Office.

TABLE OF CONTENTS

LIST OF FIGURES

LIST OF TABLES

1 INTRODUCTION

1.1 MOTIVATION

Groundwater is an essential resource in the United States. It is vital for industrial and agricultural purposes, and approximately half of the population uses groundwater for residential purposes. Rural areas and urban centers in arid regions rely heavily on groundwater. In fact, the allocation of scarce groundwater resources may become one of the most important political issues in the arid regions of the American Southwest.

However, the industrial nature of America's economy threatens the quality of groundwater throughout the nation. Spills during the production, transportation, and storage of hazardous chemicals can pollute the subsurface. Leaks from hazardous waste treatment, storage, and disposal facilities can also introduce pollutants. For these reasons, the quality of groundwater resources in the United States increasingly commands the attention of the public and those who formulate public policy.

Of the many compounds that pose a threat to groundwater quality, one of the most significant classes of chemicals is volatile organic compounds (VOC's). VOC's are a great concern for a number of reasons. The primary reason is that many of the most common VOC's are hazardous to human health. One VOC, benzene, is a known human carcinogen (Aksoy, 1988). Several others are known animal carcinogens and are suspected human carcinogens. Virtually all VOC's exhibit some toxic characteristics.

From the perspective of groundwater quality, an equally disturbing fact is that many of the most common VOC's are not only carcinogenic or toxic, but also very

persistent in the environment. In this respect, chlorinated VOC's are particularly problematic. These compounds have been used widely as industrial solvents and degreasers, as well as for dry cleaning operations. They have been introduced into the subsurface throughout the United States. Unless remedial measures are taken, they will remain there and spread for a long time.

Finally, VOC's are ubiquitous. The acronym "VOC's"includes chemicals that are used for dry cleaning, for industrial degreasing, as industrial solvents, and as fuel components for automobiles and airplanes. Undoubtedly, automobile gasoline is the VOC blend that most people in the United States encounter on an almost daily basis. It is illustrative of the omnipresence of VOC's in our society and the threat they pose to groundwater quality. In most urban areas one can find gas stations at virtually every major intersection, and it is not uncommon to find more than one per intersection. Furthermore, until very recently, gasoline was stored at these stations in underground tanks that were designed and operated with minimal concern for leakage.

Because VOC's are a significant threat to groundwater quality, hydrogeologists and engineers have been working to develop both accurate methods to model the fate and transport of VOC's and effective designs for removing these compounds from the subsurface. The purpose of this study was to test a key assumption that is presently used in models simulating the transport of VOC's. The motivation for this research was to improve the accuracy of these models, to allow for better prediction of fate and transport, and to enable more informed decision-making when choosing among various remedial design alternatives.

1.2 OBJECTIVES

This study had four objectives. All of the objectives centered on an analysis of the assumption that the liquid in the saturated domain and the vapor in the unsaturated domain are at equilibrium at the saturated-unsaturated interface. The first objective was to develop a methodology for generating laboratory data to quantify the rate of interphase mass transfer under conditions approximating those in the subsurface. The second objective was to generate such data for a single VOC. The third objective was to use the lab data for the VOC to test the assumption of equilibrium under ambient subsurface conditions. The final objective was to determine conditions under which the equilibrium assumption may not be valid for the VOC.

2 THEORY

2.1 INTRODUCTION

This chapter presents derivations of the equations that described the physical system modeled in this study. The equations governed the processes of interest in the subsurface. In simplified form, they modeled the conditions in the lab apparatus. In its most general form, the model had two dependent variables in the saturated zone and three dependent variables in the unsaturated zone.

The physical processes governing the transport of a contaminant in the subsurface for this study were: bulk transport, diffusion and dispersion, degradation reactions, and interphase mass transfer. In the saturated zone, the transport of water was assumed to be unaffected by the aqueous phase contaminant concentration. In the unsaturated zone at ambient conditions, density driven natural advection of the vapor phase was not considered significant. Furthermore, for conditions of forced advection of the unsaturated zone vapor phase, the bulk transport was assumed to be independent of the vapor phase contaminant concentration. For these reasons, the equations governing bulk transport were decoupled from the contaminant transport equations and are discussed only briefly in section 2.2. The governing equations for transport in the saturated and unsaturated zones are derived in sections 2.3 and 2.4. The equations in these two domains were coupled by equating the fluxes at the shared interfacial boundary; the mathematics of this coupling are discussed in section 2.5. General interphase mass transfer theory is presented in section 2.6. Finally, a method of dimensional analysis is discussed in section 2.7, and

the method is applied to obtain possible correlations for mass transfer coefficients in the subsurface.

2.2 GROUNDWATER FLOW EQUATION

The groundwater flow equation can be derived by writing a mass balance on a differential volume of completely saturated porous media. This follows the method of Bird et al. (1960) for deriving the equation of continuity. A differential volume is shown in Figure 2–1. N_x, N_y, and N_z are the mass fluxes in the principal directions and Δx, Δy, and Δz are the incremental lengths. The mass balance on the volume can be written as

$$[MASS\ RATE\ IN] - [MASS\ RATE\ OUT] = [MASS\ RATE\ OF\ ACCUMULATION] \tag{2–1}$$

In mathematical terms, this is

$$(N_x|_x - N_x|_{x+\Delta x})\Delta y\Delta z + (N_y|_y - N_y|_{y+\Delta y})\Delta x\Delta z + (N_z|_z - N_z|_{z+\Delta z})\Delta x\Delta y = \frac{\Delta x\Delta y\Delta z\Delta(n\rho)}{\Delta t} \tag{2–2}$$

where n is the porosity of the media and ρ is the fluid density. Dividing equation (2–2) by the differential volume, $\Delta x\Delta y\Delta z$, yields

$$\frac{N_x|_x - N_x|_{x+\Delta x}}{\Delta x} + \frac{N_y|_y - N_y|_{y+\Delta y}}{\Delta y} + \frac{N_z|_z - N_z|_{z+\Delta z}}{\Delta z} = \frac{\Delta(n\rho)}{\Delta t} \tag{2–3}$$

From the definition of the differential operator, taking the limit as Δx, Δy, Δz, and Δt go to zero yields

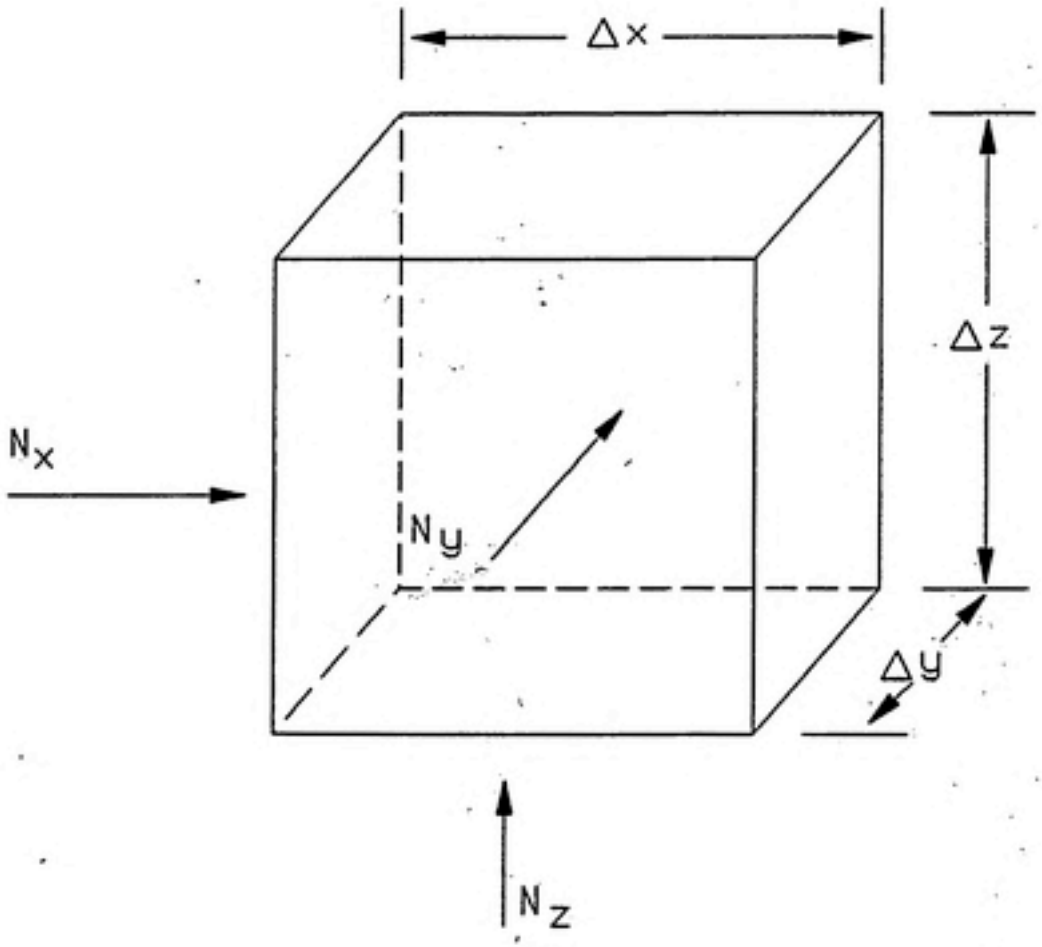

Figure 2–1. Differential Volume of Saturated Porous Media

$$-\frac{\partial N_x}{\partial x} - \frac{\partial N_y}{\partial y} - \frac{\partial N_z}{\partial z} = \frac{\partial (n\rho)}{\partial t} \tag{2-4}$$

Substituting

$$q_i \rho = N_i \tag{2-5}$$

into equation (2–4) where q_i is the specific discharge (that is, the superficial face velocity) in the direction i yields

$$-\frac{\partial (q_x \rho)}{\partial x} - \frac{\partial (q_y \rho)}{\partial y} - \frac{\partial (q_z \rho)}{\partial z} = \frac{\partial (n\rho)}{\partial t} \tag{2-6}$$

Assuming the fluid is incompressible, or assuming the spatial derivatives of ρ are small compared to the spatial derivatives of the specific discharge, yields

$$-\rho \left(\frac{\partial q_x}{\partial x} + \frac{\partial q_y}{\partial y} + \frac{\partial q_z}{\partial z} \right) = \frac{\partial (n\rho)}{\partial t} \tag{2-7}$$

At this point, Darcy's law is introduced. Henry Darcy, a nineteenth-century French engineer, determined the following empirical relationship for the specific discharge, q_i, the hydraulic conductivity, K, and the spatial derivative of the piezometric head, ϕ, in one dimension (Bear, 1979)

$$q_i = -K \frac{d\phi}{di} \tag{2-8}$$

Generalizing to three dimensions gives

$$q_i = -K_{ii} \frac{\partial \phi}{\partial i} - K_{ij} \frac{\partial \phi}{\partial j} - K_{ik} \frac{\partial \phi}{\partial k} \tag{2-9}$$

where i, j, and k represent the three principal directions in rectangular coordinates. Equation (2-9) reveals the hydraulic conductivity as a second-rank tensor. It has been shown that the hydraulic conductivity tensor is symmetrical (Marsily, 1986), thus

$$K_{ij} = K_{ji} \tag{2-10}$$

Dividing equation (2-7) by ρ and substituting equation (2-9) for the specific discharge yields

$$\begin{aligned} &\frac{\partial}{\partial x}\left(K_{xx}\frac{\partial \phi}{\partial x} + K_{xy}\frac{\partial \phi}{\partial y} + K_{xz}\frac{\partial \phi}{\partial z}\right) \\ &+\frac{\partial}{\partial y}\left(K_{yx}\frac{\partial \phi}{\partial x} + K_{yy}\frac{\partial \phi}{\partial y} + K_{yz}\frac{\partial \phi}{\partial z}\right) \\ &+\frac{\partial}{\partial z}\left(K_{zx}\frac{\partial \phi}{\partial x} + K_{zy}\frac{\partial \phi}{\partial y} + K_{zz}\frac{\partial \phi}{\partial z}\right) = \frac{1}{\rho}\frac{\partial (n\rho)}{\partial t} \end{aligned} \tag{2-11}$$

Expressing equation (2-11) more elegantly in vector-tensor notation yields one form of the groundwater flow equation

$$\nabla \cdot (\mathbf{K} \nabla \phi) = \frac{1}{\rho}\frac{\partial (n\rho)}{\partial t} \tag{2-12}$$

To write the equation with a single dependent variable, ϕ, the right side of equation (2-12) can be expressed in terms of a specific storage coefficient, S_s. The expression for S_s is derived by considering the balance of forces that must exist between the soil and the water at some point in an aquifer and the total mass of material above that point in the aquifer (Bear, 1979). The expression is

$$\frac{1}{\rho}\frac{\partial (n\rho)}{\partial t} = S_s \frac{\partial \phi}{\partial t} \tag{2-13}$$

with

$$S_s = g\rho[(1-n)\kappa_m + n\kappa_w] \tag{2-14}$$

where g is the gravitational constant, κ_m is the compressibility of the soil matrix, and κ_w is the compressibility of water. Substituting the right side of equation (2–13) into equation (2–12) yields

$$\nabla \cdot (\mathbf{K}\nabla\phi) = S_s \frac{\partial \phi}{\partial t} \tag{2-15}$$

which is a common form of the groundwater flow equation. Equation (2–15) relates changes in the piezometric head in an aquifer to the storage capacity of the aquifer.

Returning to the general form of Darcy's law, equation (2–9) , and expressing it in vector-tensor notation gives

$$\{\vec{q}\} = -[\mathbf{K}]\{\nabla\phi\} \tag{2-16}$$

Since the pore velocity, v_i, is defined in terms of the superficial velocity and the porosity by (Bear, 1979)

$$v_i = \frac{q_i}{n} \tag{2-17}$$

Darcy's law can be expressed in terms of the pore velocity as

$$\{\vec{v}\} = -\frac{1}{n}[\mathbf{K}]\{\nabla\phi\} \tag{2-18}$$

This final expression relates the spatial derivatives of piezometric head to the pore velocity flow field.

2.3 CONTAMINANT TRANSPORT: SATURATED MEDIA

The contaminant transport equations for the saturated domain are derived in this section. The introduction to this chapter explains why the groundwater flow equation and the contaminant transport equation were decoupled for the model used in this study. In addition to assuming that the liquid-phase flow field was unaffected by changes in the contaminant concentration, the model assumed that the liquid-phase flow field was fully characterized and at steady-state.

As in the previous section, the governing equation is obtained, after Bird et al. (1960), by performing a mass balance on a differential volume of saturated porous media. In this section, however, the mass balance is on a contaminant rather than on the fluid phase. The contaminant can be in either the liquid phase or the solid phase, thus two mass balances must be written. The liquid-phase mass balance is developed first.

Figure 2-2 depicts the components of flux in the liquid phase. The total flux at each face of the differential volume is the sum of the advective and dispersive fluxes. The flux terms shown at the top of the figure are the advective fluxes. These can be written mathematically as

$$J_i^A = C_l q_i \tag{2-19}$$

where J_i^A is the advective flux, C_l is the liquid-phase concentration, q_i is the superficial face velocity, and i represents the three principal directions in rectangular coordinates. An expression can also be developed for the dispersive flux in each direction. The dispersive flux at each face of the differential element is actually comprised of three dispersion terms arising from advection in each of the principal directions. Dispersion is thus a tensor. The nine dispersive fluxes are shown at the bottom of Figure 2-2. The dispersive fluxes are defined in terms of hydrodynamic

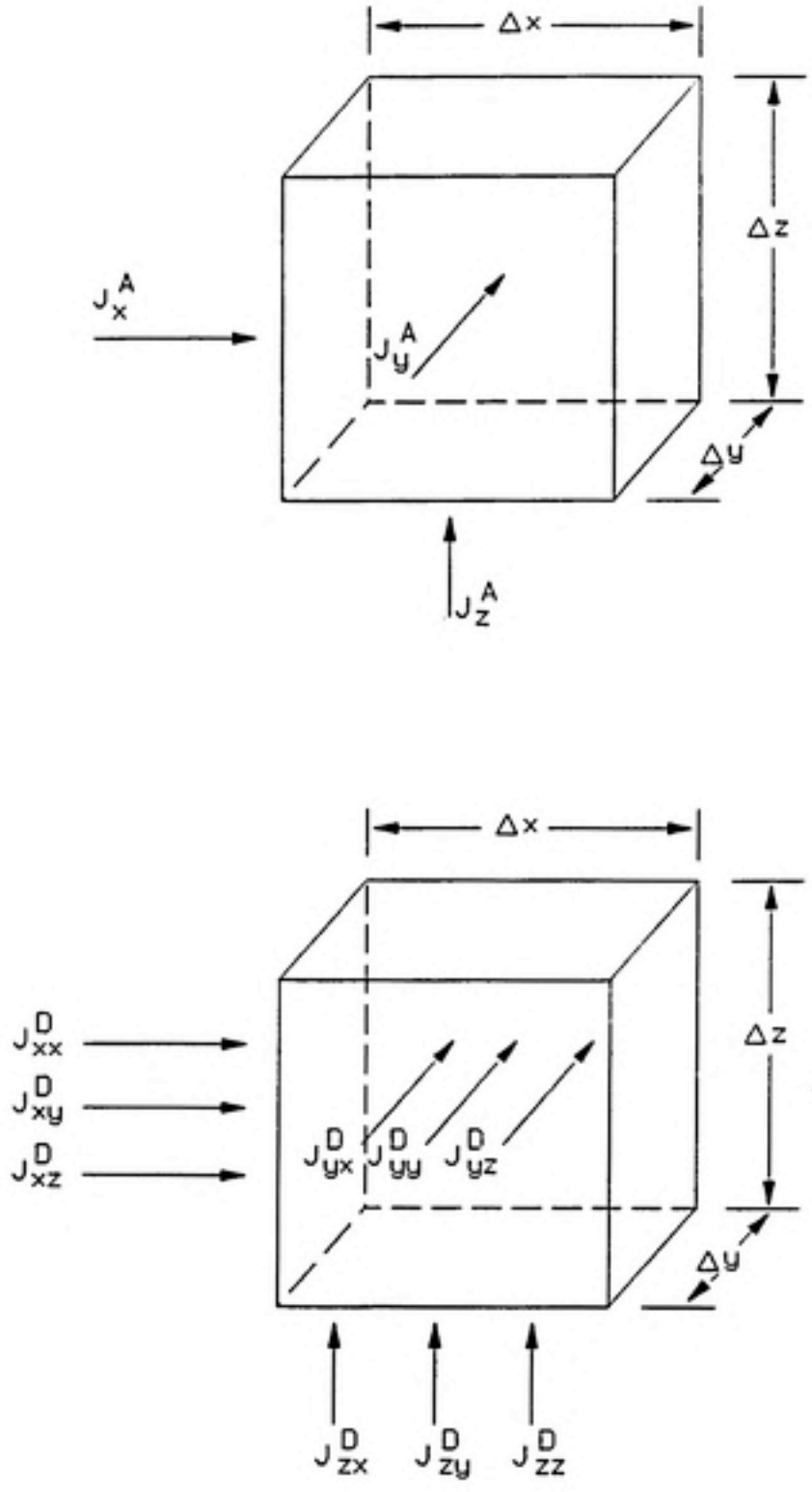

Figure 2–2. Differential Volume for Contaminant Transport

dispersion coefficients, which are comprised of mechanical dispersion and molecular diffusivity. Bear (1979) defined the hydrodynamic dispersion tensor, $\mathbf{D}_h$, by

$$\mathbf{D}_{h,ij} = \alpha_t \bar{v} \delta_{ij} + (\alpha_l - \alpha_t) \frac{\bar{v}_i \bar{v}_j}{\bar{v}} + D_l n \tau \tag{2-20}$$

where δ_{ij} is the Kronecker delta, n is the porosity of the media, τ is the tortuousity of the media ($0 < \tau \leq 1.0$), α_l and α_t are the longitudinal and transverse dispersivities for the media, and

$$\bar{v} = \sqrt{v_x^2 + v_y^2 + v_z^2} \tag{2-21}$$

with v_x, v_y, and v_z being magnitudes of the macroscopic pore velocities in the principal directions.

The total dispersive mass flux of contaminant in the principal directions is expressed as

$$J_x^D = -n \left(D_{h,xx} \frac{\partial C_l}{\partial x} + D_{h,xy} \frac{\partial C_l}{\partial y} + D_{h,xz} \frac{\partial C_l}{\partial z} \right) \tag{2-22}$$

$$J_y^D = -n \left(D_{h,yx} \frac{\partial C_l}{\partial x} + D_{h,yy} \frac{\partial C_l}{\partial y} + D_{h,yz} \frac{\partial C_l}{\partial z} \right) \tag{2-23}$$

$$J_z^D = -n \left(D_{h,zx} \frac{\partial C_l}{\partial x} + D_{h,zy} \frac{\partial C_l}{\partial y} + D_{h,zz} \frac{\partial C_l}{\partial z} \right) \tag{2-24}$$

Combining the advective and dispersive fluxes, equation (2–19) and equations (2–22) to (2–24) , yields terms the for the total mass flux

$$J_x^T = n\left[v_x C_l - \left(D_{h,xx}\frac{\partial C_l}{\partial x} + D_{h,xy}\frac{\partial C_l}{\partial y} + D_{h,xz}\frac{\partial C_l}{\partial z}\right)\right] \quad (2\text{–}25)$$

$$J_y^T = n\left[v_y C_l - \left(D_{h,yx}\frac{\partial C_l}{\partial x} + D_{h,yy}\frac{\partial C_l}{\partial y} + D_{h,yz}\frac{\partial C_l}{\partial z}\right)\right] \quad (2\text{–}26)$$

$$J_z^T = n\left[v_z C_l - \left(D_{h,zx}\frac{\partial C_l}{\partial x} + D_{h,zy}\frac{\partial C_l}{\partial y} + D_{h,zz}\frac{\partial C_l}{\partial z}\right)\right] \quad (2\text{–}27)$$

Now the liquid phase mass balance can be written in terms of the total mass flux in the principal directions. The mass balance can be expressed verbally as

$$\begin{aligned}&[MASS\ RATE\ IN] - [MASS\ RATE\ OUT]\\ &+[MASS\ RATE\ OF\ REACTION] \quad (2\text{–}28)\\ &=[MASS\ RATE\ OF\ ACCUMULATION]\end{aligned}$$

Note that this mass balance contains one more term than the bulk fluid phase mass balance in the previous section. This reaction term represents sources and sinks within the domain. For a source (e.g., a solid desorbing contaminant into the liquid phase) the term is positive. For a sink (e.g., chemical or biological degradation within the liquid phase) the term is negative. Writing the mass balance mathematically, in terms of the total fluxes J_i^T, yields

$$\begin{aligned}&(J_x^T|_x - J_x^T|_{x+\Delta x})\Delta y\Delta z + (J_y^T|_y - J_y^T|_{y+\Delta y})\Delta x\Delta z + (J_z^T|_z - J_z^T|_{z+\Delta z})\Delta x\Delta y\\ &+\left(\frac{n\Delta C_l}{\Delta t}\right)_{rxn} = \frac{\Delta x\Delta y\Delta z(n\Delta C_l)}{\Delta t}\end{aligned} \quad (2\text{–}29)$$

Dividing through by the volume, $\Delta x\Delta y\Delta z$, and taking the limit as the Δ's go to zero yields

$$-\left(\frac{\partial J_x^T}{\partial x}+\frac{\partial J_y^T}{\partial y}+\frac{\partial J_z^T}{\partial z}\right)+n\left(\frac{\partial C_l}{\partial t}\right)_{rxn}=n\frac{\partial C_l}{\partial t} \qquad (2\text{–}30)$$

Substituting equations (2–25) to (2–27) into equation (2–30) and writing the result in vector-tensor notation yields the governing equation for contaminant transport in the liquid phase

$$\frac{\partial C_l}{\partial t}=-\vec{v}\cdot\nabla C_l+\nabla\cdot(\mathbf{D}_h\nabla C_l)+\left(\frac{\partial C_l}{\partial t}\right)_{rxn} \qquad (2\text{–}31)$$

Equation (2–31) is often referred to as the advective-dispersive-reactive (ADR) equation. The reaction term in equation (2–31) includes interactions between the solid and liquid phases as well as homogeneous reactions in the liquid phase

$$\left(\frac{\partial C_l}{\partial t}\right)_{rxn}=\left(\frac{\partial C_l}{\partial t}\right)_{rxn}^{s-l}+\left(\frac{\partial C_l}{\partial t}\right)_{rxn}^{lp} \qquad (2\text{–}32)$$

Before the liquid phase governing equation can be completely defined, the solid phase governing equation must be considered. In this study, sorption onto the solid was modeled as a two-site phenomenon. This model (Cameron and Klute, 1977) postulates that two types of sorption sites exist on the solid phase: 'fast' sites and 'slow' sites. Sorption at the fast sites is an equilibrium process, while sorption at the slow sites is a mass transfer limited process. The total solid phase concentration, q_s, is

$$q_s=q_{ss}+q_{fs} \qquad (2\text{–}33)$$

where q_{ss} is the solid phase concentration for the slow sites and q_{fs} is the solid phase concentration for the fast sites. For both slow and fast sorption, linear equilibrium was assumed. Thus, the equilibrium expression for the fast sites is

$$q_{fs} = K_{ef} C_l \tag{2-34}$$

where K_{ef} is the fast site equilibrium constant. A mass balance on the fast sites yields

$$\begin{aligned} \left(\frac{\partial q_{fs}}{\partial t}\right)_{srp} &= \frac{\partial q_{fs}}{\partial t} - \left(\frac{\partial q_{fs}}{\partial t}\right)_{rxn} \\ &= K_{ef} \frac{\partial C_l}{\partial t} + k_{rf} K_{ef} C_l \end{aligned} \tag{2-35}$$

where k_{rf} is a first-order rate constant for degradation reactions at the fast sites. The two terms from the mass balance on the fast sites are incorporated into the liquid phase governing equation. The mass balance for the slow sites on the solid phase is

$$\frac{dq_{ss}}{dt} = k_s (K_{es} C_l - q_{ss}) - k_{rs} q_{ss} \tag{2-36}$$

where k_s is the mass transfer coefficient for sorption at the slow sites, K_{es} is the equilibrium constant for sorption at the slow sites, and k_{rs} is the first-order degradation constant at the slow sites (Weber and Miller, 1988). Equation (2-36) is one of the two governing equations for the saturated zone.

The term in equation (2-32) describing the interactions between the solid and liquid phases can now be expressed as

$$\left(\frac{\partial C_l}{\partial t}\right)_{rxn}^{s-l} = -\frac{\rho_b}{n} K_{ef} \frac{\partial C_l}{\partial t} - \frac{\rho_b}{n} k_{rf} K_{ef} C_l - k_s \frac{\rho_b}{n} (K_{es} C_l - q_{ss}) \tag{2-37}$$

where ρ_b is the bulk density of the solid phase. Equation (2-37) shows that the term in the ADR describing interactions between the solid and liquid phases is

comprised of: equilibrium sorption at the fast sites; first-order degradation on the solid at the fast sites; and mass transfer limited sorption at the slow sites.

Substituting equation (2-37) into equation (2-32) , then placing the resulting expression in the ADR equation yields the liquid-phase governing equation with all of the terms now explicitly defined

$$\frac{\partial C_l}{\partial t} = -\vec{v}\cdot\nabla C_l + \nabla\cdot(\mathbf{D}_h\nabla C_l) + \left(\frac{\partial C_l}{\partial t}\right)_{rxn}^{lp} - \frac{\rho_b}{n}k_{rs}K_{ef}C_l - k_s\frac{\rho_b}{n}(K_{es}C_l - q_{ss}) - \frac{\rho_b}{n}K_{ef}\frac{\partial C_l}{\partial t} \tag{2-38}$$

The last term on the right hand side of equation (2-38) can be moved to the left hand side and the retardation factor, R_f, can be defined by

$$R_f = \left(1 + \frac{\rho_b}{n}K_{ef}\right) \tag{2-39}$$

Writing Equation (2-38) in terms of R_f and assuming a first-order reaction for homogeneous liquid-phase degradation yields the final version of the liquid phase governing equation

$$R_f\frac{\partial C_l}{\partial t} = -\vec{v}\cdot\nabla C_l + \nabla\cdot(\mathbf{D}_h\nabla C_l) - k_{rl}C_l - \frac{\rho_b}{n}k_{rs}K_{ef}C_l - k_s\frac{\rho_b}{n}(K_{es}C_l - q_{ss}) \tag{2-40}$$

where k_{rl} is the first-order rate constant for liquid-phase reaction. This expression constitutes the remaining governing equation for the saturated zone.

The ADR equation and the the solid-phase slow-site equation , equations (2-40) and (2-36) respectively, are the two significant equations derived in this section. Simultaneous solution of the equations, with appropriate boundary and initial conditions, described the movement of contaminant within the saturated zone. The solid-phase concentration was then determined from equations (2-33) and (2-34) .

2.4 CONTAMINANT TRANSPORT: UNSATURATED MEDIA

Modeling the movement of contaminant in the unsaturated domain requires the simultaneous solution of three equations. The equations arise from mass balances on the three phases in the unsaturated zone and are coupled by interphase mass transfer terms. The assumptions that define the processes included in the model used for this study and that determine the form of the governing equations are:

- the vapor phase is the only mobile phase in the unsaturated zone;
- the vapor-phase flow field is known and is unaffected by changes in vapor-phase concentration;
- concentration gradients in the vapor phase do not induce natural advection;
- the aqueous phase completely wets the solid phase, thus no vapor-solid interphase mass transfer occurs;
- vapor-liquid interphase mass transfer is a nonequilibrium process;
- the equilibrium relationship between the vapor and liquid is defined by Henry's law;
- liquid-solid interphase mass transfer follows the two-site, linear equilibrium sorption model (Cameron and Klute, 1977); and
- first-order degradation reactions can occur in the liquid phase and at both the fast and slow sites on the solid phase.

From the assumptions above, it is clear that the equations for the solid phase in the unsaturated zone are the same as the solid phase equations for the saturated zone. The total solid phase concentration, q_u, is the sum of the concentrations at the fast and slow sites

$$q_u = q_{fu} + q_{su} \tag{2-41}$$

where the fast site concentration is solely dependent upon the liquid phase concentration and the fast site equilibrium constant

$$q_{fu} = K_{ef} C_l^u \tag{2-42}$$

the mass balance for the fast sites is

$$\begin{aligned} \left(\frac{\partial q_{fu}}{\partial t}\right)_{srp} &= \frac{\partial q_{fu}}{\partial t} - \left(\frac{\partial q_{fu}}{\partial t}\right)_{rxn} \\ &= K_{ef} \frac{\partial C_l^u}{\partial t} + k_{rf} K_{ef} C_l^u \end{aligned} \tag{2-43}$$

where K_{ef} is the fast site equilibrium constant and k_{rf} is a first-order rate constant for degradation at the fast sites. The mass balance for the slow sites is

$$\frac{dq_{su}}{dt} = k_s (K_{es} C_l^u - q_{su}) - k_{rs} q_{su} \tag{2-44}$$

where k_s is the slow site mass transfer coefficient, K_{es} is the slow site equilibrium sorption constant, and k_{rs} is a first-order degradation constant for the slow sites. Equation (2-44) is one of the governing equations in the unsaturated zone.

Since the aqueous phase is immobile, the aqueous-phase mass balance in the unsaturated domain does not contain advection or dispersion. However, it does include all of the reaction terms that appear in the saturated zone aqueous-phase equation plus one additional term. The additional term is for the vapor-liquid interphase mass transfer that occurs within the unsaturated zone. This term is

$$\left(\frac{\partial C_l^u}{\partial t}\right)^{v-l} = \left(\frac{1 - S_w^\circ}{S_w^\circ}\right) K_l a (C_v - H_c C_l^u) \tag{2-45}$$

where $K_l a$ is the mass transfer rate constant for vapor-liquid mass transfer within the unsaturated zone, S_w° is the degree of water saturation of the pores in the

unsaturated zone, and H_c is the Henry's constant for the contaminant. Henry's law is

$$C_v^* = H_c C_l^* \tag{2-46}$$

where the asterisk superscripts denote equilibrium values.

In summary, the terms that appear in the aqueous phase mass balance in the unsaturated zone describe: first order homogeneous degradation; liquid-vapor interphase mass transfer; slow sorption; fast sorption; and first order degradation at the fast sorption sites. The equation is

$$\begin{aligned}\frac{\partial C_l^u}{\partial t} = &- k_{rl} C_l^u + \left(\frac{1 - S_w^\circ}{S_w^\circ}\right) K_l a (C_v - H_c C_l^u) \\ &- \left(\frac{\rho_b}{n S_w^\circ}\right) k_s (K_{cs} C_l^u - q_{su}) - \frac{\rho_b}{n S_w^\circ} K_{cf} \left(\frac{\partial C_l^u}{\partial t}\right) \\ &- \frac{\rho_b}{n S_w^\circ} k_{rf} K_{cf} C_l^u\end{aligned} \tag{2-47}$$

By moving the fast sorption term to the left side of equation (2–47) , the mass balance can be expressed in terms of the retardation factor, R_f,

$$\begin{aligned}R_f \frac{\partial C_l^u}{\partial t} = &- k_{rl} C_l^u + \left(\frac{1 - S_w^\circ}{S_w^\circ}\right) K_l a_u (C_v - H_c C_l^u) \\ &- \left(\frac{\rho_b}{n S_w^\circ}\right) k_s (K_{cs} C_l^u - q_{su}) - \frac{\rho_b}{n S_w^\circ} k_{rf} K_{cf} C_l^u\end{aligned} \tag{2-48}$$

where R_f is defined here by

$$R_f = \left(1 + \frac{\rho_b}{n S_w^\circ} K_{cf}\right) \tag{2-49}$$

Equation (2–49) is the second of the three governing equations in the unsaturated zone.

The final equation to consider is the vapor-phase mass balance. Since the vapor phase is mobile, the governing equation will include the advection and dispersion terms that were defined in the previous section for the mobile water phase in the saturated zone. The vapor phase does not include a homogeneous degradation reaction term, but it does include the expression for vapor-liquid interphase mass transfer within the unsaturated domain. The governing equation for the vapor phase in vector-tensor notation is

$$\frac{\partial C_v}{\partial t} = -\vec{v_v} \cdot \nabla C_v + \nabla \cdot (\mathbf{D}_h^u \nabla C_v) - K_l a_u (C_v - H_c C_l^u) \qquad (2\text{–}50)$$

Equations (2–44) , (2–48) , and (2–50) were the three governing equations for the unsaturated zone. Simultaneous solution of these equations with appropriate boundary and initial conditions described the transport of contaminant within the unsaturated zone.

2.5 COUPLING THE SATURATED AND UNSATURATED ZONES

The equations presented in the two previous sections describe the transport of a contaminant within each of two domains: the saturated zone and the unsaturated zone. A contaminant that partitions between the aqueous and vapor phases couples the two domains, and modeling the transport of such a contaminant requires that the systems of equations be solved simultaneously. Since the two domains only interact along a single shared boundary, the governing equations for the two domains must be coupled by imposing appropriate boundary conditions. Specifically, the flux of contaminant normal to the interface at the boundary must be equal for the liquid in the saturated zone and the vapor in the unsaturated zone. Mathematically,

$$\mathbf{J}_{sat}^{lp}|_{int} = \mathbf{J}_{uns}^{vp}|_{int} \qquad (2\text{–}51)$$

Nonequilibrium interphase mass transfer is typically expressed as a function of a driving force and a mass transfer coefficient. Thermodynamics reveals that two phases in contact will approach the same fugacity; stated less esoterically, the two phases will approach equilibrium. For this reason, the driving force used in mass transfer expressions is the deviation from equilibrium. The equilibrium expression used in this study is Henry's law

$$C_v^* = H_c C_l^* \tag{2-52}$$

where H_c is Henry' constant, the subscripts indicate vapor and liquid phases, and the asterisk superscripts denote equilibrium values. Henry's law is applicable for a dilute solution in equilibrium with an ideal-gas mixture (McCabe and Smith, 1976).

The flux at the interfacial boundary in the liquid phase of the saturated zone, defined in terms of a mass transfer coefficient, is

$$D_{zl}\left(\frac{\partial C_l}{\partial z}\right)\bigg|_{int} = K_l\left(\frac{C_v^{uns}}{H_c} - C_l^{sat}\right) \tag{2-53}$$

where K_l is the overall mass transfer coefficient at the interface, based on the liquid phase, and D_{zl} is the transverse dispersion coefficient governing the flux of contaminant within the liquid phase normal to the interface. Likewise, the flux at the interfacial boundary in the vapor phase of the unsaturated zone is

$$D_{zv}\left(\frac{\partial C_v}{\partial z}\right)\bigg|_{int} = -K_l\frac{n_s}{n_u(1-S_w^\circ)}\left(\frac{C_v^{uns}}{H_c} - C_l^{sat}\right) \tag{2-54}$$

where n_s is the porosity in the saturated zone, n_u is the porosity in the unsaturated zone, S_w° is the degree of water saturation of the pores in the unsaturated zone, and D_{zv} is the transverse dispersion coefficient governing the flux of contaminant within

the vapor phase normal to the interface. Note that the mass transfer coefficient and the expression for the driving force are identical in equations (2-53) and (2-54). Combining these two terms with the porosity and water saturation terms ensures mass balance at the interface. The inclusion of two different porosity terms for the saturated and unsaturated zones may appear unnecessary since one could assume that the porosity in the subsurface does not vary greatly over the short distance represented by the two sides of the interface. This may be a reasonable assumption in modeling the subsurface. However, the different porosity terms were necessary for modeling the laboratory apparatus used in this study since the unsaturated zone was a continuous vapor phase and, therefore, had a porosity of one.

Specifying the above boundary conditions for the liquid-phase governing equation in the saturated zone and for the vapor-phase governing equation in the unsaturated zone coupled the two domains. Thus, the equations developed in the two previous sections and the boundary conditions presented here constitute a complete mathematical model for combined saturated-unsaturated transport of a contaminant which partitions between the aqueous and vapor phases.

2.6 MASS TRANSFER THEORY

Throughout this century, engineers have expended much effort generating methods for relating mass transfer coefficients to the hydrodynamics of mass transfer processes. Both empirical and theoretical approaches have been taken. Empirical methods have generally been used for the design of engineered systems. However, engineers have formulated a large number of theoretical models because these models are nominally applicable to a wide range of systems, and they engender the feeling that underlying mechanisms have been explicated. Of the many theories of mass transfer that have been developed, only a few will be discussed in this section.

All of the models presented apply only for dilute systems. One empirical approach to predicting mass transfer coefficients is presented in section 2.7.

2.6.1 FILM THEORY

The simplest theory proposed to explain resistance to interphase mass transfer is film theory, sometimes known as Lewis-Whitman film theory. This theory postulates that all the resistance to mass transfer results from stagnant layers that exist at interphase boundaries (Lewis and Whitman, 1924). Mass can only cross the film by diffusion, thus the mass transfer coefficient is a function of the film thickness and the diffusivity

$$k_i = \frac{D^f_{ai}}{l_i} \tag{2-55}$$

where k_i is the film mass transfer coefficient for phase i, D^f_{ai} is the diffusivity of component a inside the film in phase i, and l_i is the thickness of the film in phase i. At fluid-fluid interfaces, each phase may have an associated film coefficient, and the overall resistance to mass transfer across the interface is the sum of the individual resistances. One problem with the film theory that is immediately evident is the need for an estimate of the film thickness. Rarely can a reliable estimate of l_i be obtained. Another problem is that the theory compares unfavorably with existing data. Equation (2-55) predicts that the mass transfer coefficient varies linearly with diffusivity, while a significant body of experimental data, some of which is discussed in the following chapter, indicates that the exponent on diffusivity should be less than one.

2.6.2 PENETRATION THEORY

One theory of interphase mass transfer that eliminates the need for determining the elusive stagnant film thickness was first developed by Higbie (1935). This model is known as penetration theory. The theory can be illustrated by considering a falling liquid film with a wall on one side and a vapor on the other side. The film moves in the x-direction, and interphase mass transfer occurs in the z-direction, normal to the direction of flow. This model does not postulate a stagnant layer on either side of the interface. However, it does require the following assumptions:

- advection dominates diffusion in the direction of flow, the x-direction;
- diffusion dominates advection in the z-direction;
- the falling film is thick compared to the depth to which mass from the vapor penetrates;
- the vapor concentration is unchanged along the contact path; and
- the liquid at the interface is in equilibrium with the vapor throughout the contact length.

The second assumption implies that the liquid is in laminar flow; thus this model has no need to postulate a stagnant film at the interface since the entire film is essentially stagnant in the z-direction. The third assumption can be expressed mathematically as a boundary condition at the wall

$$\frac{\partial C_l}{\partial z} = 0 \,, \qquad \text{for} \quad z = 0, \quad x > 0 \tag{2-56}$$

which implies either a thick film or a short contact time. Applying the above assumptions yields an expression for the mass flux in the liquid at the interface anywhere along the contact length

$$J_l|_{int} = \sqrt{\frac{D_l v_m}{\pi x}}\left(C_{lb} - C_l^*\right) \tag{2-57}$$

where D_l is the diffusivity in the liquid, v_m is the liquid velocity at the interface, C_{lb} is the constant bulk liquid concentration some distance from the interface, and C_l^* is the interfacial liquid concentration that is in equilibrium with the vapor phase. For the parabolic flow field that exists in laminar flow, the term v_m is the maximum velocity and is equal to $(3/2)v_a$, the average liquid velocity. Integrating equation (2-57) over the entire contact length, L, and dividing by the contact length yields an expression for the average interfacial mass flux, $\bar{J}_l|_{int}$

$$\bar{J}_l|_{int} = \frac{1}{L}\int_0^L \sqrt{\frac{D_l v_m}{\pi x}}\left(C_{lb} - C_l^*\right)dx = 2\sqrt{\frac{D_l v_m}{\pi L}}\left(C_{lb} - C_l^*\right) \tag{2-58}$$

The liquid-phase mass transfer coefficient, k_l, based on the average flux appears in the equation

$$\bar{J}_l|_{int} = k_l(C_{lb} - C_l^*) \tag{2-59}$$

Comparing equations (2-59) and (2-58) reveals an expression for the liquid phase mass transfer coefficient as a function of the hydrodynamics

$$k_l = 2\sqrt{\frac{D_l v_m}{\pi L}} \tag{2-60}$$

One problem with this model is the need to determine the contact time, L/v_m. In complex systems, this term may be difficult to measure. Note, however, that the mass transfer coefficient varies as the square root of the diffusivity. This result compares favorably with much of the data that have been generated on gas absorption

in packed columns. This is surprising since the model would seem to be limited by the assumptions of short contact time, thick liquid film, and laminar flow. Higbie, however, developed this theory for use in modeling packed process unit operations. He proposed that the fluid moves in laminar flow across individual packing elements and mixes at the points where these packing elements meet.

2.6.3 SURFACE RENEWAL THEORY

A number of models exist that do not have the assumptions about flow regime and contact time that are inherent in the penetration model. Additionally, these models do not rely on a specific geometry to derive the mass transfer relationship. These models are known collectively as surface renewal theories because they consider the interfacial surface to be a transient feature that is renewed by eddies from the bulk of the fluid. In this subsection, the model first proposed by Dankwerts (1951) is explained, then variations on the theme are described briefly.

The conceptual framework makes some intuitive sense. The fluid is presumed to consist of eddies. Furthermore, the fluid can be divided into two regions: a well-mixed bulk region and an interfacial region where interphase mass transfer occurs. The eddies move between the bulk region and the interfacial region. The key feature of the model is that the amount of time an eddy spends in the interfacial region is determined by a probability distribution. Dankwerts proposed the following residence time probability distribution

$$E(t) = \frac{e^{-t/\Theta}}{\Theta} \tag{2-61}$$

where the random variable t is the residence time for an eddy in the interfacial region, $E(t)$ is the expected value for that variable, and Θ is the average residence time for eddies in the interfacial region. Eddies in the interfacial region can, for a

brief period, be treated as having semi-infinite extent; therefore, mass is transferred to the eddies at the interface according to the postulates of the penetration model. Using an expression similar to that for Higbie's penetration model, the flux at a point on the interface is

$$J_l|_{int} = \sqrt{\frac{D_l}{\pi\Theta}}\left(C_{lb} - C_l^*\right) \tag{2-62}$$

Thus, the average flux is

$$\bar{J}_l = \int_0^\infty E(t) J_l|_{int} dt = \sqrt{\frac{D}{\Theta}}\left(C_{lb} - C_l^*\right) \tag{2-63}$$

Comparing equations (2-63) and (2-59) yields an expression for the mass transfer coefficient

$$k_l = \sqrt{\frac{D}{\Theta}} \tag{2-64}$$

The mass transfer coefficient varies as the square root of the diffusivity, which is the same conclusion reached using Higbie's penetration theory. Of course, the average residence time, Θ, is an unknown that may be difficult to determine.

A number of modifications have been made to this basic version of the surface renewal theory. Perlmutter (1961) noted that Dankwerts' choice of residence time distribution requires that the most probable eddy have a residence time of zero in the interfacial region, and suggested two alternative models. The first uses two mass transfer capacitances in series to develop a residence time distribution. This model requires the determination of two residence time terms. The second model Perlmutter proposed involves modifying Dankwerts' time distribution by adding a term that represents a 'dead time' arising from stagnant pockets in the interfacial region. Once again, this model requires the determination of two time terms.

Because of data indicating that interfacial resistance to mass transfer may exist (particularly for liquid-liquid and liquid-solid interfaces and for liquids with surfactants), Dankwerts modified the model above to include an equivalent interfacial mass transfer coefficient in equation (2–59) . Perlmutter (1961) took exception with Dankwerts' approach to accounting for this interfacial mass transfer resistance. He proposed two alternatives. The first postulated nonequilibrium conditions at the interface, and the second proposed that a narrow region exists near the interface in which the effective diffusivity is reduced.

The various surface renewal models share certain features. They provide conceptually attractive descriptions of mass transfer and are applicable to a wide range of systems. All of the models result in the mass transfer coefficient varying as the square root of the diffusivity. However, they all require determination of at least one rather elusive term for the residence time distribution, and those that include interfacial resistance to mass transfer have even more unknown terms to assess.

2.6.4 BOUNDARY LAYER THEORY

One last theoretical approach must be mentioned but will not be discussed in detail. This approach is termed boundary layer theory. In general, this method entails narrowing the focus. The theories discussed above all aim to generate simple calculations that are applicable to a number of situations. In boundary layer theory, a detailed mathematical description is generated for a specific system. The geometry, the flow regime (laminar, transition, or turbulent), the nature of the momentum transfer (e.g., Newtonian, non-Newtonian), and other features of a system are defined. Mass and momentum balances are written, and the resulting system of equations is solved using appropriate boundary conditions. This approach is mathematically complex, but the resulting expression for the mass transfer coefficient is typically accurate for the system modeled. A number of systems have been modeled

with this approach. The resulting expressions for k_l depend upon the geometry of the system and the boundary conditions. The exponent on diffusivity is usually in the range 0.04 to 0.67.

2.6.5 COMMENTS ON MASS TRANSFER THEORIES

To summarize, many theoretical models for mass transfer have been proposed. The simplest model is film theory. It predicts that mass transfer coefficients vary linearly with diffusivity and requires the determination of the film thickness. More complex models, based on penetration theory and surface renewal theory, provide insight into the possible mechanisms of mass transfer and have some applicability, but they also yield expressions with terms that are not readily determined. These models predict the mass transfer coefficient should vary as the square root of the diffusivity. Highly specific and mathematically complex models based on boundary layer theory yield very good results for the systems modeled. The mass transfer coefficient generally varies with the diffusivity to the two-third's power.

To determine the utility of the theories, the theoretical predictions must be compared with experimental results. Section 3.2 reviews some experimental data that define the dependence of mass transfer coefficients on diffusivity; these data indicate significant variation in this dependence. Because of this fact, and the fact that the theoretical approaches require the determination of process specific parameters, mass transfer coefficients are typically determined from experimental data. The theories serve primarily to provide a conceptual understanding of mass transfer processes but may be used in one of two ways. In one approach, a correlation is derived and an optimal value for the exponent on the diffusivity is determined from experimental data with the theories serving as a check against egregiously inappropriate results. In the other approach, the experimental data is forced to fit a correlation with diffusivity raised to the power of 1.0, 1/2, or 2/3 and other

parameters are included in the correlation that can be optimized to fit the expression to the data.

2.6.6 ADDITIONAL COEFFICIENT EXPRESSIONS

The mass transfer coefficients calculated from the theories described above are all individual coefficients for a single phase. At fluid-fluid interfaces, each phase may have an associated coefficient. As equation (2–59) indicates, using an individual-phase coefficient requires knowledge of the interfacial concentration of the external phase. In most systems, bulk concentrations are readily determined but interfacial concentrations are not. However, individual coefficients can be added to obtain an overall mass transfer coefficient that can be used to calculate interphase mass transfer rates without knowing the interfacial concentrations. If the equilibrium is linear (but not necessarily through the origin), the rate of interphase transfer is proportional to the difference between the bulk concentration in one phase and the concentration in that same phase that would be in equilibrium with the bulk concentration in the other phase (Maddox, 1973).

For example, consider a vapor-liquid system with an equilibrium described by Henry's law. Let k_l and k_v be the liquid and vapor coefficients, respectively. Since mass transfer coefficients are essentially conductance terms, and since resistances are additive, an overall mass transfer coefficient can be defined in terms of the vapor phase by

$$\frac{1}{K_v} = \frac{1}{k_v} + \frac{H_c}{k_l} \tag{2–65}$$

Alternatively, the overall coefficient could be expressed in terms of the liquid phase by

$$\frac{1}{K_l} = \frac{1}{H_c k_v} + \frac{1}{k_l} \tag{2-66}$$

The rate of mass transfer can be expressed

$$J_v = K_v(C_v^* - C_v^b) \tag{2-67}$$

where J_v is the flux *into* the vapor phase, C_v^b is the bulk vapor concentration and C_v^* is the bulk concentration that would exist in the vapor phase if it were in equilibrium with the bulk liquid phase. Alternatively, the rate could be expressed

$$J_l = K_l(C_l^* - C_l^b) \tag{2-68}$$

where J_l is the flux *into* the liquid phase, C_l^b is the bulk liquid concentration and C_l^* is the bulk concentration that would exist in the liquid phase if it were in equilibrium with the bulk vapor phase.

In addition to the individual phase coefficients, overall coefficients may include terms for interfacial resistance. The additivity of individual resistances, however, is subject to several constraints that are frequently violated in engineered systems (King, 1964). These constraints may also be violated in some natural systems.

One additional point about mass transfer coefficients should be noted. Equations (2-67) and (2-68) are expressions for mass fluxes. To calculate the resulting change in concentration for a phase, the interfacial area and the volume of the phase must be known. These values may be obtained for systems in which two phases interact at a fairly well-defined interface, for example oxygen transfer into a slow flowing river with a calm surface. However, In many situations the interfacial area cannot be determined. Mass transfer rates determined experimentally for such systems are expressed in terms of the overall mass transfer coefficient, K_l or K_v, and

the specific interfacial area, a. Since the values of the coefficient and the area may be inseparable, they are often expressed as a single term, $K_l a$ or $K_v a$. Unfortunately, the terms $K_l a$ and $K_v a$ are not given a new name; they are simply referred to as mass transfer coefficients. Using the same name for terms with different units and different mathematical uses can cause some confusion. In this study, $K_l a$ and $K_v a$ will be referred to as *mass transfer rate constants* because the units, t^{-1}, are the same as those for any first-order rate constant.

2.7 DIMENSIONAL ANALYSIS

Since all the theoretical approaches require the determination of some variables that will be system dependent, a typical situation in the field of process design is that a theoretical approach may be used for preliminary design calculations, but an empirical method will be used for the final design of a unit. Dimensional analysis is a powerful tool for analyzing and presenting empirical data. The Buckingham-pi method is a popular technique for performing dimensional analysis (Silberberg, 1973).

First, one determines the variables (velocity, density, etc.) that are presumed to govern and define the functioning of a system. The dimensions of the variables are then written in terms of the four primary dimension: mass, length, time, and temperature. Next, one determines m, the *maximum* number of variables that can be combined *without* forming a dimensionless group. Usually, m is the number of primary dimensions represented by the variables in the problem, but it may be less. In any event, m will *never* be greater than the number of primary dimensions represented. Determining m may be the most tedious step in the process, but it is certainly the most important.

If η is the number of variables in the problem, the number of dimensionless groups that can be constructed, p, is

$$p = \eta - m \tag{2-69}$$

To construct these groupings, first choose m variables as a core group of repeating quantities. It is essential that no combination of the variables chosen as the core group forms a dimensionless group. Next, p groupings are formed by using the core group repeatedly and including one of the p remaining variables. If Q_i represents core group variables, and R_j represents the remaining variable then the p groups formed can be expressed

$$\begin{aligned}
\pi_1 &= Q_1^{\alpha_{11}} Q_2^{\alpha_{12}} \ldots Q_m^{\alpha_{1m}} R_1 \\
\pi_2 &= Q_1^{\alpha_{21}} Q_2^{\alpha_{22}} \ldots Q_m^{\alpha_{2m}} R_2 \\
&\vdots \\
\pi_p &= Q_1^{\alpha_{p1}} Q_2^{\alpha_{p2}} \ldots Q_m^{\alpha_{pm}} R_p
\end{aligned} \tag{2-70}$$

Note that the core group variables are raised to an unknown exponent while the p remaining variables are not. Now, taking each π_i group individually, solve for the dimensionless group represented by that π_i. To do this, express the dimensions of the variables in terms of the primary dimensions. Then write an equation for each primary variable summing the exponents $(\alpha_{i1}, \alpha_{i2}, \ldots \alpha_{im})$ that apply for that primary variable. Finally, solve the resulting system of m equations in m unknowns; the values determined for the α's specify the power to which each variable in a grouping is raised to generate the dimensionless group. This must be done separately for each π_i.

The Buckingham-pi method can be used to obtain potential correlations for the mass transfer coefficients of VOC's in the subsurface. For these compounds, the interfacial resistance will be dominated by the liquid phase, thus variables describing

the liquid-phase hydrodynamics must be included. The variables chosen for this analysis are:

v = pore velocity, (L/t); and,

d_p = particle diameter, (L).

μ = liquid-phase viscosity, (M/L·t);

ρ_l = liquid-phase density, (M/L^3); and,

The variables included to describe the chemical characteristics are:

D_l = diffusivity of the VOC in water, (L^2/t); and

H_c = dimensionless Henry's constant.

The general functional relationship can be expressed

$$k_l^i = f(v, d_p, D_l, \rho_l, \mu, H_c) \tag{2-71}$$

Since the dimensionless form of the Henry's constant is used, this term is ignored during the Buckingham-π analysis and is introduced at the end as a separate dimensionless group in the correlations. Under these assumptions, the system has six variables and three primary dimensions (M, L, t,), thus three dimensionless groups can be formed. The three core variables are d_p, D_l, and ρ_l. The three dimensionless groups can be expressed

$$\begin{aligned} \pi_1 &= d_p^{\alpha_{11}} D_l^{\alpha_{12}} \rho_l^{\alpha_{13}} v \\ \pi_2 &= d_p^{\alpha_{21}} D_l^{\alpha_{22}} \rho_l^{\alpha_{23}} k_l^i \\ \pi_3 &= d_p^{\alpha_{31}} D_l^{\alpha_{32}} \rho_l^{\alpha_{33}} \mu \end{aligned} \tag{2-72}$$

To solve for π_1, write an equation for each dimension in terms of the exponents on the variables.

$$\begin{aligned} &M : \alpha_{13} = 0 \\ &L : \alpha_{11} + 2\alpha_{12} + 1 = 0 \\ &t : -\alpha_{12} - 1 = 0 \end{aligned} \tag{2-73}$$

Solving for the exponents yields

$$\alpha_{11} = 1 \quad , \qquad \alpha_{12} = -1 \quad , \qquad \alpha_{13} = 0 \tag{2-74}$$

Thus

$$\pi_1 = \frac{v d_p}{D_l} \tag{2-75}$$

The first dimensionless group is a Peclet number (Pe).

Following the same procedure for π_2 yields the same dimensional balances shown in equation (2-73) and the same α-values presented in equation (2-74) . However, the dimensionless group that results is

$$\pi_2 = \frac{k_l^i d_p}{D_l} \tag{2-76}$$

which is a Sherwood number (Sh). For the final grouping,

$$\begin{aligned} &M : \alpha_{33} + 1 = 0 \\ &L : \alpha_{31} + 2\alpha_{32} - 3\alpha_{33} - 1 = 0 \\ &t : -\alpha_{32} - 1 = 0 \end{aligned} \tag{2-77}$$

Solving for the exponents yields

$$\alpha_{31} = 0 \quad , \qquad \alpha_{32} = -1 \quad , \qquad \alpha_{33} = -1 \tag{2-78}$$

The final dimensionless group, then, is

$$\pi_3 = \frac{\mu}{\rho_l D_l} \tag{2-79}$$

which is a Schmidt number (Sc). Based on this analysis, some potential mass transfer correlations for VOC's in the subsurface are

$$\begin{aligned} \mathrm{Sh} &= C_1 \mathrm{Pe}^{C_2} + C_3 \mathrm{Sc}^{C_4} + C_5 H_c^{C_6} \\ \mathrm{Sh} &= C_1 \mathrm{Pe}^{C_2} \mathrm{Sc}^{C_3} + C_4 H_c^{C_5} \\ \mathrm{Sh} &= C_1 + C_2 \mathrm{Pe}^{C_3} \mathrm{Sc}^{C_4} H_c^{C_5} \end{aligned} \tag{2-80}$$

where the C_i's are constants that must be determined empirically.

No previous researcher appears to have investigated the possibility that the aqueous-vapor mass transfer coefficients for VOC's may be correlated with the compounds' Henry's constants. In the present study, this hypothesis was tested by performing an original analysis of data previously generated by other researchers. The results of that analysis, appearing in section 3.2, support the hypothesis that k_l^i is a function of H_c.

3 PREVIOUS EXPERIMENTAL STUDIES

3.1 INTRODUCTION

This chapter presents previous experimental work related to the research performed for this study. Section 3.2 briefly summarizes some of the data that have been generated to determine the dependence of mass transfer coefficients on diffusivity. The studies described are those referred to in the previous chapter as indicating that penetration theory and surface renewal theory may be more appropriate than film theory. Section 3.2 also presents a reinterpretation of data generated by Rathbun and Tai (1988b). In their study, Rathbun and Tai correlated mass transfer coefficients with diffusivity and with molecular weight, but neither correlation fit the experimental results over the entire range of the data. The analysis of the data, which the author of the present study performed, appearing in Section 3.2 indicates that the data are more accurately correlated by an expression that includes both Henry's constant and diffusivity.

Section 3.3 summarizes investigations into the mass transfer of volatile compounds between surface water and the atmosphere. The purpose of this study is to model the movement of VOC's in the subsurface. However, a thorough search of the literature indicated that data on the mass transfer of VOC's under conditions encountered in the subsurface has not been generated, while estimates of mass transfer coefficients for VOC's in surface waters have been generated. Although the surface water data are not directly applicable to conditions in the subsurface, they represent the largest body of work that can serve as an analog to the results of this study. For this reason, section 3.3 is devoted to a presentation of these studies. Data have been generated for the volatilization of pesticides from soils and surface

waters (Glotfelty and Schomburg, 1989, and others). Although pesticides are more volatile than was originally assumed, these data are not necessarily applicable to the compounds of interest for this study and are not discussed.

3.2 INFLUENCE OF DIFFUSIVITY AND HENRY'S CONSTANT

3.2.1 DIFFUSIVITY

The discussion of mass transfer theories in section 2.6 indicated that a salient feature of the various models is the dependence of the mass transfer coefficient on diffusivity. In general

$$k_i \propto D^{\beta} \tag{3-1}$$

with the models predicting that 1.0, 1/2, and 2/3 are the most likely values for β. To determine which model, if any, is the most appropriate description of mass transfer, researchers have used a variety of experimental approaches attempting to define the correct value of β.

Kozinski and King (1966) used a continuous-flow, stirred beaker to measure the mass transfer coefficients of helium, hydrogen, oxygen, argon, and carbon dioxide in distilled water. Their apparatus corresponded to surface aeration processes. For conditions of low agitation, they found that β varied from 0.5 to 0.6. However, at high agitation, they had to correct their data for vapor entrainment in the bulk of the fluid. Doing this yielded a value for β greater than 0.6. This result is odd since most researchers (Holmén and Liss, 1984; Munz and Roberts, 1989; and others) have found that β decreases as agitation increases.

Holmén and Liss (1984) measured coefficients for hydrogen, helium, and xenon in a batch-process stirred tank. They found β to vary from 0.45 to 0.66 with an average value of 0.57. In that same paper, they reviewed lab and field data generated by other researchers and noted that much of the variation that has been reported results from inconsistent use of estimated diffusivity values. Since the calculations were typically based on the ratio of one compound to a reference compound, use of the maximum estimated diffusivity for one compound and the minimum estimated diffusivity for the other increased the scatter in the resulting values of β. They suggested that calculations should be based on the average estimated diffusivity. To illustrate their point, they corrected some of the existing data by using average estimated diffusivities; the corrected calculations did reduce the spread in the β values. Before correcting the data, the β values ranged up to 1.22 indicating film theory may not be completely wrong. However, correcting the data yielded a maximum β of 0.76.

Smith et al. (1980) used a batch-process stirred beaker to model surface aeration for removal of highly volatile chlorohydrocarbons. They calculated a value of 0.61 for β. They later extended their work to include low-volatility compounds (Smith et al., 1981). For these compounds, β varied between 0.6 and 1.0, with the higher values obtained for the less volatile compounds. Some of the variability in their data may have been due to errors in estimating Henry's constants. Roberts and Dändliker (1983) found the value of β to vary between 0.57 and 0.84 for chlorohydrocarbons undergoing surface aeration. The average value for all the compounds tested was 0.66. Munz and Roberts (1989) found that β varied with power input in a stirred tank. The value ranged from about 0.45 at high power input to about 0.6 at low power input.

Rathbun and Tai (1988b) measured the mass transfer coefficients for the nine compounds in the homologous series benzene to n-octylbenzene. They expressed

their results as the ratio of the mass transfer coefficient of each compound to the mass transfer coefficient of oxygen, $k_l^i/k_l^{O_2}$. They then correlated these results with diffusivity. The optimal value of β obtained for these compounds was 0.566. However, this yielded a correlation that only fit ethylbenzene to n-pentylbenzene well. For benzene and toluene the correlation deviated from the experimental results by 11 and 5.4 percent, respectively. For n-hexylbenzene to n-octylbenzene, the correlation deviated by 6.5, 19, and 34 percent. Furthermore, the data also fit a correlation with molecular weight raised to the -0.427-power. The data fit this correlation as well as it fit the diffusivity correlation. This is somewhat contradictory. Most correlations for diffusivity find that diffusivity varies as the negative square root of the molecular weight (Wilke and Chang, 1955; Wilke and Lee, 1955; Fuller et al., 1966; and others). Since diffusivity varies with molecular weight to the -0.5-power, if the value of 0.566 is correct for β, then the mass transfer coefficient should vary with the molecular weight to the -0.283-power.

Gowda and Lock (1986) used dimensional analysis to obtain a correlation between the liquid-phase ethylene mass transfer coefficient, the hydraulic characteristics of a stream, and the chemical characteristics of ethylene. The mass transfer coefficient for ethylene was expressed as a function of the channel width, the mean channel depth, the mean water velocity, the length of the reach, the gravitational constant, the water density, the water viscosity, and the diffusivity of ethylene in water. Six dimensionless groups were determined using the Buckingham-pi method. Two correlations were derived: one using all six groups, the other eliminating two groups that were not found to be statistically significant. The exponent on diffusivity in the resulting correlations was 1.89 and 1.59, respectively.

As this brief sampling of results indicates, when the exponent on diffusivity is estimated by finding the optimal value to fit a given data set, the resulting estimates of β can vary greatly. However, the preponderance of evidence indicates that the

predictions of surface renewal theory and penetration theory are more consistent with the data than are the predictions of film theory. The studies referenced above are examples of finding the optimal value of β that fits the data. An alternative approach is to force the data to fit the theories and introduce additional parameters to optimize the fit of the model to the data.

O'Connor (1983) took this latter approach in developing a mathematical model for the effects of wind on mass transfer coefficients in rivers. In his model, he assumed that for low wind speeds the water surface was smooth, thus film theory applied. At high wind speeds, he applied surface renewal theory. For intermediate conditions, O'Connor calculated the transfer coefficient by summing the contributions from the film resistance and from the turbulent resistance. He then compared his model to existing lab and field data. By including two dimensionless parameters, he was able to obtain a reasonable fit of the model to the data. Other examples of this approach can be found in the chemical engineering literature. For gas-liquid contacting in packed columns, a number of correlations have been developed that depend upon diffusivity to the 1/2-power for liquid-phase coefficients and to the 2/3-power for vapor-phase coefficients (Fair et al., 1973).

3.2.2 HENRY'S CONSTANT

The dimensional analysis presented in section 2.7 indicates that aqueous-vapor interphase mass transfer coefficients for VOC's may be correlated with the dimensionless Henry's constant. This hypothesis was tested by performing an original analysis on data previously generated by Rathbun and Tai (1988b) for the nine compounds in the homologous series benzene to n-octylbenzene. The results of that analysis, described below, support the hypothesis that k_l^i is a function of H_c.

Table 3–1. Parameter Values For Analysis of Data from Rathbun and Tai (1988b)

Compound	$(k_l^i/k_l^{O_2})^{(1)}$ (—)	M_i (g/gmole)	D_l ($cm^2/s \times 10^6$)	H_c at 298 K (—)
Benzene	0.606	78.11	10.9[2]	0.224[4]
Toluene	0.598	92.14	9.5[2]	0.262[4]
Ethylbenzene	0.595	106.17	9.0[2]	0.35 [5]
Ethylbenzene	0.586	106.17	9.0[2]	0.35 [5]
n-Propylbenzene	0.559	120.20	7.6[3]	0.44 [5]
n-Butylbenzene	0.535	134.22	7.0[3]	0.53 [5]
n-Butylbenzene	0.559	134.22	7.0[3]	0.53 [5]
n-Pentylbenzene	0.530	148.25	6.6[3]	0.65 [5]
n-Hexylbenzene	0.475	162.28	6.2[3]	0.78 [5]
n-Heptylbenzene	0.411	176.30	5.8[3]	0.93 [5]
n-Octylbenzene	0.357	190.33	5.5[3]	1.10 [5]

[1] Experimental values determined by Rathbun and Tai (1988b).
[2] Experimental values compiled by Hayduk and Laudie (1974).
[3] Estimated using revised Othmer-Thakar equation (Hayduk and Laudie, 1974)
$D_l = 1.3 \times 10^{-4} V^{-0.589}$
This is the same expression used by Rathbun and Tai.
[4] Experimental values from Leighton and Calo (1981)
[5] Estimated using expression from Rathbun and Tai (1988b)
$H_c = 3.5 \times 10^{-3} V_m e^{0.00570 V_m}$
where H_c [=] kPa·m^3/gmole and the molar volume, V_m is
$V_m = M_i/0.863$ [=] ml/gmole

Values for the aqueous-phase diffusivities (D_l) and the Henry's constants (H_c) for the compounds were obtained from existing experimental data and from published correlations. Table 3–1 presents the data used in the present analysis for the compounds. Rathbun and Tai used correlations to estimate all the diffusivities and Henry's constants. Some of the values in Table 3–1 are different from those that

Rathbun and Tai used; for this reason, constants for the best-fit power correlation between mass transfer coefficient and diffusivity were recalculated for the present analysis. The expression that Rathbun and Tai derived was

$$k_l^i/k_l^{O_2} = (5.65 \times 10^3 D)^{0.566} \tag{3-2}$$

As noted earlier in this section, neither this expression nor an expression using molecular weights fit the experimental results over the entire range of the data. The expression derived here using the data in Table 3-1 was

$$k_l^i/k_l^{O_2} = 476(D)^{0.577} \tag{3-3}$$

Figure 3-1 is a plot of equation (3-3) and the experimental results. As in the expression developed by Rathbun and Tai, the correlation provided a poor fit to the data. The sum of the squares of the errors (SSE) for the correlation was 1.7×10^{-2}. When the data were correlated with Henry's constant, the best fitting expression was the following linear relationship

$$k_l^i/k_l^{O_2} = 0.687 - 0.285 H_c \tag{3-4}$$

The SSE for this correlation was 2.4×10^{-3}, about an order of magnitude less than the error for the correlation given by equation (3-3) . A plot of the correlation and the experimental results appears in Figure 3-2. Clearly, the linear correlation with Henry's constant provides a better fit to the data than does the power function correlation with diffusivity. One final correlation was developed. Optimal values for the four constants in the expression

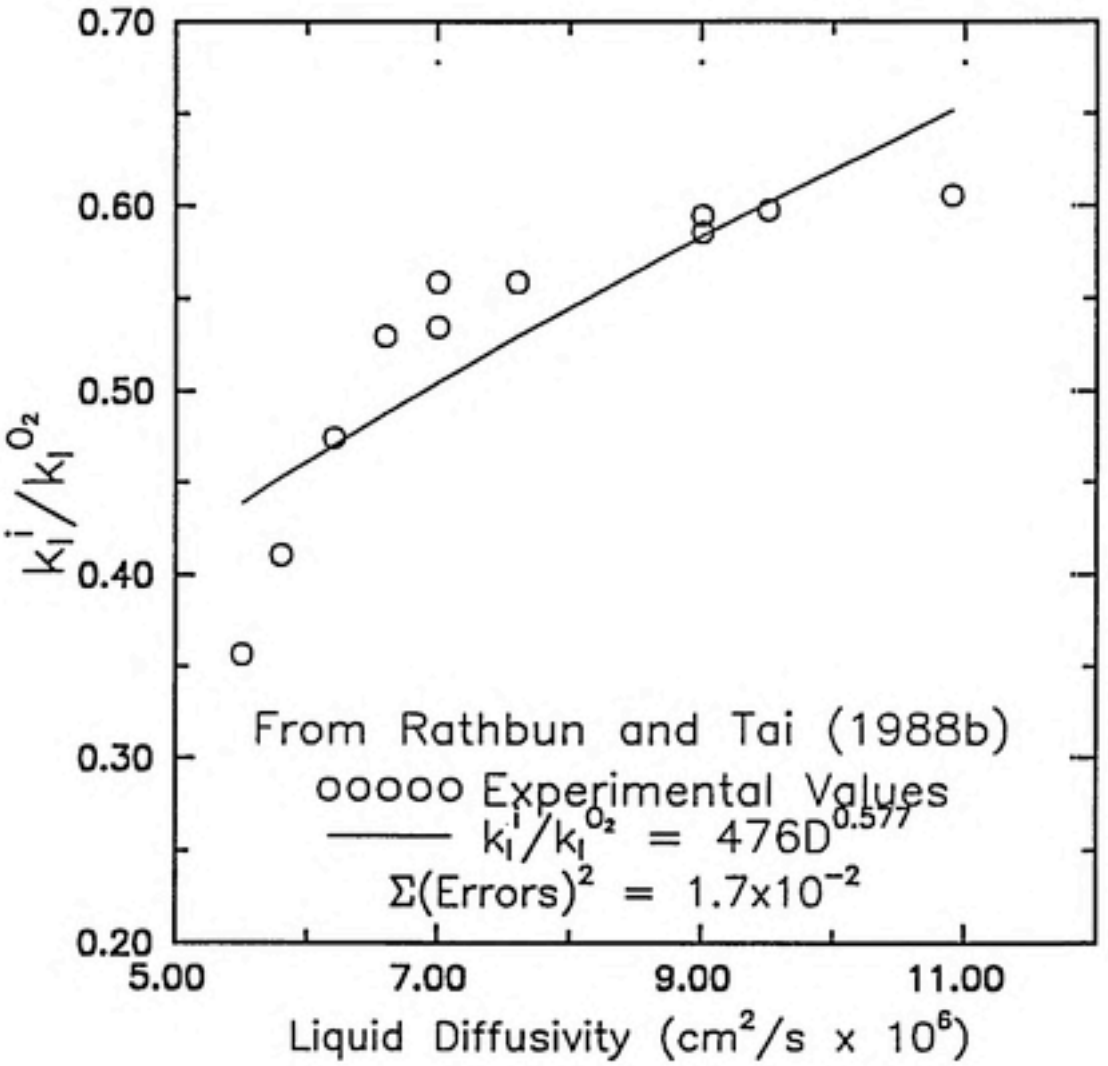

Figure 3–1. $k_l^i/k_l^{O_2}$ vs D: Based on Data From Rathbun and Tai (1988b)

$$k_l^i/k_l^{O_2} = C_1 + C_2 H_c + C_3 D^{C_4} \qquad (3\text{–}5)$$

were determined. The resulting expression was

$$k_l^i/k_l^{O_2} = 0.923 - 0.376 H_c - 520 D^{0.674} \qquad (3\text{–}6)$$

Two points about equation (3–6) are noteworthy. The SSE for the correlation was the lowest of the three correlations at 1.2×10^{-3}. In addition, the exponent on diffusivity is in agreement with boundary layer theory. Both these facts indicate that equation (3–6) is the best correlation for the data generated by Rathbun and Tai for the compounds benzene to n-octylbenzene. However, the negative coefficient on diffusivity in equation (3–6) leads to a contradiction with mass transfer theory: in this expression, k_l^i decreases as diffusivity increases. Figure 3–3 is a plot of the estimated values of $k_l^i/k_l^{O_2}$ vs the experimental values of $k_l^i/k_l^{O_2}$ for equations (3–4) and (3–6) . Table 3–2 is a comparison of the experimental values with the values obtained using the three correlations.

The analysis presented here indicates that individual phase mass transfer coefficients for VOC's may be correlated linearly with Henry's constant. Further data must be generated to determine if this will be true for compounds that do not constitute a homologous series.

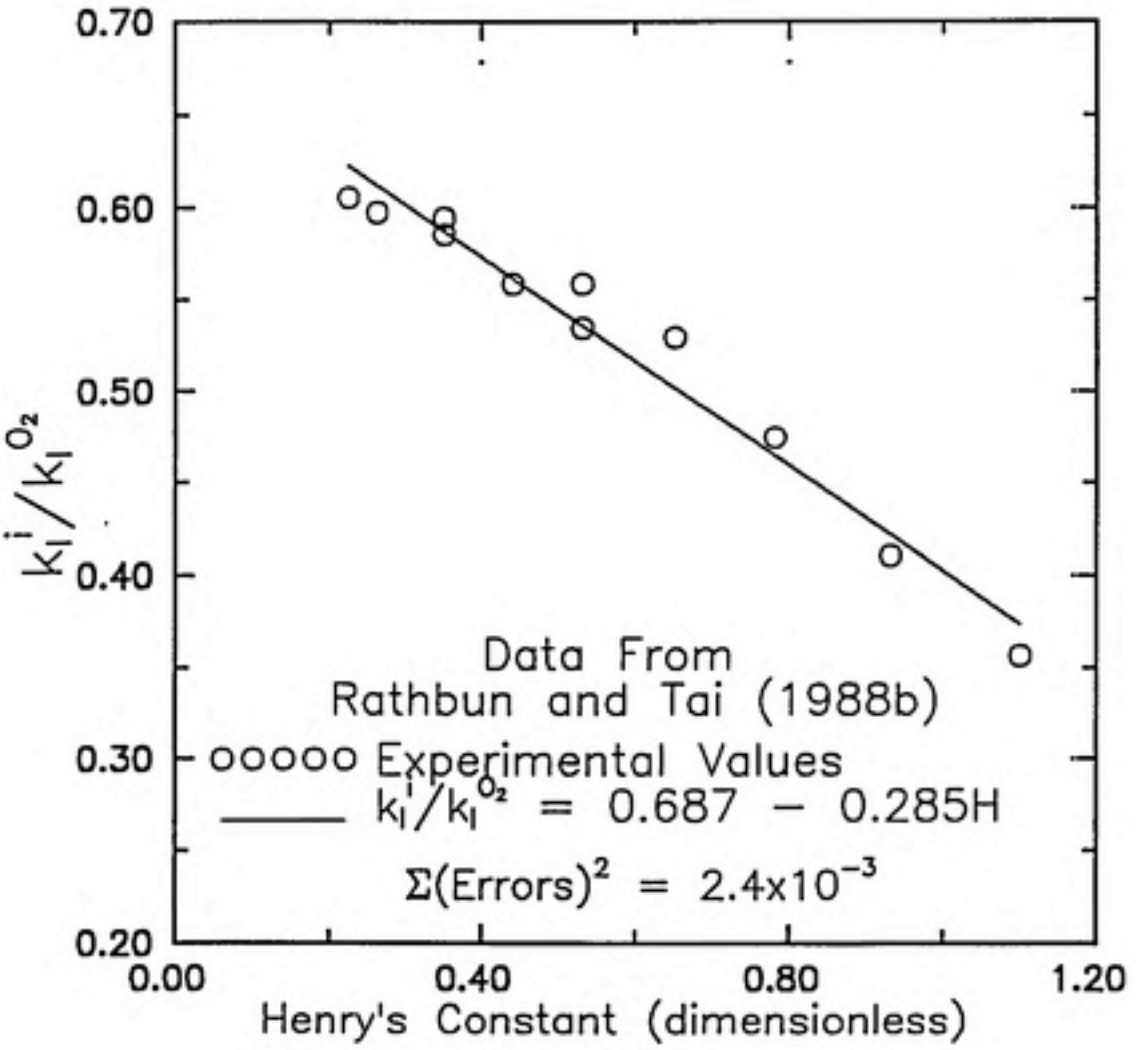

Figure 3–2. $k_l^i/k_l^{O_2}$ vs H_c: Based on Data From Rathbun and Tai (1988b)

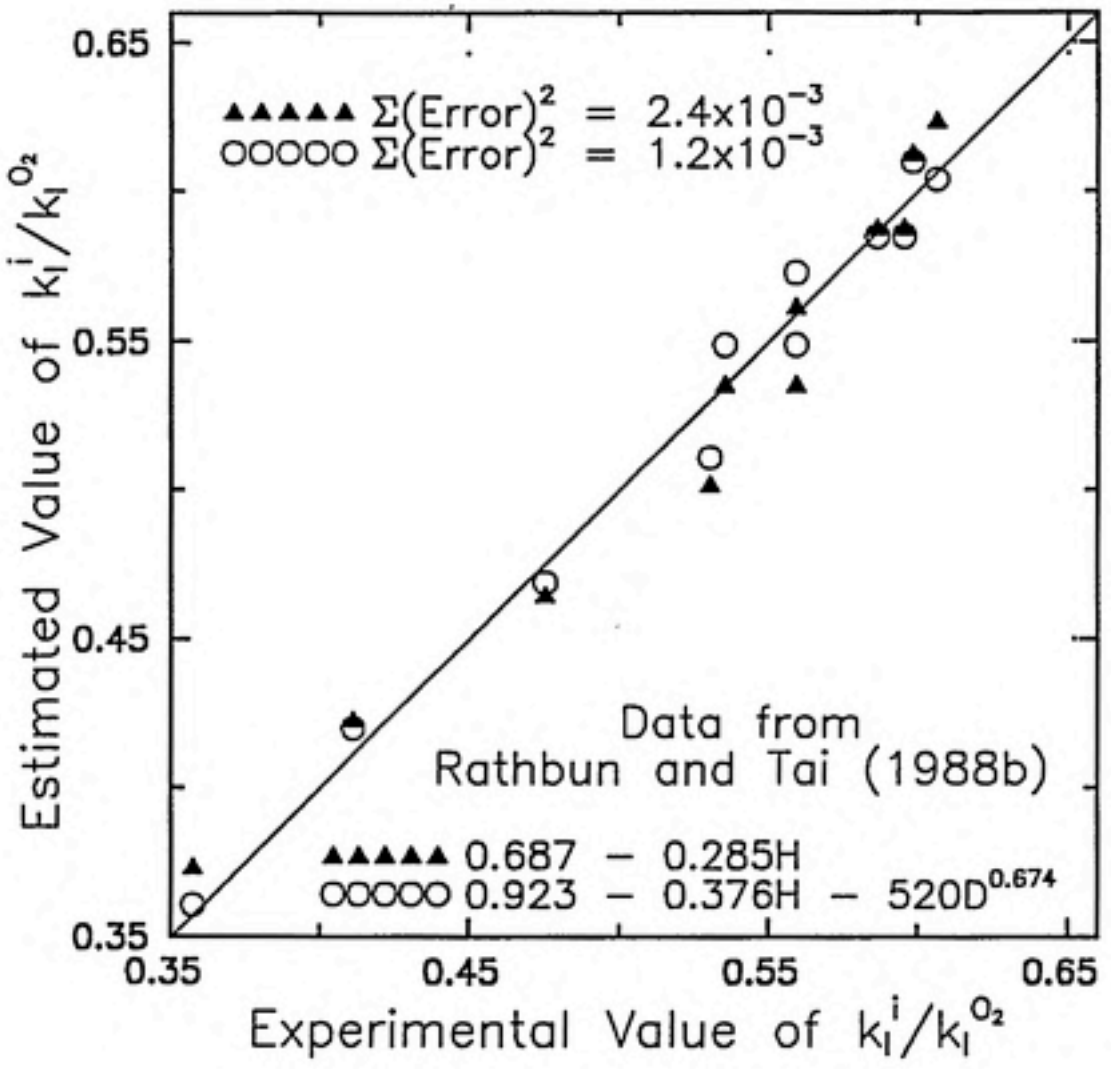

Figure 3–3. Estimated $k_l^i/k_l^{O_2}$ vs Experimental $k_l^i/k_l^{O_2}$

Table 3–2. Comparison of Experimental and Estimated Values for $k_l^i/k_l^{O_2}$

Compound	$(k_l^i/k_l^{O_2})^{(1)}$	$f(D_l)^{(2)}$	$f(H_c)^{(3)}$	$f(H_c,D_l)^{(4)}$
Benzene	0.606	0.652	0.624	0.604
Toluene	0.598	0.602	0.613	0.610
Ethylbenzene	0.595	0.584	0.588	0.585
Ethylbenzene	0.586	0.584	0.588	0.585
n-Propylbenzene	0.559	0.530	0.562	0.573
n-Butylbenzene	0.535	0.505	0.536	0.549
n-Butylbenzene	0.559	0.505	0.536	0.549
n-Pentylbenzene	0.530	0.488	0.502	0.511
n-Hexylbenzene	0.475	0.471	0.465	0.469
n-Heptylbenzene	0.411	0.453	0.423	0.420
n-Octylbenzene	0.357	0.439	0.374	0.361

(1) Experimental values determined by Rathbun and Tai (1988b)

(2) $(k_l^i/k_l^{O_2}) = 476 D_l^{0.577}$

(3) $(k_l^i/k_l^{O_2}) = 0.687 - 0.285 H_c$

(4) $(k_l^i/k_l^{O_2}) = 0.923 - 0.376 H_c - 520 D_l^{0.674}$

3.3 DATA FOR NATURAL SYSTEMS

Prior to this study, no data had been generated to estimate the aqueous-vapor mass transfer coefficients of VOC's in the subsurface. Data for the volatilization of these compounds from surface waters does exist. Although the methods for generating and correlating the data for surface water are different than those that are necessary for groundwater, the existing surface water data will be useful in understanding and evaluating the results of this study.

The physical parameters that govern the volatilization of VOC's from surface water are difficult to correlate. However, the mass transfer coefficient of oxygen absorbing into a surface water (the reaeration coefficient, $k_l^{O_2}$) and the mass transfer

coefficient of water volatilizing into the air (the evaporation rate, $k_v^{H_2O}$) can be determined. Fortuitously, the ratio of the mass transfer coefficient of a volatile compound to that of some reference compound is relatively insensitive to mixing conditions (Kaczmar et al., 1984; Smith et al., 1980, and 1981; Rathbun and Tai, 1981, 1984, 1986, and 1988b; and others). For this reason, much research has been done to determine these ratios for environmentally important volatile compounds. The evaporation of water (or any other pure liquid) is limited by resistance in the vapor phase, thus water is the reference compound for correlation of vapor-phase transfer coefficients. The absorption of a slightly soluble vapor into water is limited by liquid-phase resistance, thus oxygen (or carbon dioxide) is the reference compound for correlating liquid-phase coefficients.

Some of the earliest work on modeling aqueous-vapor mass transfer in natural systems was done by Tsivoglou (1967). He developed a method for measuring the reaeration coefficient, $k_l^{O_2}$, of a stream using radioactive tracers. A fluorescent tracer measured longitudinal dispersion, tritium measured total dispersion, and krypton-85 measured the liquid-phase transfer coefficient. The tracers were added instantaneously at one point and measurements were made at several points downstream. Rathbun et al. (1975, and 1978) improved on the method by eliminating the radioactive tracers. The modified method used a short, continuous injection of ethylene or propane to measure the liquid-phase coefficient.

Mackay and Wolkoff's (1973) method for estimating the rate of volatilization of sparingly soluble compounds from surface water is a good example of the errors that can be introduced into calculations when mass transfer limitations are ignored. They derived expressions for the rate of volatilization based on the assumptions that the liquid phase was completely mixed, thus the interfacial and bulk concentrations were approximately equal, and that the phases were in equilibrium at the interface. Based on these assumptions, they calculated half-lives for 16 organic compounds

and concluded that the compounds would not persist in water. Then, Liss and Slater (1974) published a paper applying the two-film model to mass transfer at the air-sea interface. Liss and Slater estimated the values of $k_v^{H_2O}$ and $k_l^{CO_2}$ from field and experimental data, and calculated the coefficients for other compounds by

$$k_v^i = k_v^{H_2O}\sqrt{\frac{M_{H_2O}}{M_i}} \quad \text{and} \quad k_l^i = k_l^{CO_2}\sqrt{\frac{M_{CO_2}}{M_i}} \tag{3-7}$$

where M_i, M_{H_2O}, and M_{CO_2} are the molecular weights of the compound, water, and carbon dioxide, respectively, and k_l^i and k_v^i are the individual phase coefficients. Overall coefficients were determined by adding the individual resistances. Mackay and Lienonen (1975) then used Liss and Slater's approach to improve on Mackay and Wolkoff's original estimates of half-lives, eliminating the equilibrium assumption by including mass transfer resistance. The half-lives calculated with mass transfer resistance included were one order-of-magnitude higher for benzene, toluene, and o-xylene and were three orders-of-magnitude higher for n-octane and 2,2,4-trimethylpentane. Thus, Mackay and Wolkoff's very low estimates of half-lives were simply an artifact of the equilibrium assumption.

The work published by Mackay and Wolkoff and by Mackay and Lienonen was entirely theoretical — they performed no laboratory work to verify the models. The only experimental values in the models are those determined by Liss and Slater, $k_v^{H_2O}$ and $k_l^{CO_2}$, which were based on average values for the ocean surface obtained from lab and field work by previous researchers. At the time that these theoretical models were being developed, Dilling et al. (1975) were measuring the half-lives of volatile halocarbons in water. They stirred 1.0 mg/l solutions of the compounds in a beaker and measured the concentration over time. The half-lives they measured were much longer than the predictions of the equilibrium model and reasonably close to the predictions of the mass transfer limited model. Dilling (1977) continued this

work to verify the models developed by Mackay. He compared lab measurements of half-lives with the predictions of the equilibrium and mass transfer limitation models. The equilibrium model failed entirely to predict the lab results. The mass transfer limited model, however, predicted half-lives that deviated from the lab results by no more than a factor of two. Such close agreement is rather surprising since the lab results varied with agitation, air currents, and temperature, and since the predictions were based upon gross estimates of water and oxygen exchange at the ocean surface and corrected for the organic compounds according to film theory.

The introduction of mass transfer resistance terms into volatilization expressions for compounds in surface waters was a significant improvement over the equilibrium assumption. However, Liss and Slater's method for calculating individual phase resistances as the square root of the ratio of molecular weights implicitly assumes that film theory applies. Most correlations for diffusivity find that diffusivity varies as the negative square root of the molecular weight. Thus, if mass transfer coefficients are correlated as the negative square root of the molecular weight, this implies that the exponent on diffusivity is unity. Wolff and van der Heijde (1982) developed a model of volatilization from surface waters that explicitly assumed film theory was applicable. They used experimental data to correlate wind speed with the mass transfer coefficient in the vapor and liquid phases. Then they calculated the film thickness by dividing the mass transfer coefficient by diffusivity. At low velocities the value for film thickness increases rapidly, approaching 12 cm for the vapor phase and 0.3 cm for the liquid phase at zero velocity.

Mackay and Yeun (1983) performed lab experiments with a wind-wave tank to determine correlations for gas and liquid coefficients, and to test for interactions in multicomponent systems. They found that the liquid-phase coefficients correlated with the negative square root of the Schmidt number (Sc). Since Sc is the ratio of kinematic viscosity to diffusivity, this corresponds to a correlation with the square

root of diffusivity. However, they did not optimize the exponent on Sc; they simply chose a value of $-1/2$ and found that the data fit this model. For the vapor-phase coefficient, they chose an exponent of $-2/3$ for the Schmidt number and found that this correlation fit the data. The mass transfer coefficients measured for single solute systems were the same as those measured for multi-component systems, thus simultaneous volatilization of several compounds did not affect the individual volatilization rate of each compound.

Rathbun and Tai (1982) provided a method for estimating the fraction of the resistance that each phase contributes to the overall resistance for volatile compounds in surface waters. They reviewed the literature to obtain an average value of $k_v^{H_2O}$ for the open ocean and a range of values for $k_v^{H_2O}$ in a canal at wind speeds from 0.56 m/s to 5.2 m/s. They also obtained a range of values from the literature for k_l^i for benzene, chloroform, and methylene chloride in rivers. They plotted the percent of the resistance in the liquid film as a function of Henry's constant using three pairs of the coefficients obtained from the literature: the largest k_v^i and the smallest k_l^i (liquid resistance predominates), the smallest k_v^i and the largest k_l^i (vapor resistance predominates), and intermediate values of k_v^i and k_l^i (both phases contribute significantly to the overall resistance). Since the overall resistance, based on the liquid phase, is

$$\frac{1}{K_l^i} = \frac{1}{k_l^i} + \frac{1}{H_c k_v^i} \tag{3-8}$$

then the percent resistance in the liquid phase is

$$\frac{100}{k_l^i K_l^i} = \frac{100}{1 + \frac{k_l^i}{H_c k_v^i}} \tag{3-9}$$

For the intermediate coefficient values ($k_v^i = 0.93$ cm/s, $k_l^i = 3.5 \times 10^{-3}$ cm/s) over 90 percent of the resistance is in the liquid phase for compounds with $H_c > 0.04$.

Rathbun and Tai have done a significant amount of work correlating mass transfer coefficients of VOC's with $k_v^{H_2O}$ and $k_l^{O_2}$. They developed a methodology for determining k_l^i for compounds with dimensionless Henry's constants greater than 0.04 and showed that (for benzene, toluene, chloroform, and methylene chloride) the ratio of k_l^i to $k_l^{O_2}$ is independent of both mixing conditions and the presence of other volatile compounds (1981). They developed a laboratory method for measuring the gas-phase mass transfer coefficients for organic compounds using the pure compounds and referencing k_v^i to $k_v^{H_2O}$ (1986). They then used this method to measured the coefficient ratio for seven ketones as a function of temperature, vapor pressure, molecular weight, and diffusivity. Ketones were chosen because they are intermediate between liquid-phase control and vapor-phase control of the overall resistance. Rathbun and Tai later extended this work to compounds with low Henry's constants (1988a). They measured k_v^i and K_l^i and used these values with estimates of H_c to calculate k_l^i. Their estimates of k_l^i were frequently negative because K_l^i was dominated by k_v^i; under such conditions the value of k_l^i calculated in this manner is very sensitive to the estimate of H_c used.

The results of the studies summarized above are not readily applicable to volatilization in the subsurface. However, some of the results (particularly Rathbun and Tai, 1984 and 1988b; and Mackay and Yeun, 1983) assisted in evaluating the data generated in this study. Additionally, the calculations of Rathbun and Tai (1982) indicate that the mass transfer coefficients determined in this study were dominated by the liquid-phase resistance. This expectation was employed in the design of the experimental procedure and the data were analyzed to test this assumption. Finally, the alternative analysis, presented in section 3.2, of Rathbun and Tai's data for the homologous series of benzene compounds (1988b) suggests

that a mass transfer correlation for VOC's in the subsurface should include Henry's constant.

4 MATERIALS AND METHODS

4.1 INTRODUCTION

The purpose of this study was to quantify the rate of liquid-vapor interphase mass transfer of volatile organic compounds (VOC's) with low aqueous solubilities under conditions approximating those in the subsurface. The movement of such compounds between the aqueous and vapor phases under these conditions is typically assumed to be an equilibrium process. For this study, the deviation from equilibrium mass transfer was attributed to a resistance in the aqueous phase, which was expressed as a mass transfer coefficient. One goal was to develop a methodology for measuring mass transfer coefficients under conditions approximating those in the subsurface.

The methodology developed involved pumping an aqueous solution containing a single dissolved VOC through a horizontal column. The lower half of the column was packed with glass beads and the upper half of the column was a continuous vapor phase. The aqueous phase completely saturated the lower portion of the column, and the water level was maintained level with the upper extent of the beads. Nitrogen was supplied to the upper half of the column to continuously remove volatilized organic from the column.

All samples were obtained under steady-state conditions. To ensure steady-state conditions, at least three bed volumes of the contaminated water were pumped through the column before the first data point was obtained. For all subsequent data points from a given run, at least one bed volume of water was pumped between sampling. A single column run provided between two and six data points; most column runs provided three data points.

A single data point consisted of the following: a sample of liquid influent, a sample of liquid effluent, and a sample of the vapor effluent. The information for each data point also included the liquid flow rate, the vapor flow rate, and the vapor phase temperature. Liquid-phase and vapor-phase sampling and analysis are described in sections 4.4.1 and 4.4.2.

Two columns were used. The first, a circular cross-section column, was used to generate 20 data points at four velocities (spanning one order of magnitude) and at one influent concentration. The second, a square cross-section column, was used to generate 143 data points at eight velocities (spanning two orders of magnitude) and at three influent concentrations (spanning one order of magnitude).

To analyze the data obtained for the VOC's, the porous media had to be characterized. The following properties of the glass beads were measured: porosity, particle density, bead size, longitudinal dispersivity, and transverse dispersivity. The methods used to measure the first three bead properties are discussed in section 4.2. The dispersivities were measured by performing tracer studies using fluoride for the conservative tracer. These analyses are discussed in section 4.4.3. The mass transfer data were analyzed using two computer codes. A discussion of the codes and the use of the codes to analyze the data is presented in section 4.5.

4.2 MATERIALS

The volatile organic compound used was toluene. Toluene was chosen for several reasons. First, toluene is a significant component of gasoline and other fuels that are stored in large quantities in underground tanks. Furthermore, pure toluene is an ubiquitous industrial chemical transported in trucks and on rail throughout the country. For these reasons, it poses a serious threat to groundwater resources. Additionally, toluene is volatile enough that vapor phase transport may represent a significant aspect of its subsurface migration and may also present opportunities for

remediation via enhanced volatilization. At the same time, toluene is not so volatile that it fails to persist in subsurface water at concentrations requiring remediation.

Hexane was used to extract the toluene from the aqueous phase, granular activated carbon (GAC) was used to adsorb the toluene from the vapor phase, carbon disulfide (CS_2) was used to extract the toluene from the GAC, and the internal standard used during gas chromatographic analyses of both liquid extractants was 2,2,4-trimethylpentane. All chemical used were reagent grade or higher and all were obtained from Fisher Scientific Co.

The vapor phase was 99.99 percent nitrogen, supplied from a pressurized tank. Nitrogen was chosen to prevent aerobic biodegradation of toluene during the experiments.

The GAC used for vapor phase sampling was obtained from SKC Inc., located in Eighty-Four, PA. The GAC was packed in sealed glass vials about 0.6 cm in diameter and 6 cm long. Each vial contained 150 mg of carbon packed into two separate aliquots. The first aliquot consisted of 100 mg and was on the inlet side of the vial. This was the portion onto which all of the sample was adsorbed. The second aliquot consisted of the remaining 50 mg and was used to ensure that breakthrough of the first aliquot had not occurred during sampling. The maximum flow rate through the vials was 30 ml/min. More detailed information on the use of the vials for analysis of the vapor phase is presented in section 4.4.2.

The porous media used consisted of glass beads obtained from McMaster Carr of Brunswick, NJ. Glass beads were chosen to eliminate sorption of organic contaminant onto the porous media. These beads ranged in size from 0.30 to 0.45 mm. The beads were washed and wet-screened prior to use to remove attrited particles. Then, porosity, bulk density, and particle density were all measured by displacement. About 20 ml of water was placed in a 40-ml vial and weighed. Then, being careful not entrap any air, glass beads were added and the vial was lightly tapped

to pack the beads in the same manner that the beads in the column were packed. The volume of beads added was 25.0 ml. The vial was weighed again to determine the mass of the 25 ml of glass beads, thus yielding the bulk density. The excess water was then removed, leaving the water level with the beads. The saturated beads were weighed and the volume of water was determined by difference. This provided the measurement of porosity and of particle density. Seven duplicates of these measurements were performed and the results were averaged. The results appear in Table 4–1.

Table 4–1. Measured Properties of Glass Beads

Parameter	Average	Standard Deviation
Particle Density (g/ml)	2.44	0.031
Bulk Density (g/ml)	1.52	0.015
Porosity	0.379	0.006

The pump used to force the water through the column was a Pump-22, purchased from Harvard Apparatus of South Natick, MA. This syringe pump consists of a stepping motor that drives a lead screw. The lead screw moves a 'pusher' forward, and the pusher drives the syringe plunger into the syringe barrel. The pump can use a wide range of syringe sizes and thus produces flow rates ranging from 0.03 μl/min to 55 ml/min. The pump is controlled by a microprocessor to provide highly accurate and reproducible flow.

4.3 APPARATUS

A schematic of the experimental apparatus appears in Figure 4–1. The glass column lays horizontal in the middle of the drawing. The column had two influent ports and two effluent ports: the upper ports for vapor and the lower ports for liquid. The lower portion of the column was filled with glass beads, while the upper portion was a continuous vapor phase. Water was forced through the column with a syringe pump, entering the column on the left in the figure. The water flowed from the syringe through 1/8-inch Teflon tubing, then through a small section of 1/4-inch glass tubing (the influent sample port), then into the endcap and the column. The glass tubing was connected to the Teflon tubing and the Teflon endcap with stainless steel fittings. The water level was maintained level with the upper extent of the beads. The aqueous effluent passed through the endcap, through a short section of 1/4-inch glass tubing (the effluent sampling port) then into the sidearm of a vacuum flask. The flask had to be vented to maintain ambient pressure in the effluent line to prevent the water level from rising above the bead level. However, to prevent the release of toluene vapor into the lab, the flask had to be sealed. To address these conflicting concerns, the flask was sealed with a rubber stopper containing a single hole into which a Pasteur pipette packed with GAC was placed. This maintained ambient pressure in the effluent flask while preventing the release of toluene vapor.

The vapor flow was countercurrent, thus the nitrogen enters the column from the right side in Figure 4–1. The nitrogen was supplied from a pressurized tank. It was saturated with water vapor prior to entering the column to prevent the evaporation of water at the interface that would occur if dry nitrogen were introduced to the column. This evaporating water would have artificially increased the rate of VOC transfer to the vapor phase. The nitrogen passed through 1/8-inch stainless

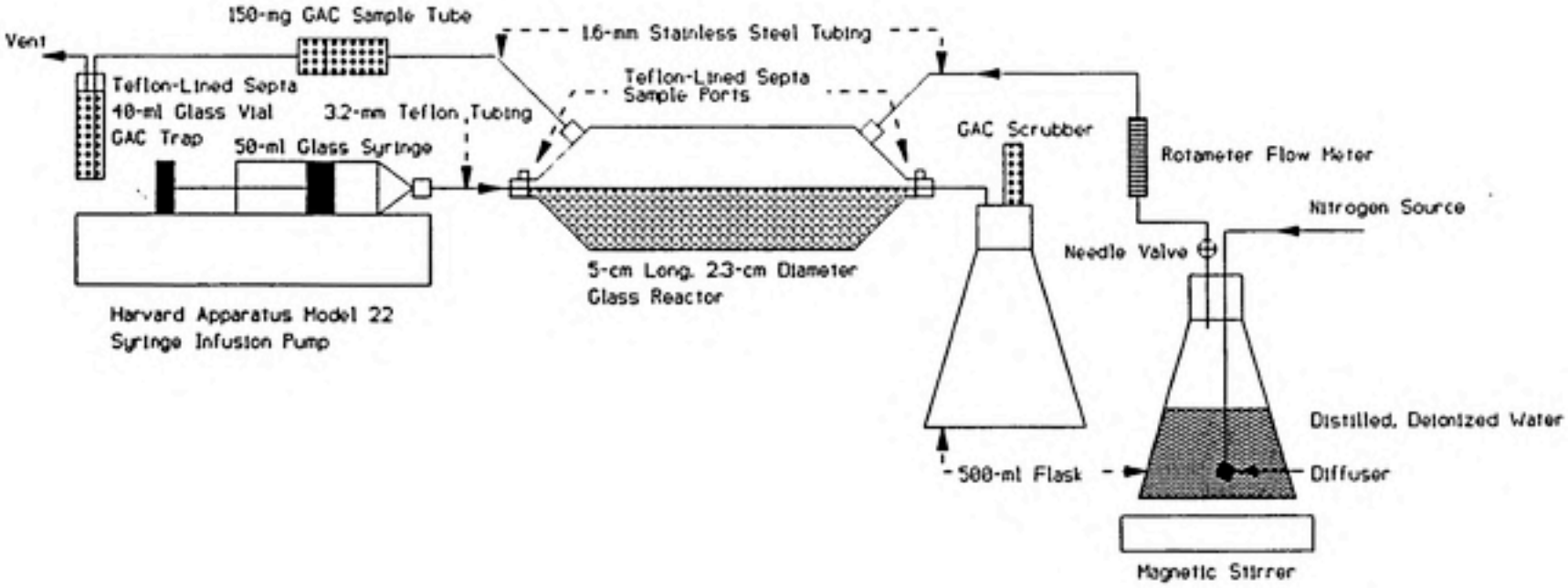

Figure 4-1. Schematic of Laboratory Apparatus

steel tubing then into a glass frit submerged in deionized water inside a sealed Erlenmyer flask, rising through the water and becoming saturated with water vapor. The wet nitrogen then passed through a valve and a flowmeter before entering the column. The valve and flowmeter simply provided control of the vapor flow; the measurement of the vapor flow was performed with a bubble flow meter that was attached at the outlet of the vapor line, on the left in the drawing. The vapor exited the column through 1/8-inch stainless steel tubing.

The vapor phase sample port was a short section of 1/4-inch Teflon tubing attached to the 1/8-inch stainless steel vapor effluent tubing. The GAC sample vials fit snugly into the 1/4-inch Teflon tubing. Between sampling periods, a spent GAC sample vial was attached to the Teflon tubing. Since the GAC in this vial was completely loaded with toluene, the vapor was then passed through a 40-ml vial full of fresh GAC prior to flowing into the bubble flow meter and out into the ambient lab air. This prevented the release of toluene into the lab.

Two different glass columns were used in this study. The first column had a circular cross-section of diameter 2.54 cm and a length of 5.08 cm. In this column, the beads filled the converging and diverging ends of the column, thus creating vertical components in the aqueous phase advection. This nonuniform flow field increased the vertical flux beyond what would result solely from transverse dispersion in a uniformly horizontal flow field, thus helping to ensure that interfacial resistance limited the interphase mass transfer. However, the circular cross section was not amenable to numerical modeling with a two-dimensional code, while using a three-dimensional code would have significantly increased the computational burden.

A second column was designed: to ensure a uniform horizontal flow field minimizing vertical components of advection, thus isolating transverse dispersion as the mode of transport of organic compound to the interface; and to facilitate the

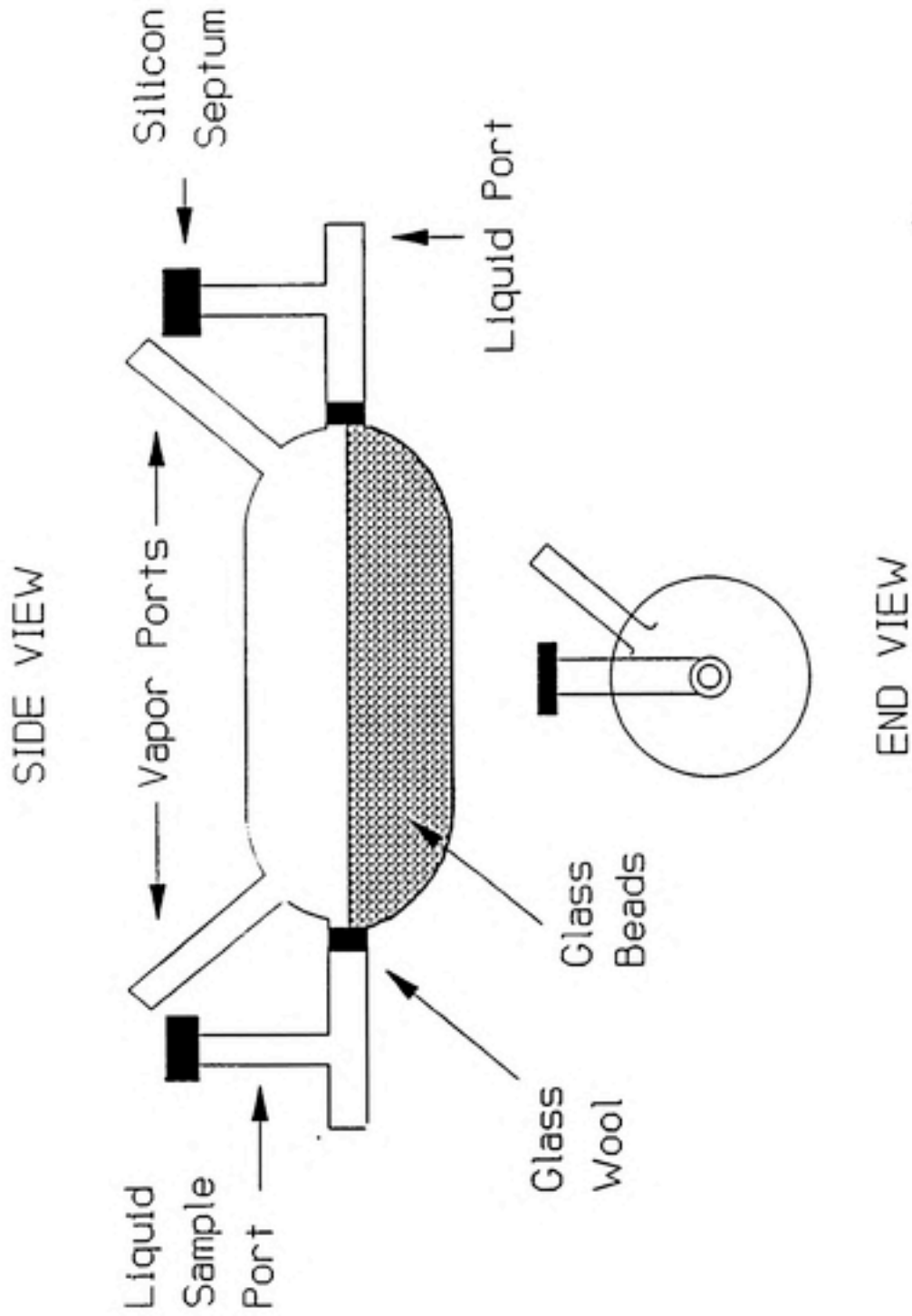

Figure 4–2. Circular Column

use of a two-dimensional code for modeling the system. This column had a square cross section of dimension 2.51 cm and a length of 5.08 cm. To seal the column and to provide for liquid and vapor influent and effluent, removable Teflon endcaps were designed and machined. These endcaps also allowed for the use of variable column lengths. Figure 4–3 shows a cross-section of the column with endcaps and an internal view of the endcaps. Each endcap had two ports; the lower one for the liquid phase and the upper one for the vapor phase. The beads in the column occupied the lower 1.3 cm, while the upper 1.18 cm was continuous vapor phase. The o-ring that slid over the column was compressed between the metal plate and the machined Teflon face to hold the endcap to the column. The column was sealed by the compression of the glass face at the end of the column against the stainless steel screen and the machined Teflon surface.

Sample ports for the aqueous phase were similar for the two columns. Essentially, they consisted of 1/4-inch glass tubing formed into inverted tees with silicon septa sealing the tops of the sample ports. In the case of the circular column, these glass tees were permanently attached to the column. For the square column, detachable glass tees were connected to the stainless steel fittings that screwed into the Teflon endcaps. The tees were sealed in the fittings with Teflon ferrules. The configuration for both columns allowed liquid influent to be sampled immediately prior to entering the column and liquid effluent to be sampled immediately after exiting the column.

4.4 ANALYTICAL METHODS

4.4.1 AQUEOUS-PHASE SAMPLING AND ANALYSIS

All aqueous-phase samples were extracted with hexane and the hexane extractant was analyzed using gas chromatography (GC). All GC methods used a

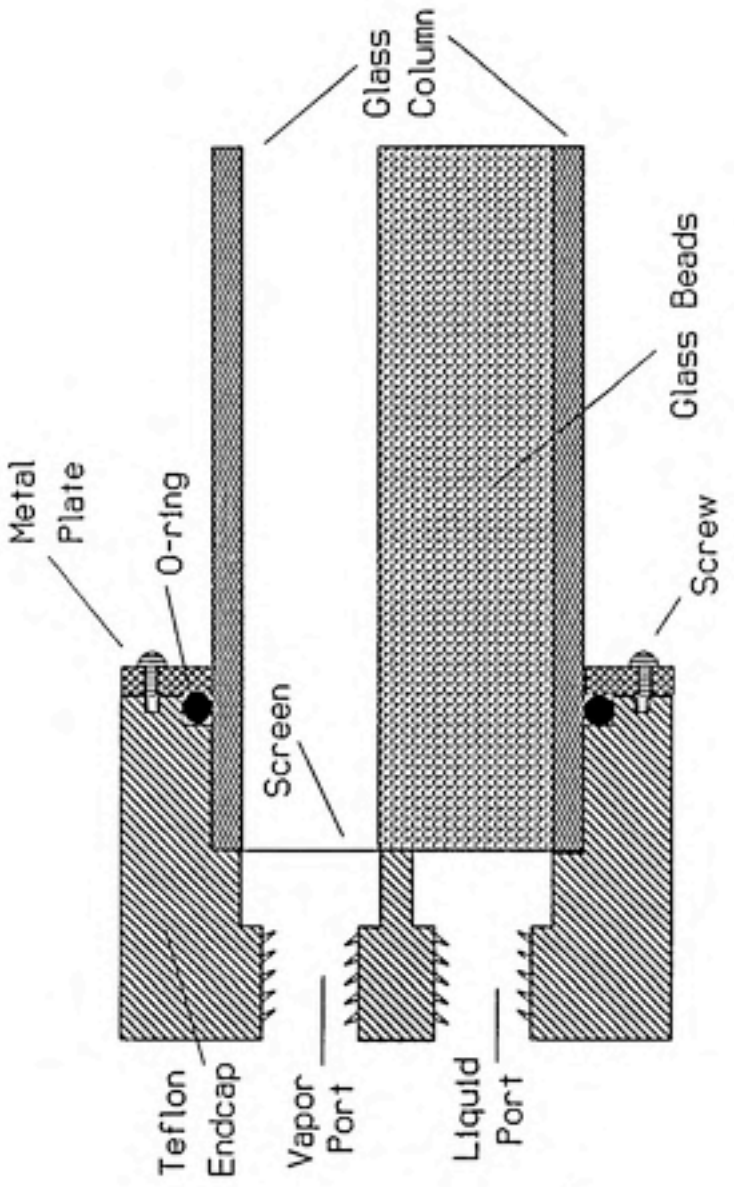

Figure 4–3. Longitudinal Cross-Section of Square Column and an Endcap

30-meter DB-5 column and flame ionization detection. The internal standard was 2,2,4-trimethylpentane.

The primary criterion in developing a methodology for analyzing aqueous phase samples was that all operations had to eliminate any possibility of exposure to the air of all solutions that contained analyte. This criterion had to be strictly applied to aqueous solutions and could be relaxed only minimally for organic solutions. For this reason, all aqueous samples were obtained by inserting the needle of a gas-tight syringe through the septum of a sample port, drawing the sample into the syringe, removing the syringe from the sample port, then injecting the aqueous phase directly into a sealed 4.0-ml vial containing the organic phase. Using this procedure, the aqueous phase was never exposed to the atmosphere. Then, the two phases were agitated during the extraction of the analyte into the organic phase by wrapping the vial in foam and placing it in a 'Junior Orbit Shaker '(from Lab-line Instruments Inc. of Melrose Park, IL) for 10 minutes at 3000 rpm. Finally, the vial was opened and the organic phase was removed, using a Pasteur pipette, and placed into a GC autosample vial, which was immediately sealed. This was the only period during which a solution containing the analyte was exposed to the air, and the exposure lasted for only several seconds.

Another criterion for obtaining the sample was that only a small volume of sample could be removed, thus minimizing system upsets. For example, at the lowest velocity (0.2 m/day) the volumetric flow rate was only 1.07 ml/hr; therefore, removal of 0.25 ml from the influent line resulted in a subsequent 15 minute period during which no water flowed into the column. A 250 μl syringe was used, so the volume removed was slightly greater than 0.25 ml. The excess water was removed from the syringe and the 250 μl water sample was extracted with 2.0 ml of hexane as described above.

A test was performed to determine the percent recovery of toluene using two toluene concentrations, 250 μl of aqueous phase, and 2.0 ml of hexane. Twelve samples of water with known concentrations were extracted following the same procedure used throughout the study. The recovery of toluene was found to be 92.9 percent. This is an overall recovery; the fraction not recovered represents the toluene that remained in the aqueous phase, that was lost to the head space of the extraction vial, and that volatilized during transfer to autosample vials. Additionally, hexane samples of known concentration were stored in GC autosample vials for ten days at about 5 °C. These samples did not exhibit any loss of toluene. Since all samples obtained from column runs were stored at that temperature for less than ten days, storage of the samples did not introduce any measurable errors or bias into the results.

Analysis of the hexane solutions was performed using gas chromatography. The conditions under which the samples were analyzed depended upon the sample concentrations. Samples with concentrations greater than 10 mg/l toluene were analyzed with a split-flow method. For the split-flow method, the column temperature was isothermal at 70 °C; the column flow was 0.8 to 1.0 ml/min; the split flow was 28 to 36 ml/min; the septum purge flow was about 4 ml/min; the volume of sample injected was 1.0 μl; and the concentration of internal standard was 50 mg/l.

Samples with concentrations less than 10 mg/l were analyzed with a splitless method, which utilized a temperature program. The intent was to increase the amount of sample that entered the column and reached the detector. This was done by recondensing the sample at the entrance to the column using an initial column temperature of 40 °C and by turning the split flow off when the sample was injected. After 45 seconds of isothermal conditions with the split flow off, the split flow was automatically begun and a temperature ramp of 5 °C/min was initiated. The run was terminated when the temperature reached 75 °C. For the splitless

method, the column flow was 0.8 to 1.0 ml/min; the split flow was 28 to 35 ml/min; the septum purge was about 5 ml/min; the volume of sample injected was 1.0 or 2.0 μl; and the concentration of internal standard was 1.7 mg/l.

For all analyses, the standard curve was generated using four standards that were dilutions of a single stock standard. The concentrations of the standards were chosen to bracket the sample concentrations. A fifth standard was used to check the standard curve. This known standard was generated by diluting a stock known that was created independent of the stock standard. The concentration of the known standard was chosen to be representative of the sample concentrations to be analyzed during a given run.

To make the standards, 40-ml vials were filled with hexane then sealed with silicon septa to prevent the internal standard concentration from changing during the standard preparation. Using a syringe to puncture the septa, between 5 and 10 ml of hexane were withdrawn from the 40-ml vials and injected through septa into 5-ml and 10-ml vials. These latter vials were used to make the stock standards and the dilutions. Several μl of pure toluene were injected through the septa of 10-ml vials to produce the desired stock standard and stock known concentrations. Using a syringe, between 100 μl and 1.0 ml were withdrawn from the stock vials and injected through septa to 5-ml and 10-ml vials to generate the desired standard concentrations. During all withdrawals and injections of liquid from sealed vials, a needle without a syringe attached was pierced through the septum to prevent vacuum or overpressure from developing, while also preventing direct contact of the volatile compounds with the atmosphere.

A standard curve was considered suitable for use if: (i) the correlation coefficient was greater than 0.9995; and (ii) the estimated concentration of the known standard agreed to within 5.0 percent of the known standard concentration. For most runs, the correlation coefficient was greater than 0.9998 and the estimated

concentration of the known standard was within 3.0 percent of the known value. A full round of standards was injected to calibrate the instrument after every 10 to 15 samples.

All split-flow analyses were run with duplicate injections of samples and standards, while most splitless analyses did not employ duplicate injections. For those runs employing duplicate injections, the standard curve was calculated using all eight standard injections and sample concentrations were determined by averaging the concentrations from the two injections.

4.4.2 VAPOR-PHASE SAMPLING AND ANALYSIS

All vapor phase samples were obtained by passing the vapor through vials containing granular activated carbon (GAC), thus adsorbing the toluene onto the GAC. The toluene was then extracted from the GAC with carbon disulfide (CS_2), and the extractions were analyzed using gas chromatography (GC). The GC method used a 30 meter DB-5 column and flame ionization detection. The internal standard was 2,2,4-trimethylpentane.

The primary criterion in developing a method for analyzing the vapor phase was that breakthrough of toluene could not occur in the GAC vials. To prevent breakthrough, two conditions had to be met. The first condition was that the vapor phase flow rate through the vial had to be less than 200 ml/min (NIOSH, 1984). The second condition was that the amount of toluene sorbed had to be less than the capacity of the GAC. Estimates of the capacity of activated carbon for toluene were obtained from data published by the National Institute for Occupational Safety and Health (1984) and by White et al. (1970). Using these estimates of the GAC capacity and an estimate of the rate of mass transfer of toluene into the vapor phase under the conditions of the study, it was determined that the capacity of the GAC would only be exceeded for sampling times on the order of hours. Although both

criteria were met for all vapor phase samples taken, the second aliquot of GAC in the vials (a 50-mg portion on the downstream side) was extracted and analyzed to ensure that breakthrough had not occurred.

Another criterion for obtaining the sample was that the vapor phase flow be minimally disturbed to prevent the introduction of large errors into the data. One aspect of this was that the pressure drop throughout the vapor loop had to be the same during sampling periods as it was during the periods between sampling. To do this, a GAC vial was placed online at all times. Ultimately the capacity of this vial was exhausted; however, the pressure drop across the vial remained essentially the same as for the fresh vials that were used to sample the vapor. To obtain a sample, this 'dummy' sample vial was rapidly removed and replaced by a fresh vial; the new sample vial was exposed for a measured period of time while the vapor-phase flow rate was measured; finally, the 'dummy' vial was placed back online and the vial containing the vapor sample was sealed and stored at about 5 °C.

To extract the toluene, the vial was broken and the two aliquots of GAC were placed into separate 4-ml vials, which were sealed with Teflon-lined septa. Then, 2.0 ml of CS_2 were injected into each vial through the septa using a gas-tight syringe. The GAC in a vial was agitated slightly to remove any air that was entrained when the CS_2 was injected. The vials were allowed to stand for one hour with gentle agitation (a brief swirling of the liquid in the vial) at 15 minute intervals. Next, each vial was opened and a Pasteur pipette was used to immediately transfer the CS_2 into a GC autosample vial which was quickly sealed. The CS_2 was exposed to the air for several seconds during this transfer.

A series of tests were performed to determine the percent recovery of toluene from the GAC using two values of toluene loadings. Six samples of GAC with known toluene loadings were extracted and the recovery of toluene was found to be 90.0 percent. Additionally, samples of GAC with known toluene loadings were

stored in a refrigerator for one month at about 5 °C. These samples did not exhibit any loss of toluene. Since all vapor phase samples obtained from column runs were stored on the GAC at that temperature for less than one month, storage of the samples did not introduce any measurable errors or bias into the results.

Analysis of the CS_2 solutions was performed using gas chromatography. All of the samples were analyzed using a split-flow method. For this method, the column temperature was isothermal at 70 °C; the column flow was 0.8 to 1.0 ml/min; the split flow was 28 to 36 ml/min; and the septum purge flow was about 4 ml/min. The volume of sample injected depended upon the sample concentration: for samples with toluene concentrations greater than 10 mg/l the volume was 1.0 μl, and for those with concentrations less than 10 mg/l the volume was 2.0 μl. Splitless analysis of the low-concentration samples was not performed because the initial temperature necessary for splitless analysis with CS_2 is difficult to obtain unless the GC is configured for cryogenic analyses. The concentration of internal standard was varied to correspond with the concentration of toluene in the samples.

Standard curves were generated in the same manner described in section 4.4.1, and the same criteria that were applied to standard curves for hexane analyses were also applied to curves generated for CS_2 analyses. All analyses were run with duplicate injections of samples and standards The standard curve was calculated using all eight standard injections and sample concentrations were determined by averaging the concentrations from the two injections.

4.4.3 MEASURING DISPERSIVITIES

To analyze the data for the water-toluene system, the glass beads had to be fully characterized. Porosity, bulk density, particle density, and longitudinal dispersivity were all measured. The procedures for measuring the first three properties, and the results of those measurements, are described in section 4.2. Attempts were

made to measure the transverse dispersivity exogenous to the water-toluene data; although these attempts were unsuccessful, a description of the methods used is included in the following discussion. Ultimately, a value of transverse dispersivity was determined endogenously. A discussion of both the data manipulation necessary to determine simultaneously the transverse dispersivity and the mass transfer coefficient from the water-toluene data set and the ramifications of using this approach appears in section 5.3.

Longitudinal dispersivity was measured in the square column with the same bead packing that was used for all of the square column water-toluene data. Fluoride was the conservative tracer and the measurements were made using a fluoride-specific ion probe manufactured by Orion Instruments. The velocity used was 1.07 m/day and the fluoride influent concentration was 2080 mg/l. Each sample was collected over approximately five minutes by allowing the effluent to flow into a vial containing 2.0 ml of total ionic strength adjuster buffer (TISAB) and approximately 17 ml of deionized water. The volumetric water flow rate was 5.7 ml/hr, therefore the collection period provided about 0.5 ml of sample.

The standard curve was determined using four points: 211 mg/l, 160 mg/l, 101 mg/l, and 42.6 mg/l. The standards were prepared by dissolving 0.1738 mg of NaF in 100 ml of deionized water, then diluting this stock standard using 90 percent deionized water and 10 percent TISAB. The standard curve was checked against a known sample obtained from a separate dissolution and dilution than the standards. A measurement was made of the known sample, and the value for fluoride concentration calculated from this measurement and the standard curve was compared to the known value. Each time the calibration curve was used, the concentration determined for the known sample was less than 1.0 percent different from the known concentration. All standards were within the linear response range for the probe, and the correlation coefficient was 0.9999 for all calibrations.

Based on the lowest standard concentration and a dilution factor of about 42, the lower limit of detection of the effluent concentration was about 1.0 mg/l. Effluent was measured from 30 minutes to 165 minutes, with the concentration increasing from 1 mg/l to 2080 mg/l. Steady-state was achieved at about 145 minutes. The value of longitudinal dispersivity was determined by minimizing the errors between the measured values of effluent concentration and the effluent concentration determined from the one-dimensional unsteady-state solution to the advective-dispersive equation. The optimal value of longitudinal dispersivity was 0.199 cm.

In an attempt to measure the transverse dispersivity using the square column, the column was completely filled with beads and oriented horizontally but rotated 90 degrees from the position shown in Figure 3-3. This placed the two ports on each endcap in the same horizontal plane. Next, both ports on the inlet side were connected to syringes of the same size, and both syringes were placed on the syringe pump. Thus, as the syringe pump pusher moved forward, the flow into each port was equal. One syringe was filled with deionized water and the other was filled with deionized water containing about 2100 mg/l fluoride. Three bed volumes were pumped through the column to achieve a steady-state fluoride concentration profile, then triplicate measurements of fluoride concentration in the two outlet ports were made.

To analyze the results of the transverse dispersivity tests, a Galerkin finite element solution to the advective-dispersive equation in two-dimensions was used. By dividing the outlet concentration profile into a portion online with the fluoride influent and a portion offline from the fluoride influent and by averaging the concentration in each portion, the code calculated the concentration that could be expected in the effluent from the two outlet ports for a given set of hydraulic conditions. The expectation was that the code could be used to calculate the optimal

value of transverse dispersivity for a given velocity by minimizing the errors between a number of data points and the numerical calculations. Furthermore, if the transverse dispersivity test were performed repeatedly and the optimal dispersivities determined for the various runs were consistent, then one could reasonably state that this methodology accurately determined the transverse dispersivity for the beads.

Two criteria were chosen to determine if the results from a given run could be used to estimate the dispersivity. First, the volumetric flow from the two outlet ports had to be equal. Second, a mass balance on the fluoride had to recover 95 to 105 percent. Several problems developed in attempting to meet both of these criteria. There was great difficulty in achieving equal volumetric flow from the two outlet ports, and it was never determined whether the differing outlet flows represented a nonuniform flow field in the column or whether the flow field in the column was uniformly unidirectional and the difference in the outlet flows was purely an artifact of the outlet port configuration.

Of the many tracer tests made, only three were used to estimate the transverse dispersivity, and none of these met both criteria given above. One had outlet flows that differed by about 40 percent and mass balances of 3.9, 6.4, and 6.9 percent; the transverse dispersivity calculated was 0.036 cm. The second run also had outlet flows that differed by about 40 percent, but the mass closures were 5.8, 4.1, and 4.1 percent; the dispersivity calculated was 0.15 cm. Finally, the last run used to estimate transverse dispersion had flows that differed by about 15 percent and mass closures within 1.0 percent; the dispersivity was 0.14 cm. An explanation of the difficulty of reconciling any one of these values with the water-toluene data appears in section 5.3.

4.5 COMPUTATIONAL METHODS

As explained in section 4.1, all samples were taken at steady state. Each data point included measurements of aqueous influent concentration, aqueous effluent concentration, vapor effluent concentration, vapor flow rate, and vapor-phase temperature. The two aqueous phase concentrations were used to calculate mass transfer coefficients, and the concentration of the vapor phase was used to calculate a mass balance for each data point. Mass transfer coefficients were also calculated using the liquid influent concentration and the vapor effluent concentration. The mass transfer coefficients were calculated using two computer codes, one based on an analytical solution and one based on a numerical solution. The following discussion explains how the codes were used to calculate mass transfer coefficients and presents a brief verbal explanation of the two codes. Section 5.4 presents a comparison of the results obtained with the two codes. Appendix B presents a more complete mathematical description of the two models.

Both the analytical and numerical codes allowed for the calculation of a depth averaged concentration at the column outlet. In both codes, the depth averaged effluent concentration was a function of the influent concentration, the pore velocity, the transverse dispersion coefficient, and the mass transfer coefficient. A mass transfer coefficient could be calculated for any data point by specifying the first three parameters using lab data, then varying the value of the mass transfer coefficient until the estimated depth averaged effluent concentration equaled the value determined in the lab. An optimal mass transfer coefficient could be determined for each velocity by using all of the data points generated at that velocity and minimizing the sum of the squares of the errors (SSE). This was done by inputting liquid influent and effluent concentrations, a transverse dispersivity, and two k_l's that were thought to bracket the optimal k_l for the given α_t. The code minimized the SSE

using FMIN, a function subprogram from Kahaner et al. (1988). FMIN uses a combination of the golden section search and successive parabolic interpolation.

The first computer code used to calculate the mass transfer coefficient was based on an analytical solution for one-dimensional, unsteady-state diffusion with interphase mass transfer at one boundary. Figure 4–4 illustrates the process modeled. One boundary was a no-flow boundary and the other boundary was the interface across which mass moved. Mass transfer at the boundary was governed by two terms: the mass transfer coefficient; and the difference between the concentration in the media at the interface and the concentration in the media that would be in equilibrium with the external phase.

This analytical solution was used to approximate the two-dimensional steady-state conditions that existed in the column by: orienting the direction of diffusion in the analytical solution with the vertical direction in the column; replacing the diffusivity in the analytical solution with the dispersion coefficient in the column; and replacing the time term in the unsteady-state solution with the time of travel for a given position in the column. The result of the last modification was that every point in the column was represented by the time required for fluid to travel from the inlet to that point under steady-state conditions. Thus, the effluent from the column was represented by the residence time of the fluid in the column. Using the analytical code to model the conditions in the column implicitly assumed that the effect of longitudinal dispersion on the steady-state concentration profiles in the x and z directions could be neglected.

The second code used to determine mass transfer coefficients from the lab data was a two-dimensional Galerkin finite element code (Huyakorn and Pinder, 1983). This was the same code used to simulate aqueous-vapor phase mass transfer under ambient conditions (these results appear in section 5.4). The code consisted of a saturated domain and an unsaturated domain which were coupled by equating the

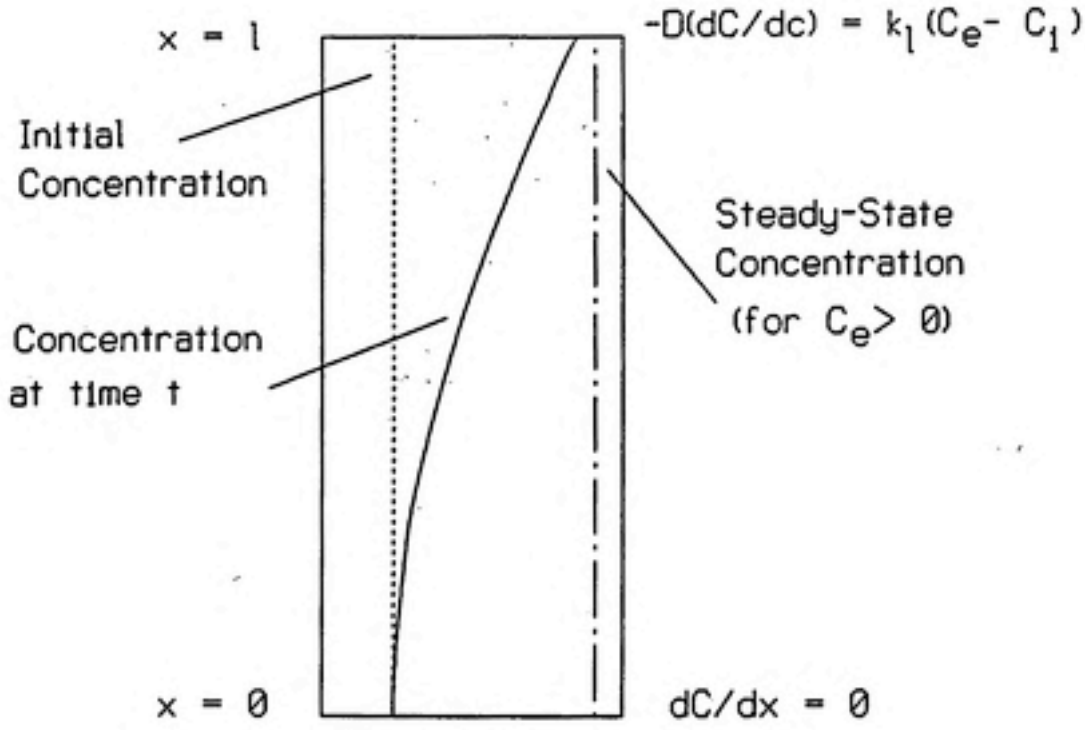

Figure 4–4. Model for the Analytical Solution

mass flux of contaminant across the interface. These interfacial boundary conditions were expressed in the same manner as the interfacial boundary condition in the analytical model. The saturated zone included terms for advection and dispersion in the aqueous phase, fast and slow sorption onto the solid phase, and first-order degradation reactions in the aqueous and solid phases. The unsaturated zone included terms for advection and dispersion in the vapor phase, mass transfer limited transport between the vapor and aqueous phases within the unsaturated domain, fast and slow sorption onto the solid phase, and first-order degradation reactions in the aqueous and solid phases.

The numerical code was simplified to simulate the conditions in the lab apparatus. In the saturated zone, sorption onto the media was eliminated because glass beads were used. In the unsaturated zone, a porosity of 1.0 was assigned since this domain consisted of a continuous vapor phase. Finally, the reaction terms in the aqueous and vapor phases of both domains were eliminated. Thus, transport in the saturated zone consisted solely of advection and dispersion and transport in the unsaturated zone consisted solely of advection and diffusion.

Both of the codes assumed that the velocity field throughout the column contained no vertical components. For the code based on the analytical solution, this assumption was unavoidable since the governing equation for the model contains no advection term. The numerical code, on the other hand, could be readily modified to include vertical components of advection, and one might expect that this would increase the accuracy of the resulting calculations. However, two features of the system being modeled negated any apparent increase in accuracy that might result from this modification. First, the small scale of the column implies that relatively small absolute errors in measuring the exact configuration of the saturated domain would result in comparatively large errors in estimates of the vertical components of the flow field. Additionally, reliable estimates of the transverse dispersivity were

never obtained exogenous to the toluene data. These two facts indicate that the errors which would have been introduced by including vertical components of advection could negate the increase in accuracy which might be expected from including vertical components. Furthermore, since the transverse dispersivity was not determined exogenous to the toluene data, it had to be estimated simultaneously with the mass transfer coefficients. Since dispersion is a tensor, including vertical advective components would have greatly increased the complexity of the calculations necessary to determine the mass transfer coefficients and the transverse dispersivities simultaneously; all of this additional complexity would result in dubious increases in the accuracy of the mass transfer coefficient estimates.

Since the boundary conditions at the interface for both models assume that the interfacial concentrations of both phases are known, the rate of mass transfer is not expressed in terms of bulk concentrations. Expressions based on individual phase coefficients typically include a bulk concentration and an interfacial concentration, and expressions based on overall coefficients typically include the bulk concentration for both phases. Since the expression used in these codes includes neither bulk-phase concentration, the coefficient could be referred to as an interfacial coefficient rather than an overall or an individual-phase coefficient. However, since the the coefficient was found to correlate with liquid-phase hydrodynamics while not correlating with vapor-phase hydrodynamics, the term is referred to as a liquid-phase coefficient and is denoted by k_l.

5 RESULTS AND DISCUSSION

In this chapter, the results from the circular column and the square column are presented first. Then, a discussion of the results follows. Finally, a simulation of VOC transport under ambient subsurface conditions is presented. All the mass transfer coefficients plotted and tabulated in this chapter were calculated with the analytical code and were based on liquid-phase analyses.

5.1 RESULTS: CIRCULAR COLUMN

The first column used for this study had a circular cross section. The column is described in section 4.3, and a drawing of the column appears in Figure 4–2. The data generated with the circular column comprised 20 data points at four velocities spanning one order of magnitude. The toluene concentration in the influent ranged from 143 ppm to 196 ppm, and the pore velocities were: 0.4 m/d, 0.85 m/d, 1.2 m/d, and 4.0 m/d. Lower-bound values for k_l were obtained using the analytical code and a transverse dispersion coefficient of 0.25 cm^2/s. Lower-bound values for each data point are given in Table 5–1. Optimal lower-bound values of the mass transfer coefficient were obtained by combining all the data at a given velocity; these results are presented in Table 5–2. An explanation of the calculation of optimal values appears in section 4.5.

Table 5–1. Lower-Bound Values for k_l: Circular Column

Pore Velocity (m/d)	Lower-Bound k_l (cm/s $\times 10^4$)
4.00	5.9
4.00	5.6
4.00	5.5
4.00	4.0
4.00	4.0
4.00	3.0
1.17	3.4
1.17	2.8
1.17	2.8
1.17	2.6
1.17	2.1
0.847	3.6
0.847	3.6
0.847	3.4
0.847	3.4
0.847	3.3
0.847	2.9
0.400	2.3
0.400	2.1
0.400	1.9

5.2 RESULTS: SQUARE COLUMN

The data set generated with the square column was much more extensive than that generated with the circular column. The set consisted of 143 data points at eight pore velocities and at three influent concentrations. Six data points were obtained at each influent concentration for each velocity. The pore velocity ranged from 0.20 m/d to 19.5 m/d. The influent concentration ranged from 24 mg/l to 260 mg/l. Vapor phase velocities varied by about a factor of three. The influent concentration was varied to determine if the liquid phase concentration had an effect on the mass transfer coefficient. The variation in vapor phase velocity was

Table 5–2. Lower-Bound k_l: Circular Column

Pore Velocity (m/d)	Lower-Bound k_l (cm/s $\times 10^4$)
4.00	4.6
1.17	2.8
0.847	3.3
0.400	2.0

inherent in the apparatus design; although fortuitous, this variation provided some indication of the relative importance of the vapor phase mass transfer resistance.

The data were first analyzed to determine the mass balance for each data point. This was calculated by the ratio of the interphase mass flow rates based on the vapor- and liquid-phase analyses. The interphase mass flow rate based on the the vapor-phase analysis is

$$\dot{m}_v = \frac{C_c \times V_c}{\epsilon_v t_v} \tag{5–1}$$

where C_c is the concentration in the CS_2, V_c is the volume of CS_2 used to extract the GAC, ϵ_v is the recovery efficiency for the vapor phase analysis (90 percent), and t_v is the period of time the GAC was exposed to the vapor-phase effluent. The interphase mass flow rate based on the liquid-phase analysis is

$$\dot{m}_l = \left(\frac{V_h}{V_w}\right)\left(\frac{C_{hi} - C_{he}}{\epsilon_l \dot{V}_l}\right) \tag{5–2}$$

where C_{hi} and C_{he} are the toluene concentrations in the hexane extractions of the aqueous influent and effluent, V_h and V_w are the volumes of hexane and water used in the extraction, ϵ_l is the recovery efficiency for the liquid phase analysis (93.9 percent), and $\dot{V}_l$ is the liquid-phase volumetric flow rate. The mass balance was the ratio of $\dot{m}_v$ over $\dot{m}_l$. Figure 5–1 is a plot of the mass balance as a function of the pore velocity.

The mass balances exhibit considerable spread. The highest value, 1.70, was obtained at 1.9 m/d and the lowest value, 0.48, was obtained at 19.5 m/d. The largest spread was at 19.5 m/d, while the smallest spread was at 0.20 m/d. Overall, however, the values vary about a mean of approximately 1.0. This can be seen clearly in Figure 5–1. Another plot of mass balance versus velocity that demonstrates the tendency of the values to vary about 1.0 appears in Figure 5–2. For this figure, the six mass flow rates generated at each velocity for each influent concentration were averaged for the vapor- and liquid-phase analyses prior to calculating the ratio of $\dot{m}_v/\dot{m}_l$. Averaging the mass flow rates prior to calculating the ratio reduces the spread considerably. The highest value in Figure 5–2 is 1.17, and the lowest value is 0.78.

Before all of the data points generated at a single velocity could be used to determine k_l at that velocity, the variation of the coefficient with changes in liquid phase concentration had to be estimated. One way to do this would have been to calculate optimal estimates of the coefficient at each of the three influent concentrations, then compare the results. Alternatively, analysis of the variation of normalized effluent concentration with variation in influent concentration would provide the same information. This last point can be demonstrated by manipulating the governing equation for the liquid phase in the saturated zone. The equation was

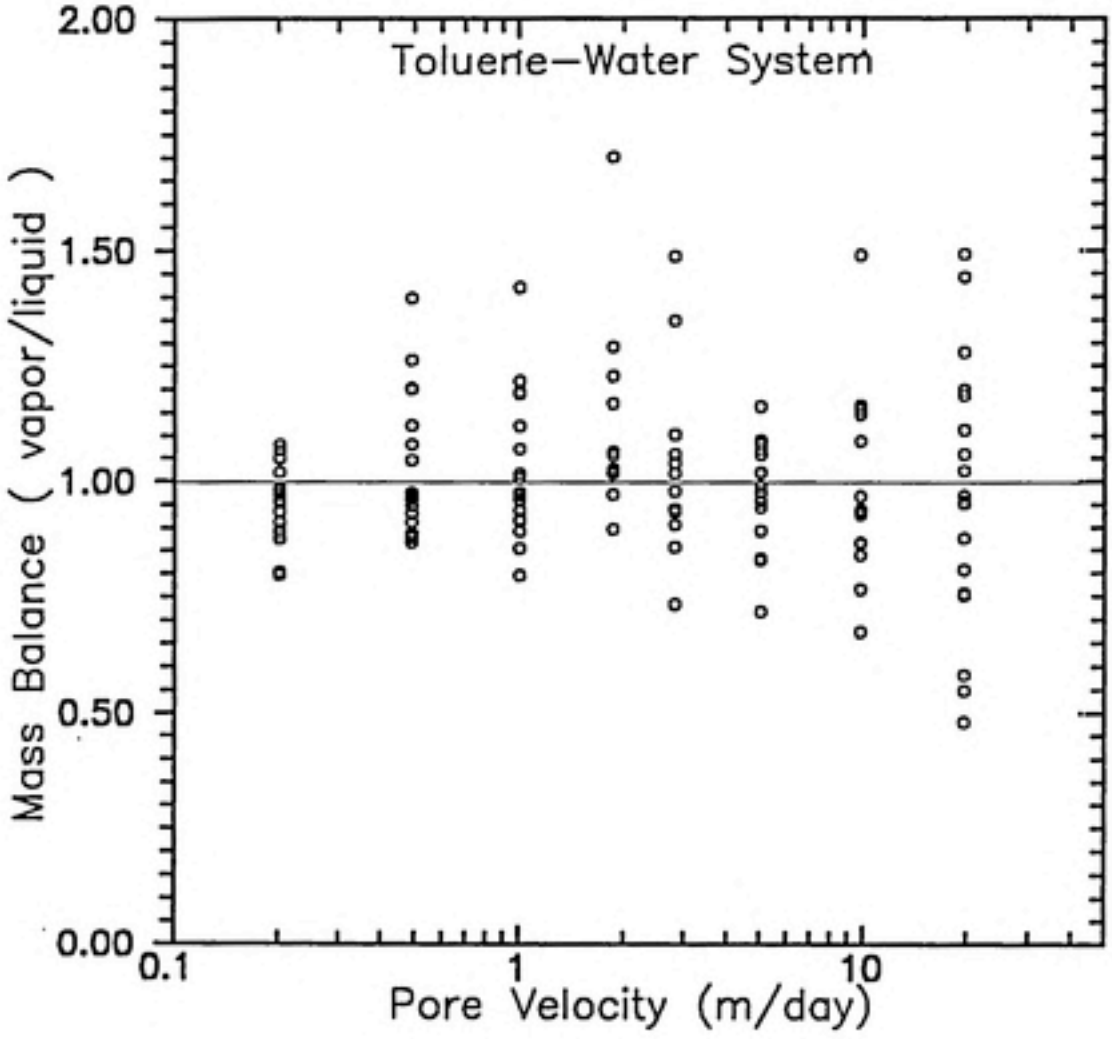

Figure 5–1. Mass Balance vs Pore Velocity

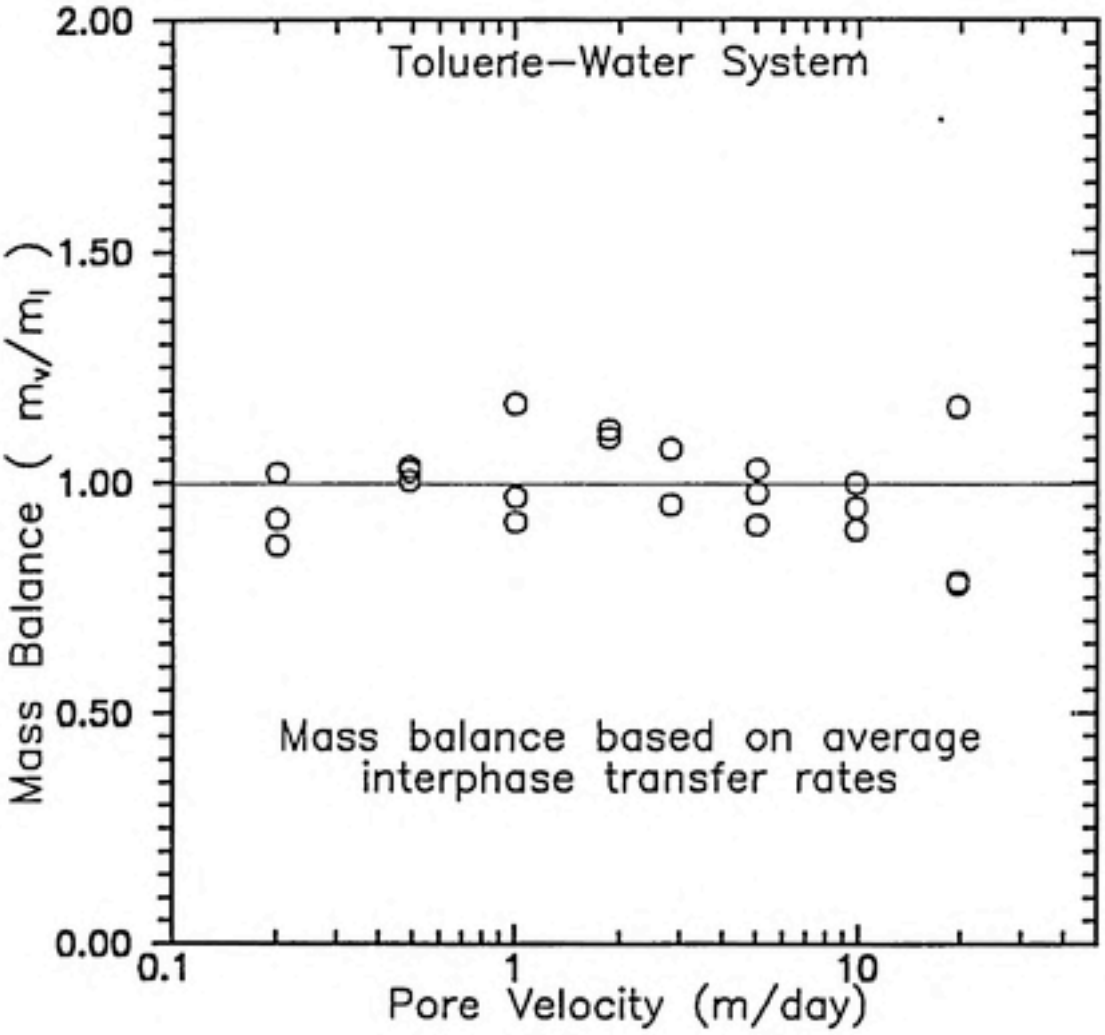

Figure 5–2. Mass Balance Based on Average Interphase Mass Transfer Rates

$$\frac{\partial C_l}{\partial t} = -\vec{v}\cdot\nabla C_l + \nabla\cdot(\mathbf{D}_h\nabla C_l) + \left(\frac{\partial C_l}{\partial t}\right)_{rxn}^{l-s} + \left(\frac{\partial C_l}{\partial t}\right)_{rxn}^{lp} \qquad (5\text{–}3)$$

with the boundary conditions

$$\begin{aligned}
C_l &= C_i \quad , \quad \text{for} \quad x = 0 \quad , \quad 0 \le z \le z|_{int} \\
\frac{\partial C_l}{\partial x} &= 0 \quad , \quad \text{for} \quad x = L \quad , \quad 0 \le z \le z|_{int} \\
\frac{\partial C_l}{\partial z} &= 0 \quad , \quad \text{for} \quad z = 0 \quad , \quad 0 \le x \le L \\
D_t\frac{\partial C_l}{\partial z} &= k_l\left(\frac{C_v}{H_c} - C_l\right) \quad , \quad \text{for} z = z|_{int}
\end{aligned} \qquad (5\text{–}4)$$

where C_i is the liquid-phase influent concentration, L is the column length, k_l is the mass transfer coefficient, $z|_{int}$ is the location of the saturated-unsaturated zone interface, and D_t is the liquid-phase transverse dispersion coefficient. By dividing through by the influent concentration, the equation and the boundary conditions can be written in terms of a normalized concentration. Thus, if the mass transfer coefficient is independent of liquid phase concentration, then a plot of the normalized effluent concentration versus the influent concentration should have a slope of zero. In other words, the equation is linear with respect to concentration if $k_l \neq \mathrm{f}(C_l)$.

Plots of normalized effluent concentration vs influent concentration were made for each of the eight velocities, and the correlation coefficient was determined for each plot. In addition, a statistical test was performed on the hypothesis that the slope was zero, and the *attained significance level*, or *p*-value, was calculated. The attained significance level is a measure of the probability that an hypothesis is correct: the lower the *p*-value, the lower the probability that the hypothesis is correct. Thus, a *p*-value of zero is a clear indication that the hypothesis is wrong. For the calculations done here, the hypothesis was that the slope was zero. Table 5–3 presents the correlation coefficients and the *p*-values for the eight plots. Figure 5–3

is a plot of normalized effluent concentration vs influent concentration for 2.8 m/d and 1.0 m/d. The p-value for 2.8 m/d was about the median value (although it did have a positive slope, while most were negative). The p-value for 1.0 m/d is the lowest, and Figure 5–3 shows a clear trend.

Table 5–3. Statistics for Linear Regressions of C_e/C_i vs C_i

Pore Velocity (m/day)	Correlation Coefficient	p-Value
19.54	-0.391	0.110
9.77	-0.118	0.460
5.01	0.375	0.140
2.81	0.417	0.085
1.86	-0.249	0.322
1.00	-0.868	0.000
0.489	-0.479	0.043
0.201	-0.542	0.019

Although the vapor phase velocity only varied by a factor of three, a similar analysis was performed on the data for this variable. For each pore velocity, plots of normalized effluent concentration vs vapor-phase velocity were made, correlation coefficients were determined, and p-values were calculated. The results appear in Table 5–4. Half the plots had positive correlation coefficients and half had negative. Also, half the plots had p-values less than five percent; but of those with low p-values, half exhibited a negative trend and half exhibited a positive trend.

Finally, the optimal values for the mass transfer coefficient were calculated for each velocity. An explanation of the calculation of optimal values is presented in section 4.5. The optimal values calculated were dependent upon the value for

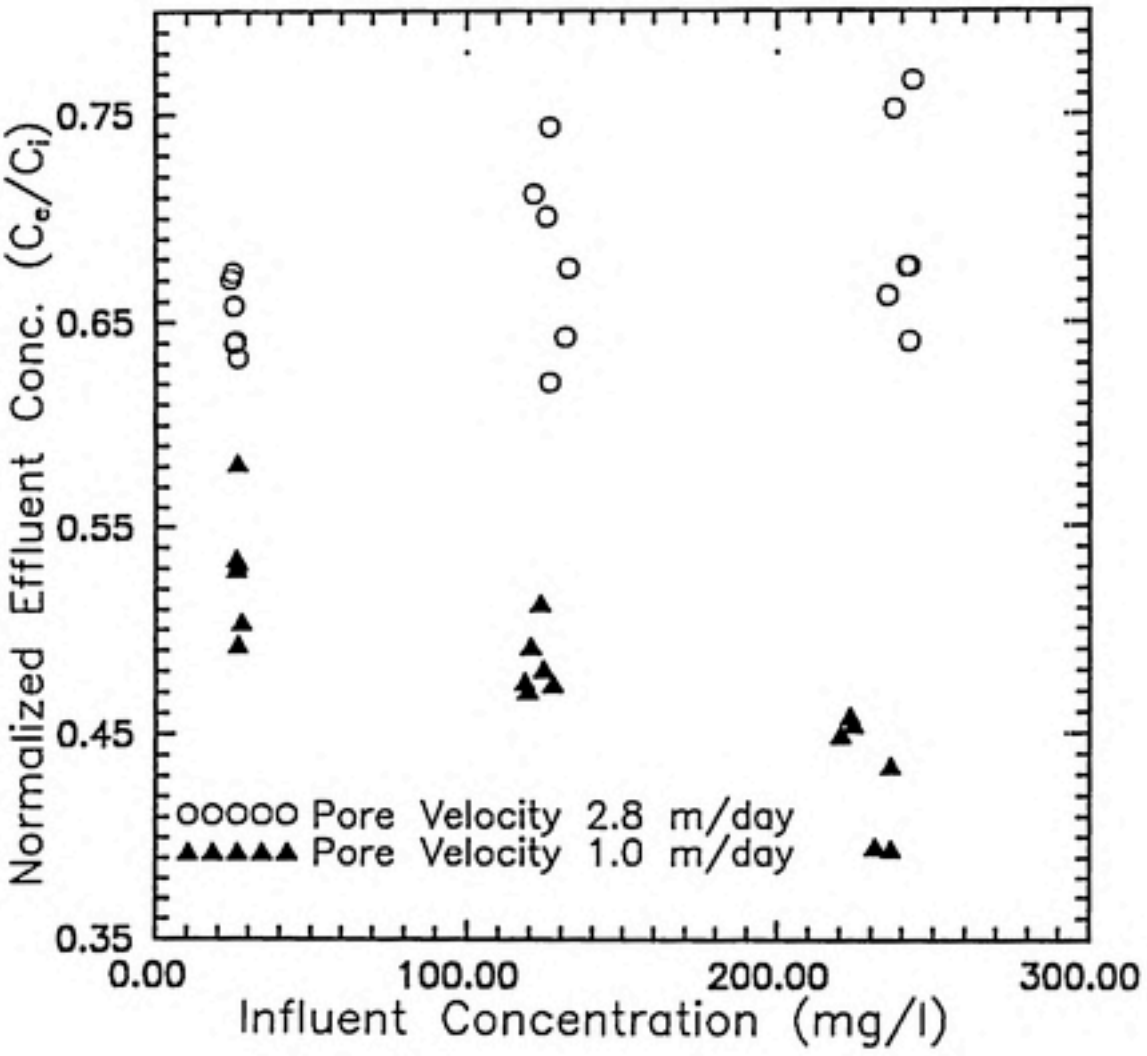

Figure 5–3. Normalized Effluent Concentration vs Influent Concentration

Table 5–4. Statistics: Linear Regressions of C_e/C_i vs Vapor Velocity

Pore Velocity (m/day)	Correlation Coefficient	p-Value
19.54	0.566	0.013
9.77	-0.298	0.234
5.01	-0.133	0.610
2.81	0.387	0.114
1.86	0.627	0.004
1.00	-0.493	0.037
0.489	0.072	0.779
0.201	-0.489	0.038

transverse dispersivity chosen; the reasons for this phenomenon, and the implications it has for interpreting the results, are discussed in section 5.3. Figure 5–4 is a plot of the optimal upper-bound and lower-bound values as a function of velocity. The upper- and lower-bound values are tabulated in Table 5–5. Between 2.8 and 19.5 m/d, the upper-bound is less than 4 percent higher than the lower-bound. At 1.86 and 1.0 m/d, the upper-bound is higher by 13 and 8 percent, respectively. Only below 1.0 m/d do the values differ significantly: by 30 percent at 0.5 m/d and 56 percent at 0.2 m/d. For most of the range of the data, the upper- and lower-bound values are essentially equal.

Figure 5–5 provides a visual representation of the scatter in the data. It is a plot of the upper-bound values obtained for each data point along with the best fit curve calculated from all 143 data points. The figure also shows two confidence intervals, both at the 95 percent confidence level. The largest interval was calculated using all 143 data points. The smaller interval was calculated by omitting the data at 19.5 m/d; The best-fit curve obtained by omitting the data at 19.5 m/d was

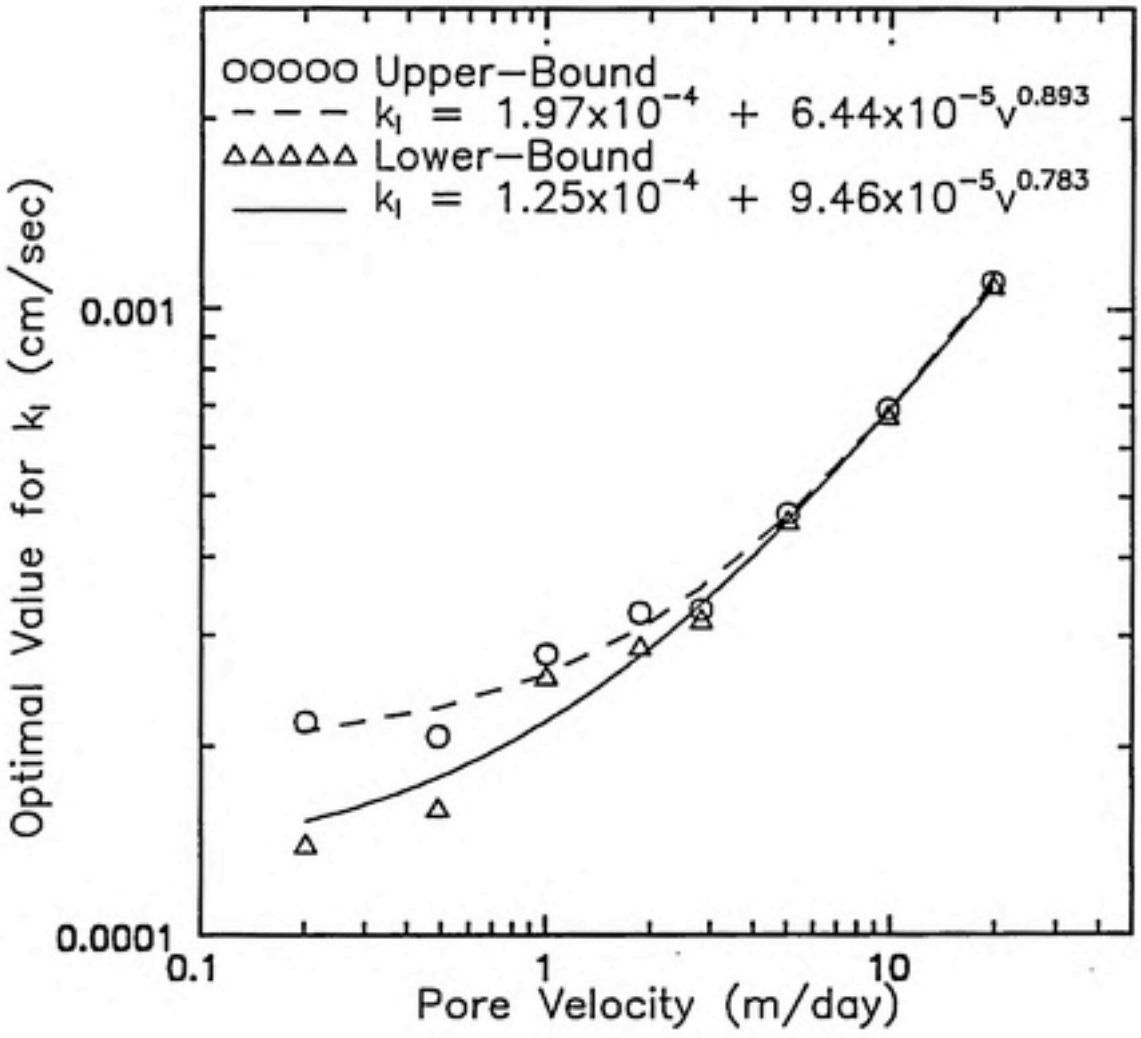

Figure 5–4. Optimal Upper- and Lower-Bound k_l with Best-Fit Curves

within 2 percent of the curve obtained using all the data. Thus, omitting the data at the high velocity did not alter the best-fit curve significantly, but it did reduce the range of the 95 percent confidence interval by about half.

Table 5–5. Upper-Bound and Lower-Bound k_l: Square Column

Pore Velocity (m/d)	Upper-Bound k_l (cm/s $\times 10^4$)	Lower-Bound k_l (cm/s $\times 10^4$)
19.54	11.1	11.0
9.77	6.94	6.80
5.01	4.71	4.60
2.81	3.31	3.20
1.86	3.27	2.90
1.00	2.81	2.60
0.489	2.08	1.60
0.201	2.19	1.40

5.3 DISCUSSION OF LAB RESULTS

5.3.1 CIRCULAR COLUMN

Because the flow field in the circular column included vertical components of advection, interphase mass transfer was probably limited by the interfacial resistance. For this reason, the lower-bound estimates for the data from this column were expected to be close to the actual values of k_l. The major source of error arose from the fact that the column was not symmetrical in the x-z plane about the centerline, an assumption required for the use of a two-dimensional solution.

The computer code (discussed in section 4.5) based on an analytical solution to diffusive transport with interphase mass transfer was used to analyze the data from the circular column. Initially, an attempt was made to determine simultaneously an

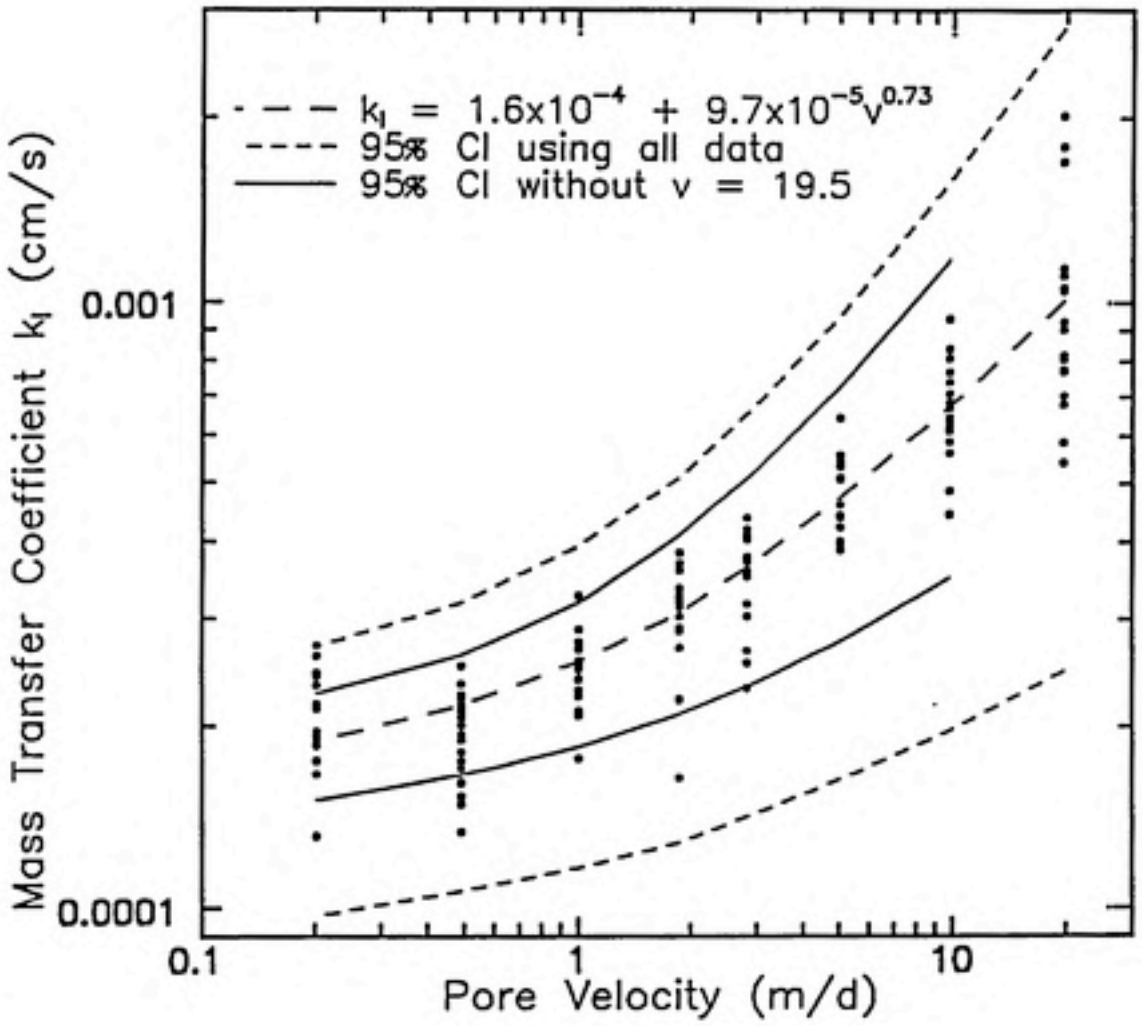

Figure 5–5. Individual Upper-Bound Values and Confidence Intervals

optimal value for the mass transfer coefficient and an optimal value for the effective transverse dispersivity at each velocity by minimizing the sum of the squares of the errors (SSE). However, the data had no global minimum for the two variables; at a given velocity, for every transverse dispersivity that was chosen, the optimal mass transfer coefficient yielded the same SSE. As the effective transverse dispersivity was increased, the value of the mass transfer coefficient at which the minimum SSE was obtained decreased.

Figure 5–6 demonstrates this problem using data from the square column. It is a plot of SSE vs mass transfer coefficient as a function of the transverse dispersivity for a pore velocity of 1.8 m/d. As the transverse dispersivity increases, the minimum point moves to the left in the figure, but the minimum value for SSE remains unchanged at 247. Note that as the transverse dispersivity is increased to a very high value (116 cm in the figure), the mass transfer coefficient that yields the minimum SSE reaches a minimum (2.9×10^{-4}). This is the lower-bound value for k_l at that velocity, and it represents the condition for which interphase mass transfer is the sole limiting process.

For these reasons, the best information that could be extracted from the data obtained with the circular column were estimates of the lower-bound values for the mass transfer coefficient. The effective transverse dispersion coefficient was increased until further increases in the dispersion value did not change the value of the mass transfer coefficient at which minimum SSE was achieved. In this manner, 0.25 cm^2/sec was determined to be a sufficiently high value for the transverse dispersion coefficient. Figure 5–7 is a plot of the individual lower-bound values for each data point and of the optimal lower-bound values obtained at each velocity. The depth of saturated media used for these calculations was the maximum depth, 1.2 cm.

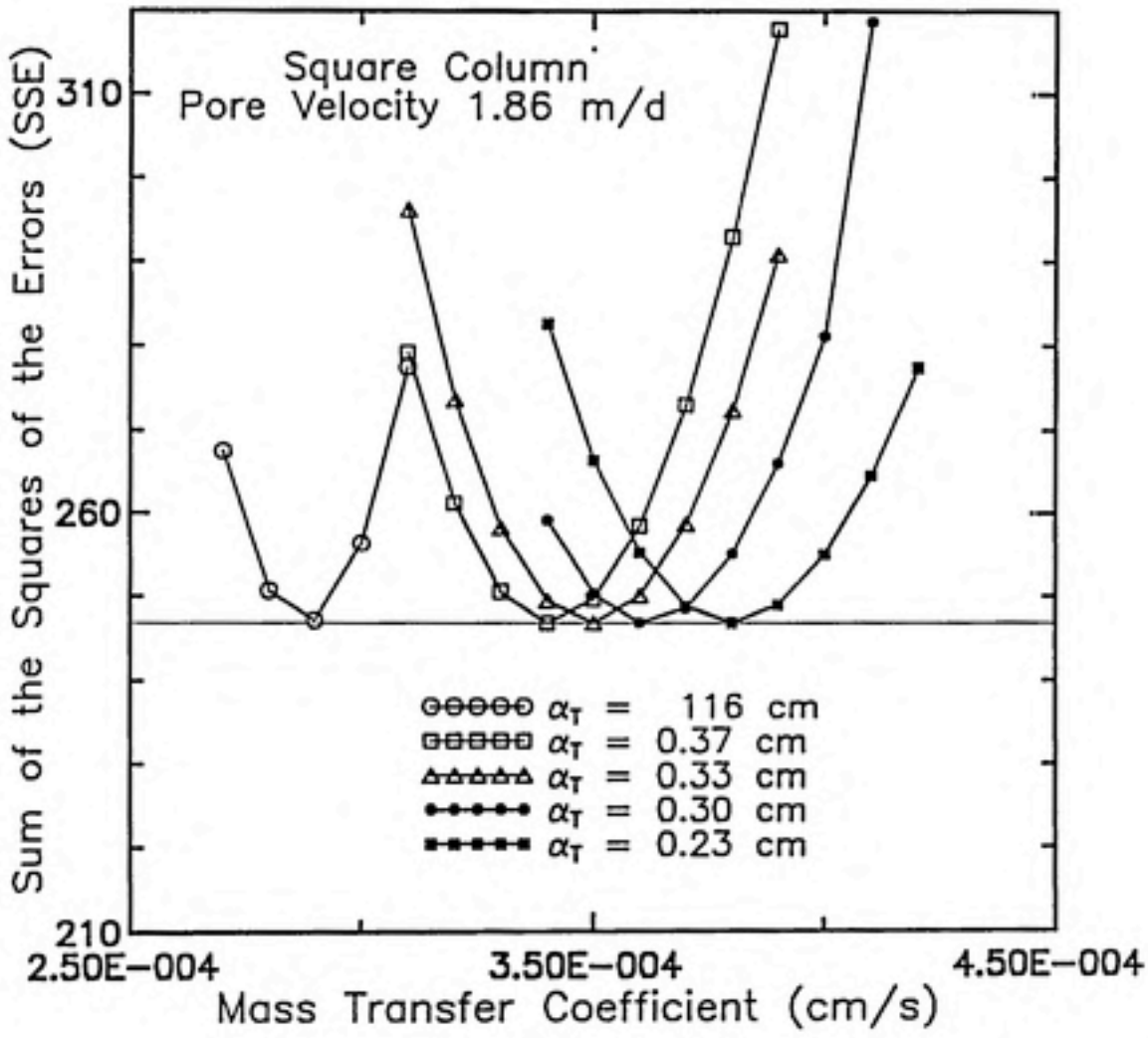

Figure 5–6. Determining an Optimal Lower-Bound Value for k_l

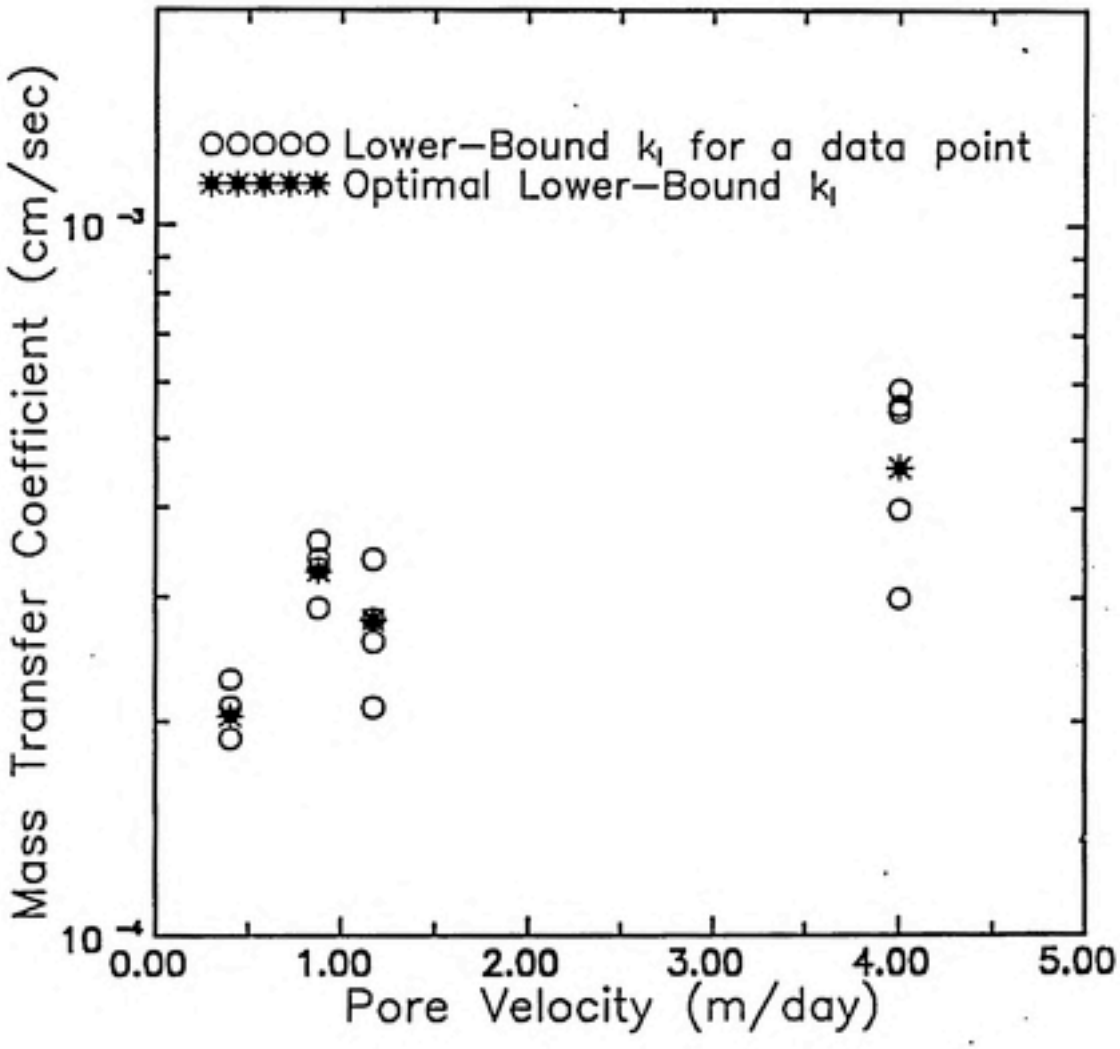

Figure 5–7. Individual and Optimal Lower-Bound k_l: Circular Column

5.3.2 SQUARE COLUMN

5.3.2.1 Mass Balances

The scatter present in the mass balance data shown in Figure 5–1 was expected. In fact, the trend observed is precisely what was expected. Almost all of the scatter at the high pore velocities results from the liquid-phase calculations. This can be explained by considering the calculation of interphase mass flow rates based on the liquid- and vapor-phase analyses

$$\dot{m}_l = \left(\frac{V_h}{V_w}\right)\left(\frac{C_{hi} - C_{he}}{\epsilon_l \dot{V}_l}\right) \quad , \quad \text{and} \quad \dot{m}_v = \frac{C_c \times V_c}{\epsilon_v t_v} \tag{5-5}$$

The vapor-phase mass flow rate is based upon only one concentration measurement, but the liquid-phase calculation is based upon the difference between two concentration measurements. The scatter in the value that results from the subtraction will include scatter from both concentration measurements. This problem becomes more pronounced at higher pore velocities because the difference between the influent and effluent concentrations is less. Thus, for a given absolute error in the analysis, the relative error increases.

This fact can be seen in Figure 5–8, a plot of the interphase mass flow rate calculated for each data point. To compare data for different concentrations at the same velocity, the mass flow rates have been normalized by dividing by the influent concentration. At the high velocities, the scatter in the liquid-phase analyses is much greater than the scatter in the vapor-phase analyses. As velocity decreases, so does the scatter in the liquid-phase analyses. At the low velocities, most of the scatter results from the vapor-phase analyses. Both curves have approximately the same mean values, however. This fact, and the previously noted tendency of the mass balances to scatter around zero, indicates that the quantity of data obtained

in this study should minimize the effects of the scatter on the final estimates of k_l if the data are analyzed with a technique that simultaneously uses all eighteen data points for each velocity. However, the results shown in Figure 5-5 indicate that care must be exercised when generating data at the high velocities to ensure the smallest possible confidence interval on the parameters values for any correlation which may be developed. In that figure, although the best-fit curves calculated with and without the data at 19.5 m/d were essentially the same, the confidence interval for the curve that included the data at the highest velocity was about twice the interval for the curve which excluded that data.

5.3.2.2 Concentration Effects

Since the data gathered at each velocity were for three influent concentrations, using all the data simultaneously from a single velocity to find an optimal k_l implies that k_l is independent of concentration. For this reason, the data were analyzed to ascertain the effect of influent concentration. Gibbs and Himmelblau (1963) used precise methods to measure the concentration dependence of the k_l of CO_2 in water under turbulent conditions. They concluded that k_l was moderately dependent upon concentration over significant concentration ranges. This dependence was of the same degree to which diffusivity was affected by concentration. In this study, the concentration only varied by one order-of-magnitude. This fact, combined with the scatter in the data, indicates that a concentration dependence for k_l may be difficult to detect in this data. Furthermore, Rathbun and Tai (1984) found volatilization to be independent of concentration for 1,2-dichloroethane over five orders of magnitude.

Reviewing the statistical parameters tabulated in Table 5-3, the data from 1.0 m/day had a p-value of zero, thus a trend was clearly detectable at that velocity. However, an overall analysis of the data indicates that there really is no clear trend.

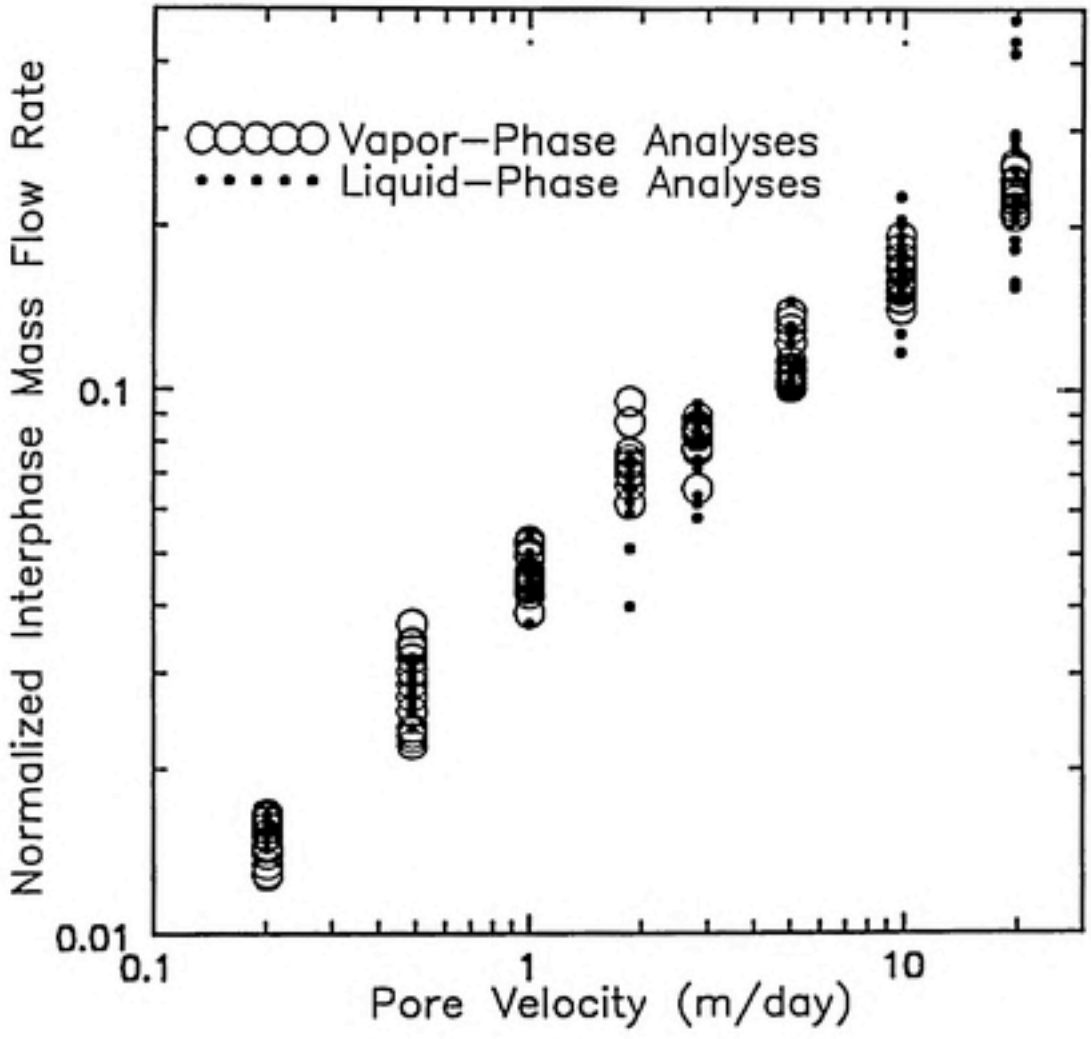

Figure 5–8. Normalized Interphase Mass Flow Rate

For two of the plots, the correlation coefficients indicate a positive trend, while the remaining six appear to have a negative trend. Furthermore, only three of the plots have a p-value of less than 5 percent. There appears to be no detectable dependence of k_l on concentration. Plots of normalized effluent concentration versus influent concentration for 1.0 m/d and 2.8 m/d appear in Figure 5–3.

5.3.2.3 Vapor-Phase Velocity

Table 5–4 displays the statistical parameters calculated for the plots of normalized effluent concentration vs vapor-phase velocity. Half the plots had positive correlation coefficients and half had negative. Also, half the plots had p-values less than five percent; but of those with low p-values, half exhibited a negative trend and half exhibited a positive trend. This indicates that the data do not exhibit a detectable dependence of k_l on the vapor-phase velocity.

The independence of the liquid-phase mass transfer coefficient from the vapor-phase velocity is a reasonable result if the vapor-phase resistance predominated under the conditions of this study. However, no data were generated that allow direct estimation of the vapor-phase resistance. An estimate of the percent resistance in the liquid phase was obtained from literature on other natural systems. Mackay and Yeun (1983) estimated a "still-air" k_g of (0.10 ± 0.05) cm/s for mass transfer of surface water agitated by the viscous drag of wind. Using this value for k_g, the percent resistance in the liquid phase varied from 95.6 (for $k_l = 1.2 \times 10^{-3}$ cm/s) to 99.2 (for $k_l = 2.0 \times 10^{-4}$ cm/s).

5.3.2.4 Upper- and Lower-Bound Estimates for k_l

Since the liquid-phase mass transfer coefficient was independent of influent concentration, all the data at a given velocity could be used to find an optimal estimate for the mass transfer coefficient, k_l, at that velocity. However, one difficulty remained: using the methods described in section 4.4.3, a reliable estimate for the transverse dispersivity, α_t, had not been obtained. Furthermore, as Figure 5–6 demonstrated, the data could not be used to determine simultaneously an optimal mass transfer coefficient and an optimal transverse dispersivity.

To obtain some estimate of the transverse dispersivity, the toluene-water data were used to calculate a lower-bound value for α_t. This was done by modeling the system assuming that mass transfer at the interface occurred at equilibrium into a vapor-phase of zero concentration. Mathematically, this required a boundary condition of zero for the liquid-phase concentration at the interface. Using all the data at each velocity, an optimal estimate of the transverse dispersivity under these assumptions was calculated. Since any resistance to mass transfer would decrease the flux normal to the boundary if α_t were held constant, the existence of mass transfer resistance would require a higher α_t than calculated by this method. Thus, the transverse dispersivity calculated under these assumptions represented a lower-bound value. This value was found to be a function of the pore velocity. Figure 5–9 is a plot of these dispersivity values. The fact that the optimal α_t calculated under these assumptions varies with pore velocity is a clear indication that the mass transfer coefficient is a function of velocity.

Using the lower-bound values for the transverse dispersivity as a starting point, an upper bound was determined for the mass transfer coefficient. Figure 5–10 illustrates the approach used to calculate the upper-bound mass transfer coefficients. The figure is a plot of optimal estimates of the mass transfer coefficient for different

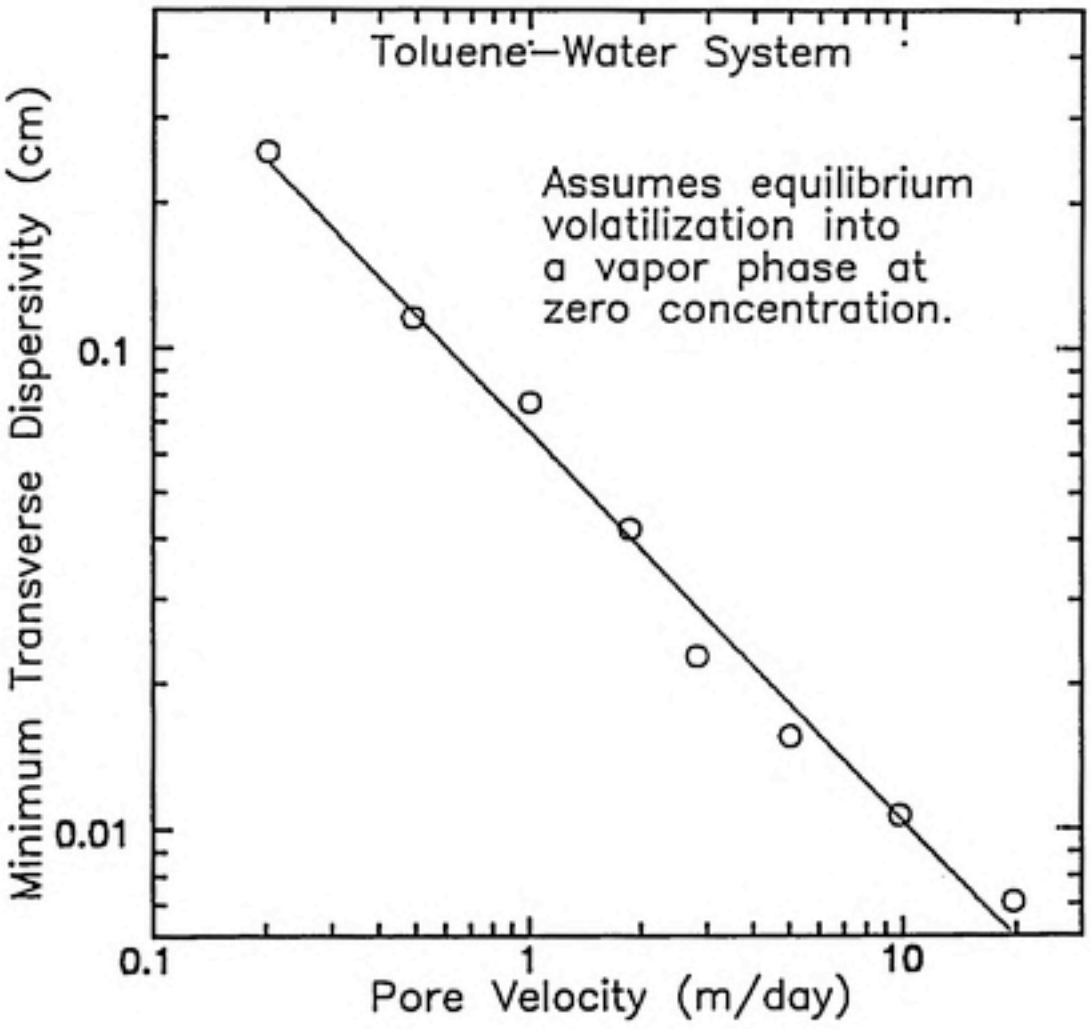

Figure 5–9. Lower-Bound Values for Transverse Dispersivity

values of transverse dispersivity. The lowest value for α_t in the figure is 0.15 cm. Referring to Figure 5–9 reveals that this value is lower than the minimum α_t determined for a pore velocity of 0.20 m/d. Thus, in Figure 5–10 the value for the optimal k_l goes toward infinity as the pore velocity approaches 0.20 m/d. When the value for α_t is increased to 0.30 cm (higher than the minimum α_t for 0.20 m/d) the optimal k_l at 0.2 m/d is finite; however, the optimal k_l increases as the pore velocity decreases from 0.50 m/d to 0.20 m/d. This result contradicts mass transfer theory and the implications of Figure 5–9, both of which indicate that k_l should decrease as the pore velocity decreases. Thus, the transverse dispersivity is increased until the optimal estimates for k_l at 0.50 and 0.20 m/d are about equal. This occurs at $\alpha_t = 0.75$ cm, and the values for k_l determined for this dispersivity represent upper-bound estimates.

The fact that the lower-bound α_t shown in Figure 5–9 increases as the velocity decreases from 0.50 to 0.20 m/d indicates that the value for k_l is decreasing between these two velocities. Thus, it is likely that the lower-bound estimates for k_l represent the true values since equal values for k_l at the two velocities would result in equal values for the lower-bound α_t's. However, one certain conclusion is that k_l is between the upper- and lower-bound values. The region defined by these bounds is fairly small for most of the flow regime. Above 2.8 m/d these values differ by less than 4 percent; only for velocities below about 1 m/d do the values differ by more than 15 percent. Table 5–5 lists the upper- and lower-bound values, and Figure 5–11 is a plot of these values and the lower-bound values for the circular column. One notable feature of this plot is the close fit of the circular and square column results. Considering the discrepancies between the circular column and the assumptions of the models used to analyze the data, it is remarkable that the circular column produced such good results. This may not be true, however, for compounds with higher mass transfer coefficients.

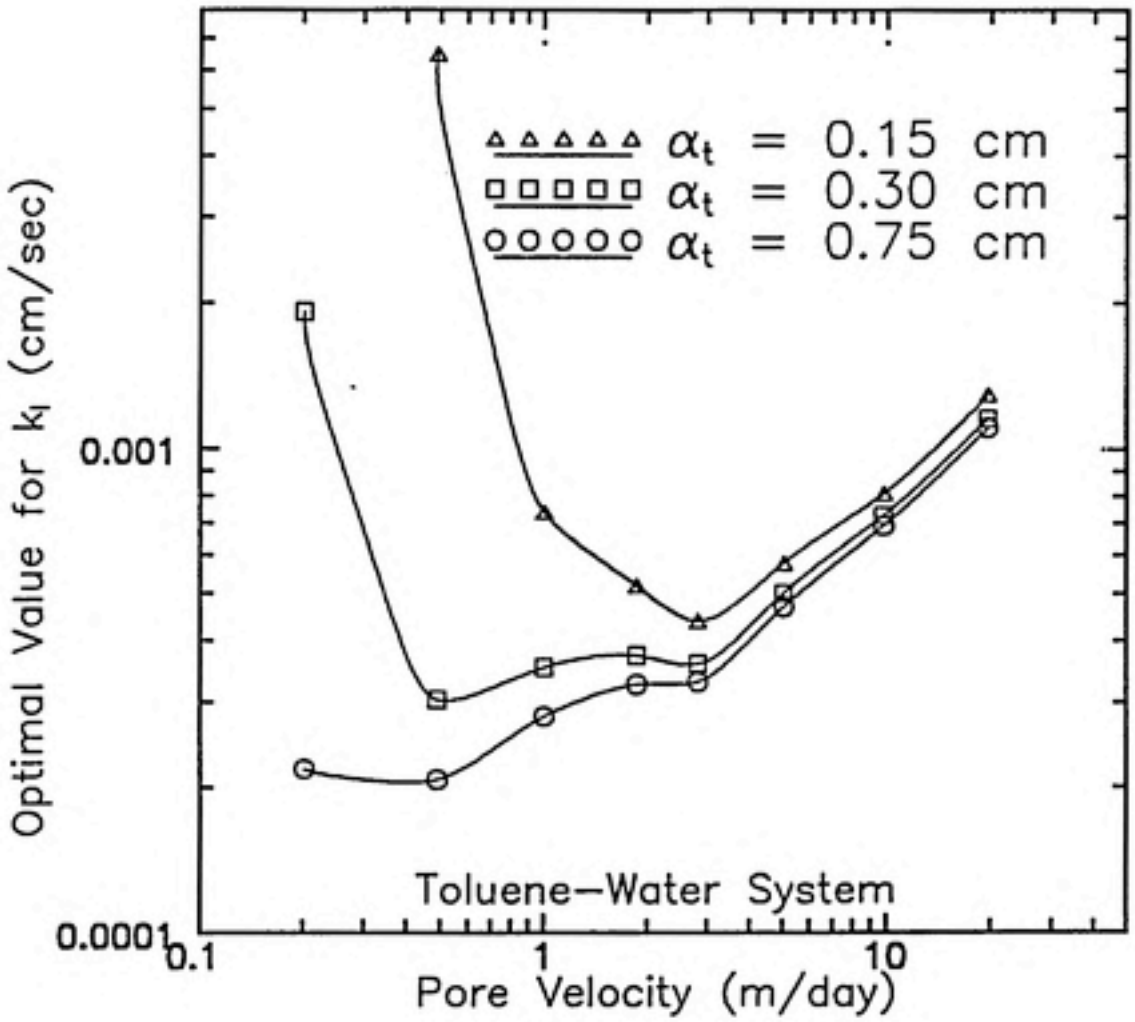

Figure 5–10. Optimal k_l as a Function of Pore Velocity and α_t

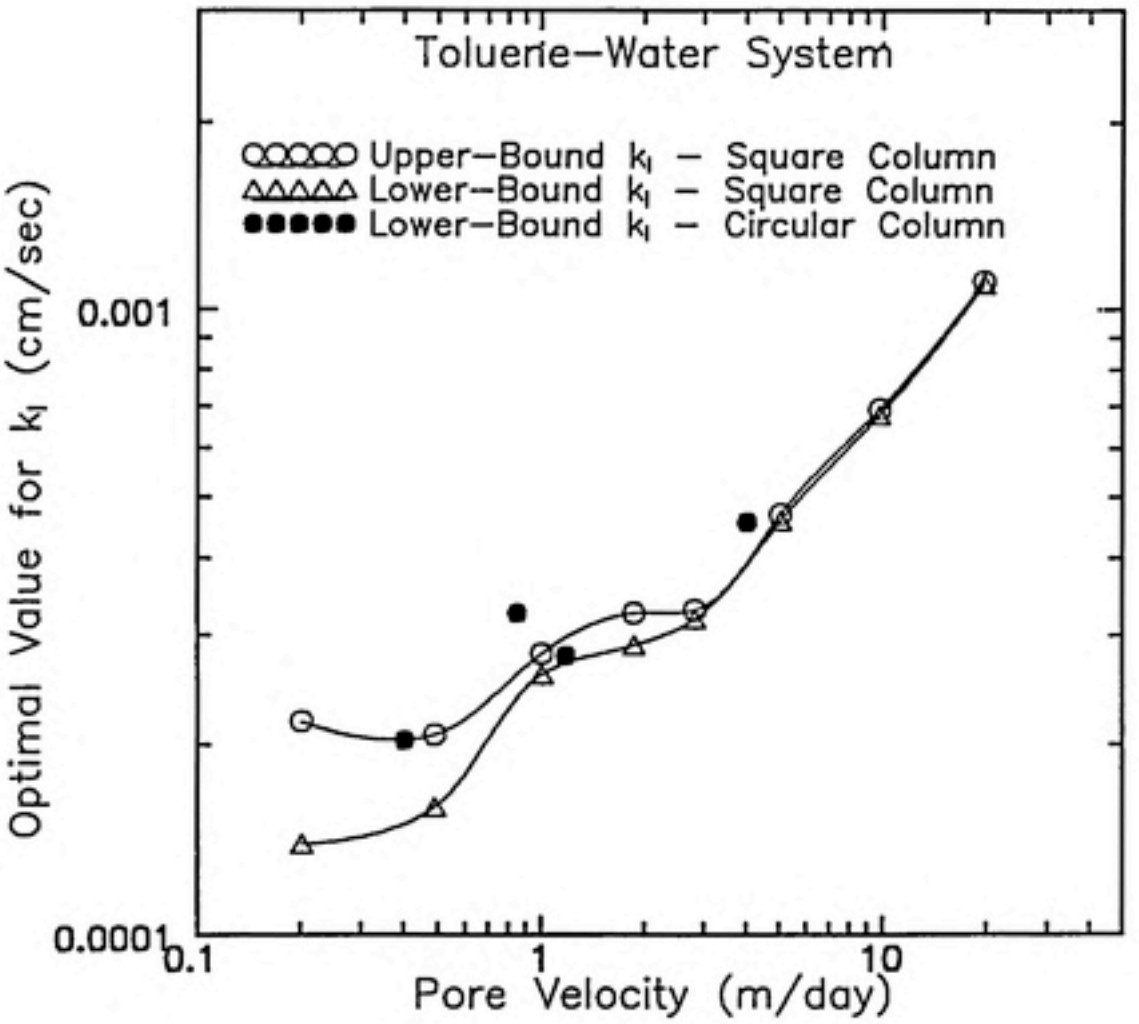

Figure 5–11. A Comparison of Results from Both Columns

Although the lower-bound values for k_l probably represent the best estimates, it is somewhat problematic that the transverse dispersivity could not be determined exogenous to the mass transfer coefficient data. One solution to this problem may be to use a compound with a high mass transfer coefficient to measure the transverse dispersivity in-situ. For a large enough k_l, the mass transfer would be dispersion limited. Under these conditions, a data set similar to the one generated here for the k_l estimates would allow for the estimation of α_t. Unfortunately, based on the literature values for the ratio $k_l^i/k_l^{O_2}$, few compounds have higher k_l's than toluene. In fact, the best candidate might be oxygen.

One aspect of the inability to determine α_t is that, for compounds for which the upper- and lower-bound estimates deviate considerably, the estimates of k_l obtained will depend upon the lowest velocity used to generate a data set. This can be illustrated by using the toluene data set to generate the plot shown in Figure 5–12. Since the ultimate goal of this research is to obtain a correlation between k_l, the compound characteristics, and system hydrodynamics, the figure is a plot of the Sherwood number versus the Reynolds number. The lowest curve is for the results obtained using the complete data set. The middle curve represents the results that would have been obtained had the same data been generated, but without the pore velocity of 0.20 m/day. Performing the analysis described above to obtain an α_t that yields about the same k_l for the two lowest velocities in the data set results in an α_t of 0.30 cm being used to generate the middle curve. The upper curve represents the results that would have been obtained had the data set only gone down to a velocity of 1.8 m/d. These curves deviate little at the high velocities, but show greater deviation at the low velocities. Furthermore, the deviation throughout the velocity range will be greater for compounds exhibiting a larger separation between the upper- and lower-bound values than toluene exhibited. This analysis indicates that either a method must be developed for determining the transverse dispersivity

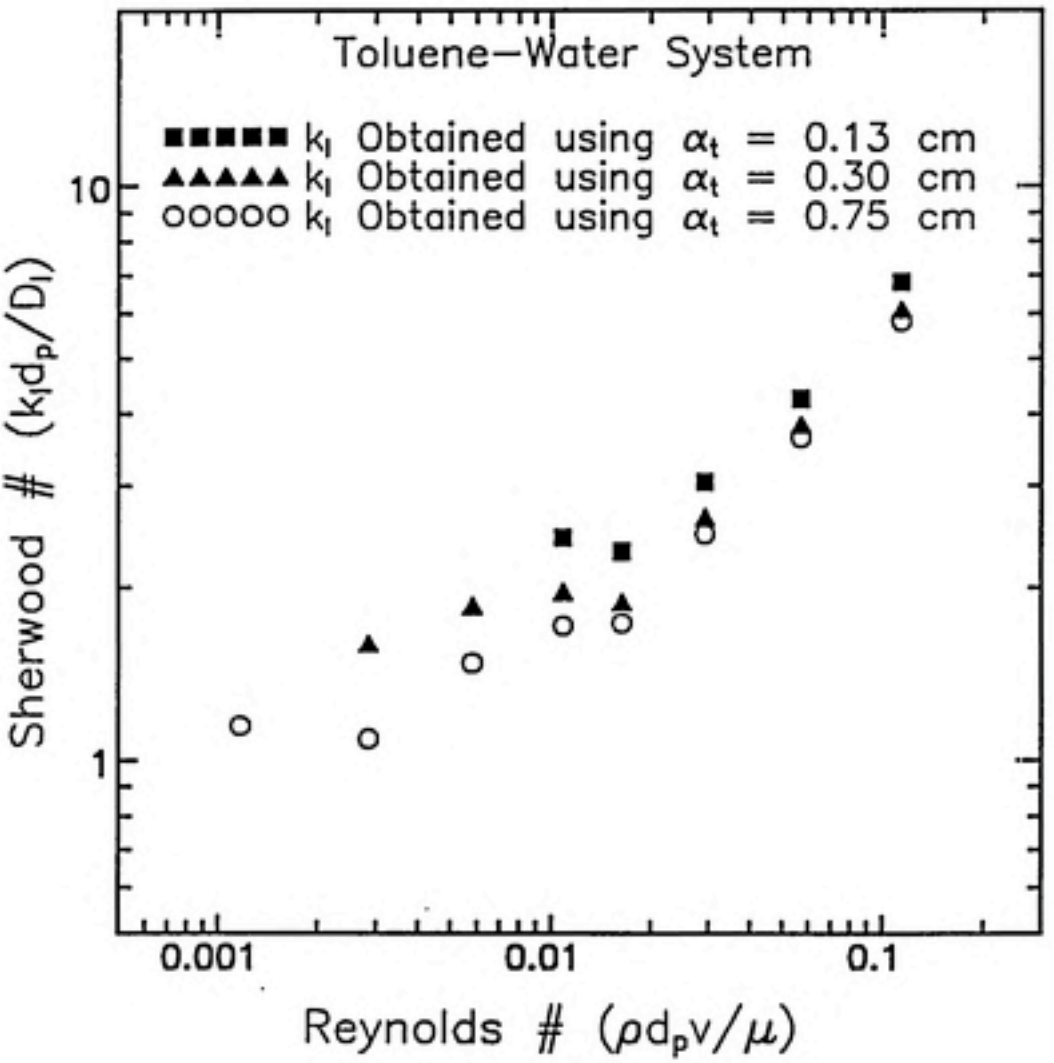

Figure 5–12. Sherwood Number vs Reynolds Number for Various α_t's

in-situ, or any data set generated must extend to the lowest velocity possible and attention must be paid to the amount of deviation that is found between the upper- and lower-bound values.

5.4 COMPARISON OF THE COMPUTER CODES

The two codes described in section 4.5 returned comparable values for the optimal k_l estimates. Table 5-6 lists the optimal k_l's for an α_t of 0.75 cm using both codes and analyses of the liquid phase. The optimal values from the two codes agreed to within 11 percent. This suggests that the assumptions in the analytical code did not introduce significant error, at least for the conditions encountered during this study. However, since it is difficult to know a priori that this will be the case, it is suggested that the analytical code only be used for 'first-cut' analysis of the data. The numerical code should return more accurate estimates than the analytical code when the longitudinal dispersion is significant and when the concentration of VOC in the vapor phase is greater than several percent of the equilibrium vapor-phase value. For this reason, it is recommended that the numerical code be used for calculating k_l for all future work and that only values for k_l obtained from the numerical code be used to determine a mass transfer correlation based on multiple VOC's.

Table 5-6 also lists the estimates obtained using the numerical code and the vapor-phase mass transfer rate data. Estimates based on the vapor phase actually used the liquid influent concentration in addition to the vapor-phase data. A liquid effluent concentration was calculated from the liquid influent concentration and the vapor phase mass transfer rate, then these two liquid concentrations were used to find optimal k_l values. A comparison of the liquid-based and the vapor-based calculations using the numerical code reveals good agreement. Below 19 m/d the k_l estimates differed by 15 percent or less. The largest difference, 30 percent, was

Table 5–6. Upper-Bound k_l from Both Computer Codes

Pore Velocity	$k_l^{(1)}$ (cm/s) Numerical		$k_l^{(1)}$ (cm/s) Analytical
(m/d)	Liquid Basis[2]	Vapor Basis[3]	Liquid Basis[2]
19.5	11.9×10^{-4}	9.05×10^{-4}	11.1×10^{-4}
9.77	7.33×10^{-4}	6.48×10^{-4}	6.94×10^{-4}
5.01	5.01×10^{-4}	4.54×10^{-4}	4.71×10^{-4}
2.81	3.53×10^{-4}	3.82×10^{-4}	3.31×10^{-4}
1.86	3.52×10^{-4}	4.06×10^{-4}	3.27×10^{-4}
1.00	3.08×10^{-4}	2.69×10^{-4}	2.81×10^{-4}
0.489	2.31×10^{-4}	2.36×10^{-4}	2.08×10^{-4}
0.201	1.96×10^{-4}		2.19×10^{-4}

(1) Optimal values of k_l determined for $\alpha_l = 0.75$ cm
(2) Based on liquid influent and effluent concentrations
(3) Based on liquid influent concentration and vapor-phase mass transfer rate measurement

obtained at 19.5 m/d, the velocity for which the variance in the liquid-phase data was greatest. To be consistent, either liquid or vapor analyses should be used for the entire data set. The variance of the liquid analyses was greater at high pore velocities, while the variance of the vapor analyses was greater at low velocities. Therefore, neither can be said to be preferable to the other for the entire range of this data set. This will probably be true for data on other VOC's; thus, the choice of which phase analyses should form the basis for the k_l calculations will be specific to a data set.

A plot of the results in Table 5–7 appears in Figure 5–13. Figure 5–14 shows best-fit power function curves based on the optimal values in Table 5–7. The best-fit power functions differ by less than 12 percent throughout the range of the data.

All mass transfer coefficients listed and plotted previously in this chapter were based on the liquid analyses and used the analytical code. The results from the analytical code were chosen simply to provide consistency in data presentation. As

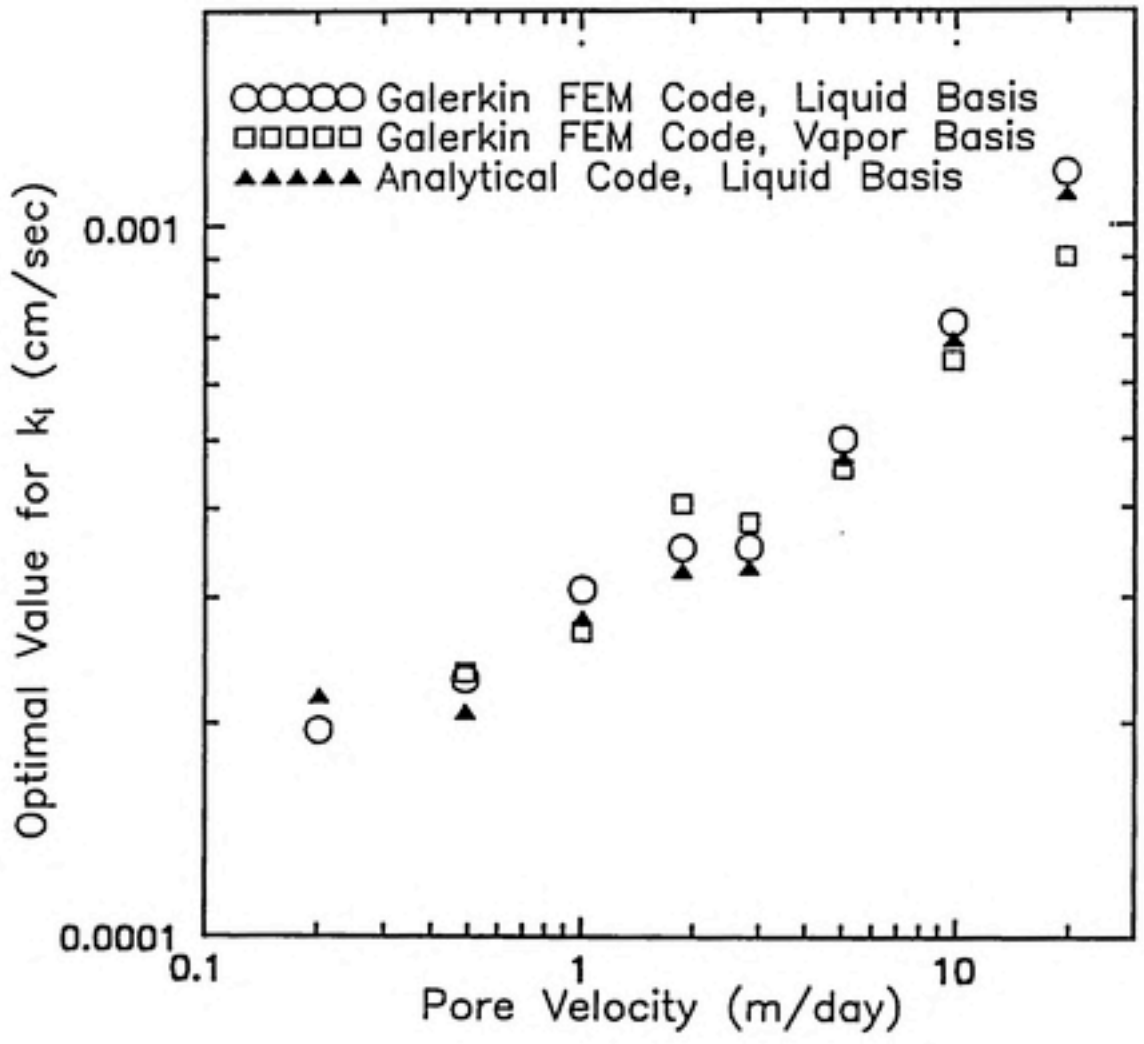

Figure 5–13. k_l from the Numerical and Analytical Codes

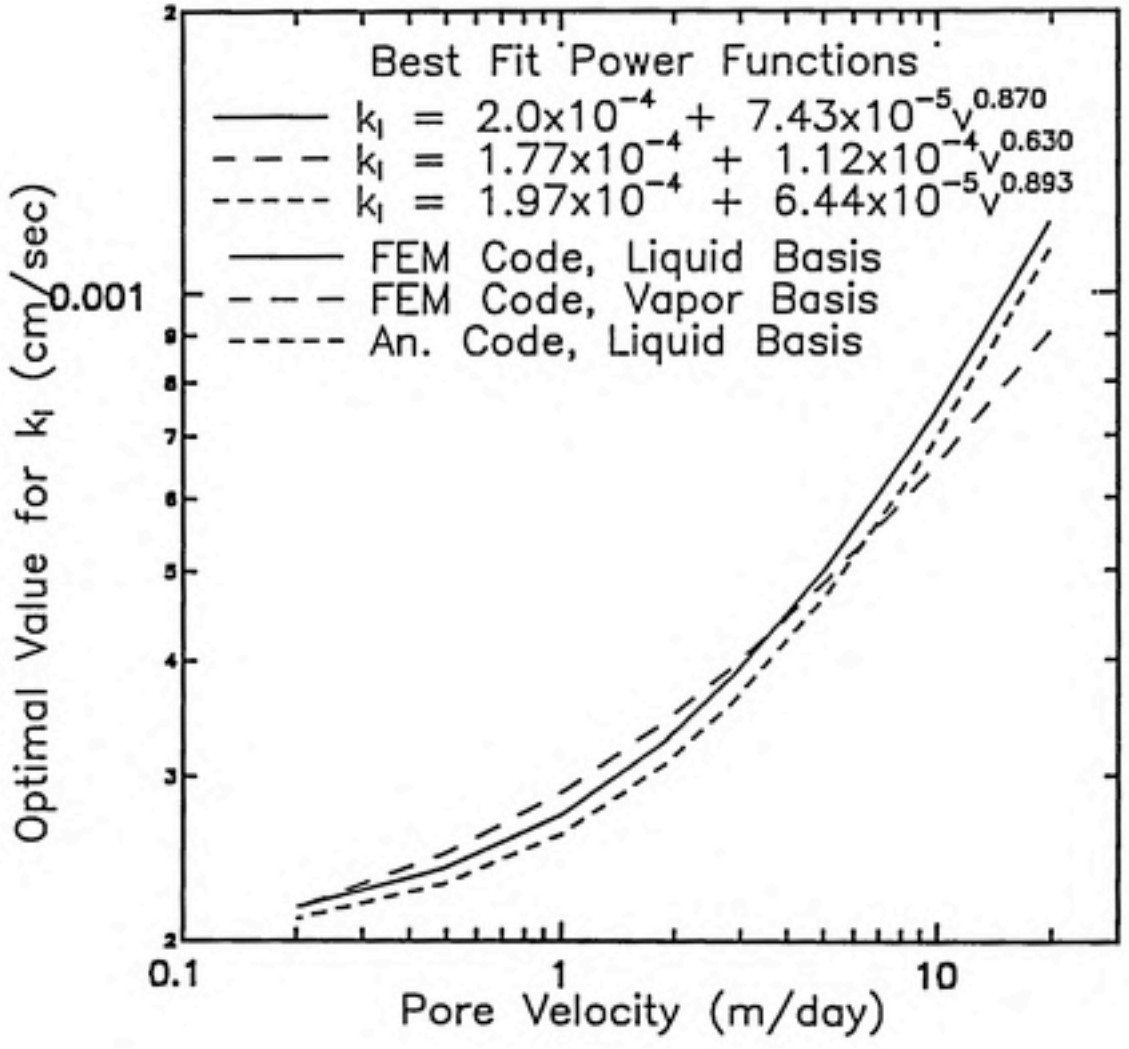

Figure 5–14. Best-fit Power Functions for k_l

noted above, the analytical code is best for initial calculations, but the numerical code should be used for subsequent work and for the ultimate goal of obtaining a mass transfer correlation for a number of VOC's.

5.5 Computer Simulation Under Ambient Conditions

A two-dimensional Galerkin finite element code was used to simulate the approach to equilibrium at the saturated-unsaturated interface for a continuous release of toluene under ambient conditions. The conditions used for the simulation are presented in Table 5–7. The continuous release at a constant concentration represents a situation that may occur if a spill of toluene reaches the phreatic surface and some immobile organic phase is entrained in the saturated zone. Under these conditions, the mass transfer of toluene from the entrained organic phase is rapid and the concentration of toluene in water at the organic-aqueous interface quickly reaches the solubility value (Poirier-McNeill, 1989). Thus, the region of entrained organic phase may act as a continuous source of constant concentration for a long time. For the simulation, the contaminated region occupied the upper 60 cm of the aquifer.

The pore velocity chosen was at the low end of the range studied in this investigation because field data suggest that the specific discharge near the water table may drop rapidly to low values (Ronen et al, 1986). In fact, the velocity used in this simulation is about 40-times higher than the velocity measured by Ronen et al. within approximately 35 cm of the phreatic surface. Because the mass transfer data do not extend to lower velocities, the choice of 0.20 m/d was as close to the results of Ronen et al. as possible. The value of the mass transfer coefficient was near the upper-bound for 0.20 m/d. Therefore, this simulation provided a conservative estimate of the time to equilibrium.

Table 5–7. Conditions and Parameter Values for Simulation

Parameter	Value	Units
Pore Velocity	0.20	m/d
Mesh Peclet #	2.0	
Mesh Courant #	1.0	
α_l	10.0	cm
α_t	1.0	cm
Porosity	0.40	
S_w°	0.50	
Concentration at $\chi = 0$	100	mg/l
H_c	0.26	
D_l	9.5×10^{-6}	cm^2/s
D_v	8.49×10^{-2}	cm^2/s
k_l	2.0×10^{-4}	cm/s
$K_l a$	1.08×10^{-2}	s^{-1}

The mass transfer rate constant for liquid-vapor interphase mass transfer within the unsaturated zone was the product of $k_l = 1.0 \times 10^{-4}$ cm/s and a specific area of 107.6 cm^{-1}. This k_l value for the immobile water was chosen for two reasons. First, extrapolating the lower-bound estimate for k_l to zero velocity yielded approximately this value. While it may not be advisable to extrapolate mass transfer coefficient expressions beyond the region for which data were obtained, results from surface water modeling provided a second justification for this value of k_l. Mackay and Yeun (1983) indicated their best estimate of the "still-air" value for k_l was $(1.0 \pm 0.5) \times 10^{-4}$ cm/s. Since wind was the primary source of liquid-phase agitation in their model, their "still-air" value corresponded to zero pore velocity in the subsurface. The specific area was calculated by the ratio of capillary pressure over surface free energy.

For a coarse porous media with porosity 0.40, degree of water saturation 0.50, and a capillary pressure of 0.40 meters of water under these conditions, the specific area at 20°C is 107.6 cm^{-1}.

Figure 5–15 shows the approach to equilibrium at three positions down-gradient from the source. Position, χ, is expressed as time of travel: the distance from the source divided by the pore velocity. The x-axis in Figure 5–15 is dimensionless time, θ, which is the time since the release began divided by the time of travel to a point. The y-axis is the ratio of the vapor-phase concentration at the interface to the the vapor-phase concentration that would be in equilibrium with the liquid phase concentration at the interface. Three features of the figure are notable: (*i*) as χ increases, the steady-state concentration ratio at the interface approaches the equilibrium value; (*ii*) the steady-state vapor-phase concentration at the interface is only about 95 percent of the equilibrium value; and (*iii*) as χ increases, the time at which steady-state is achieved decreases. Although the VOC does not actually achieve equilibrium, the time to steady-state for the VOC will be referred to as the 'time to equilibrium', θ_e.

The third item above is partly an artifact of the use of θ for the x-axis. This can be seen in Figure 5–16, which is a plot of the approach to steady state for a conservative, nonvolatile tracer under the same conditions as the simulation of the toluene release. Once again, the x-axis is θ, however the y-axis is the ratio of concentration at some time to the steady-state concentration. As in Figure 5–15, the time to steady-state, θ_{ss}, decreases with increasing χ. Since this is a conservative tracer, the steady-state concentration ratio is 1.0. The reason θ_{ss} decreases as the distance from the source, χ, increases is that the system Peclet number increases with increasing distance. The limiting value for large distances from the source is about 2.0 to 2.5.

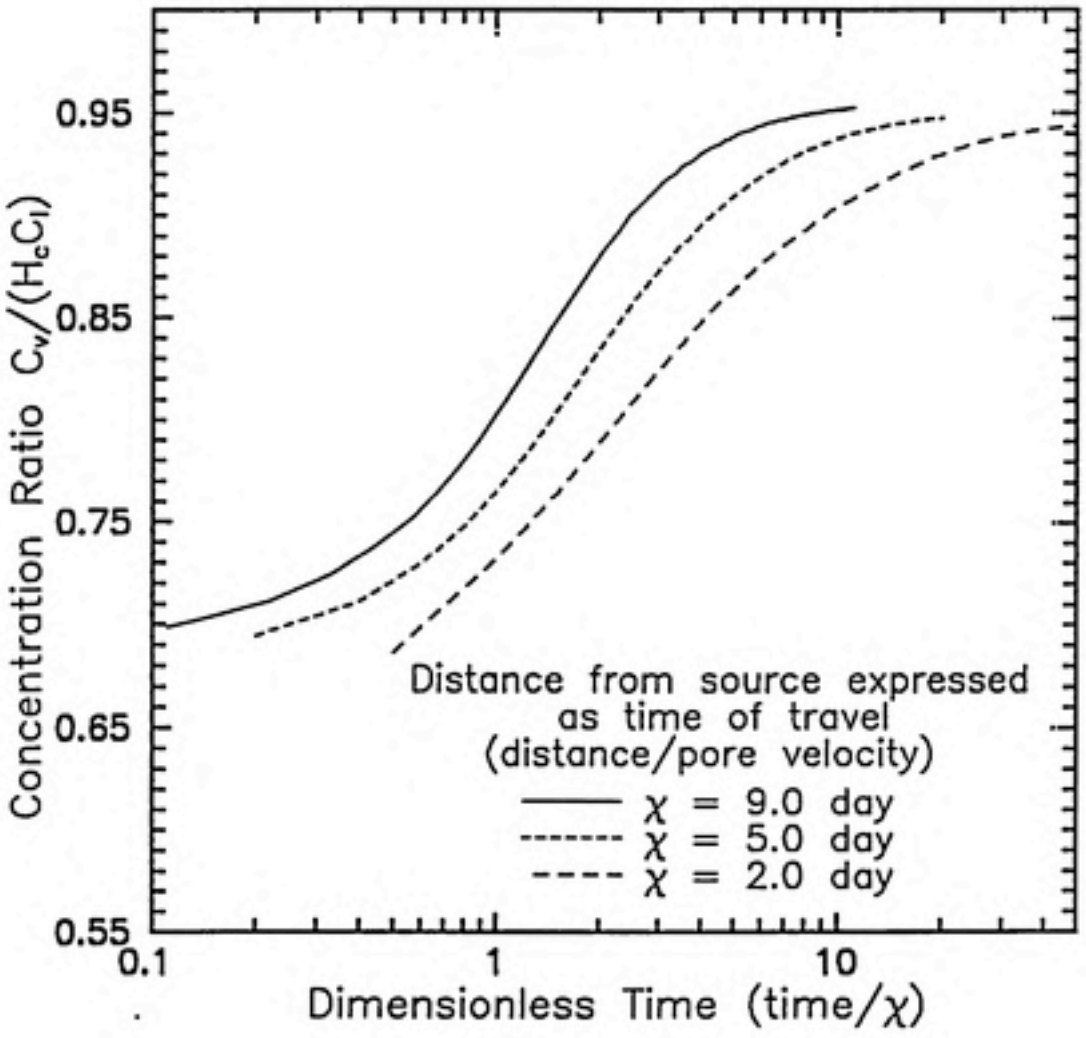

Figure 5–15. Approach to Equilibrium in the Vapor Phase at the Interface

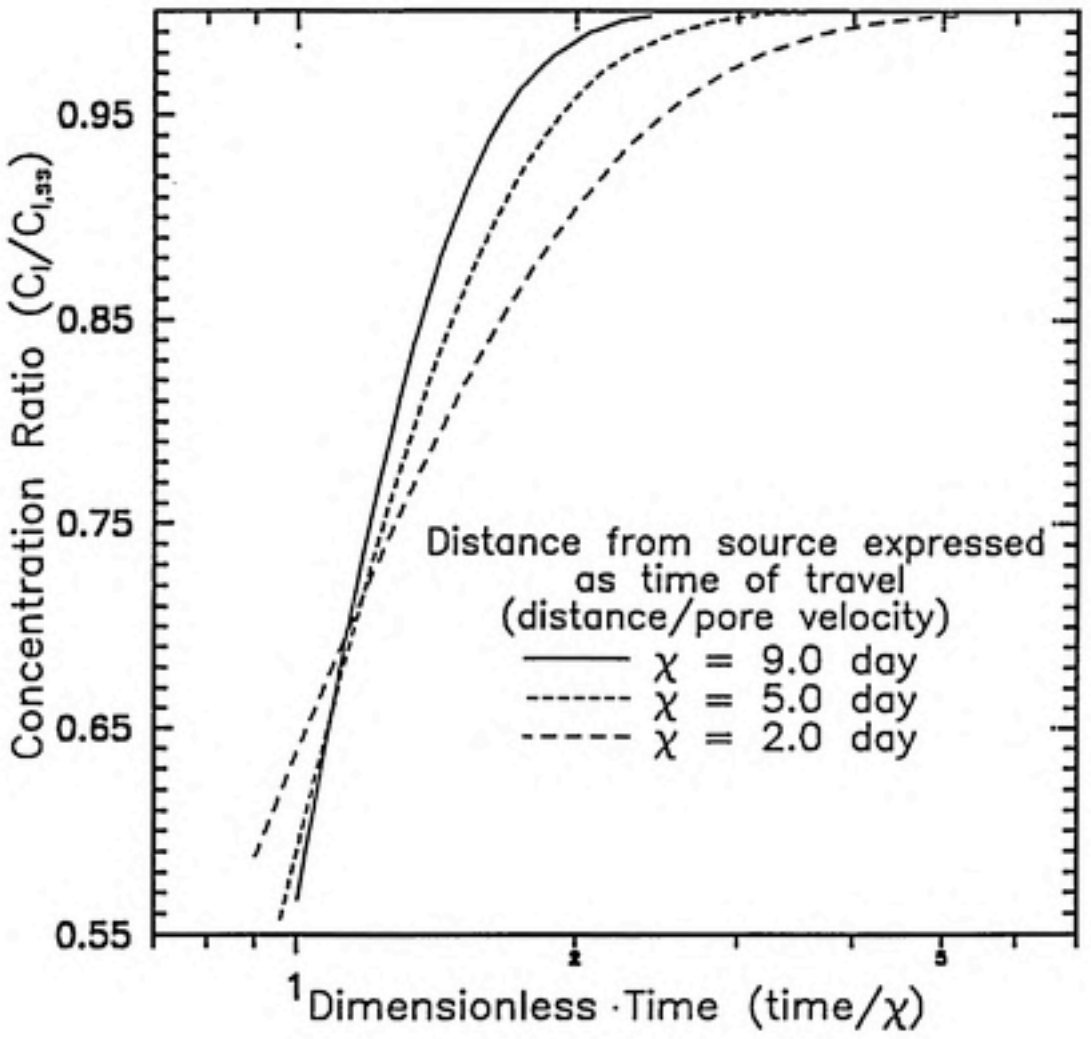

Figure 5–16. Approach to Steady-State for a Conservative Tracer

To more clearly delineate the extent to which mass transfer limitation is delaying the approach to steady-state, plots of the approach to steady-state for the conservative tracer and the approach to equilibrium for toluene at each of the three χ values were made. These appear in Figures 5–17 to 5–19. These figures can be used to determine θ_{ss} and θ_e for the three positions. These values, and the ratio θ_e/θ_{ss} are presented in Table 5–8. The ratio decreases with increasing χ but does not equal 1.0. This illustrates two points. First, the third item noted in Figure 5–15 is not entirely an artifact of the dimensionless time plot. Second, mass transfer limitation is delaying θ_e for the VOC significantly beyond the delay which arises from dispersion alone.

Table 5–8. θ_e, θ_{ss}, and the Ratio θ_e/θ_{ss} for Different χ

χ (days)	θ_e (–)	θ_{ss} (–)	θ_e/θ_{ss} (–)
2.0	23	5.0	4.6
5.0	13	3.0	4.3
9.0	6.0	2.3	2.6

A rough estimate of the time to equilibrium under other ambient conditions may now be obtained. Using the approximation that the concentration of a conservative tracer will reach steady-state at 2 to 2.5 times the time of travel, and that θ_e/θ_{ss} is about 2.5 for distances greater than 10 χ from a source, the time to equilibrium for a point down-gradient from a release is about 5 to 6.3 times the time of travel. Thus, for a point one month down-gradient from a toluene source, the interfacial vapor concentration will be about 95 percent of the equilibrium value within five to six months. From this simulation, it appears that the equilibrium

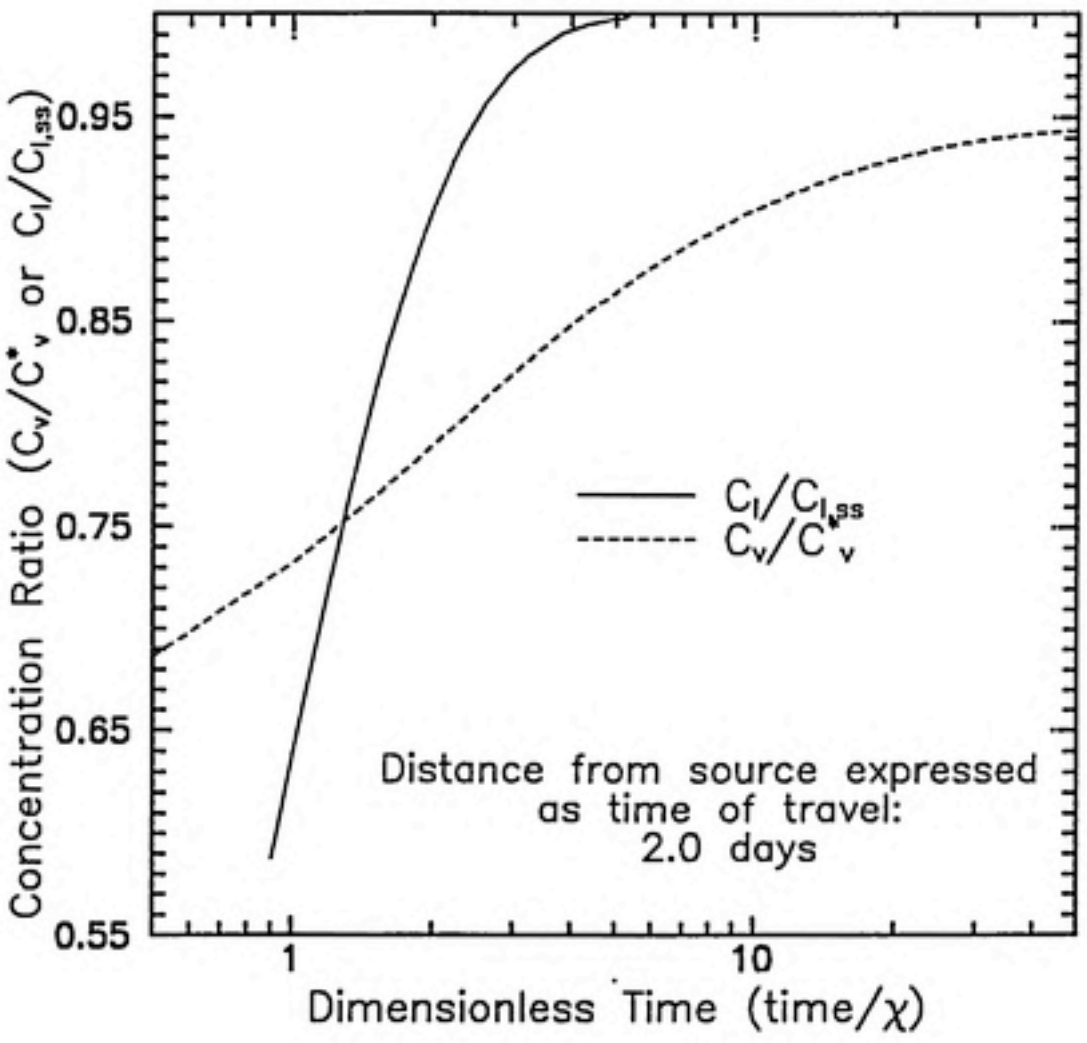

Figure 5–17. Approach to Steady-State and to Equilibrium: $\chi = 2.0$ days

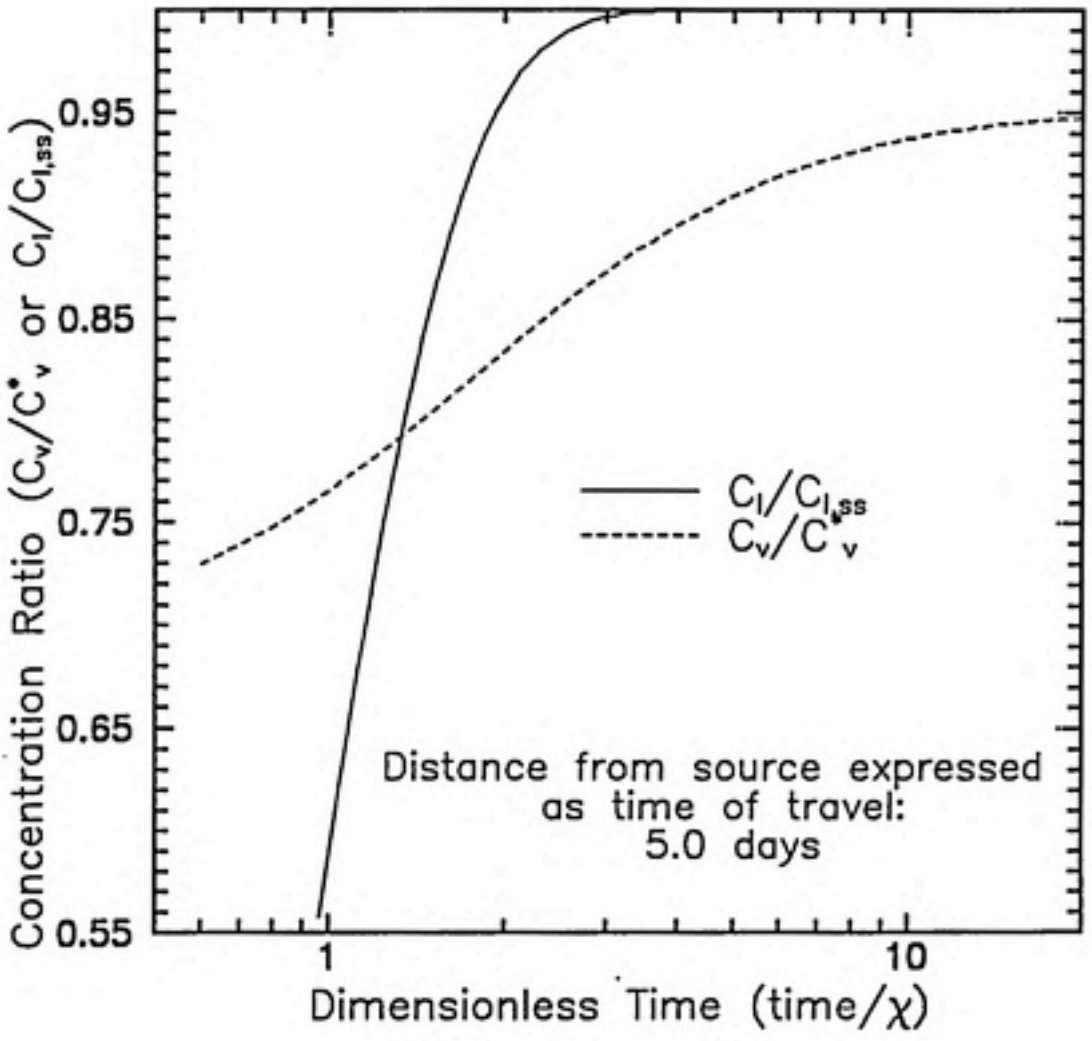

Figure 5–18. Approach to Steady-State and to Equilibrium: $\chi = 5.0$ days

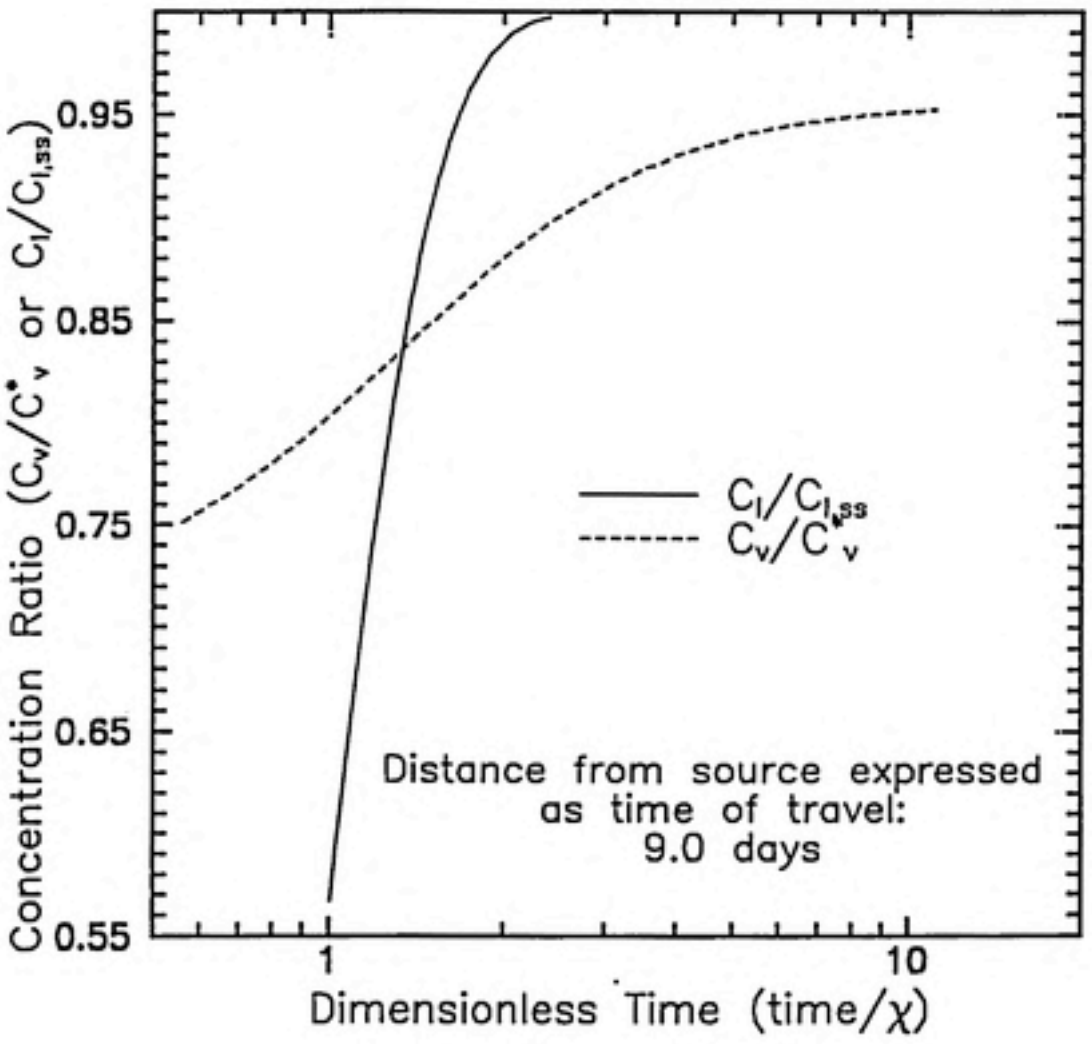

Figure 5–19. Approach to Steady-State and to Equilibrium: $\chi = 9.0$ days

assumption may not be valid for a significant portion of the area within a plume. Even under ambient conditions, only the points within 5 to 6 times-of-travel will have interfacial vapor concentrations near equilibrium.

Of course, these conclusions do not apply for conditions of enhanced volatilization. Evaluating the equilibrium assumption for situations in which the vapor phase is advected will require a significant amount of computer simulation under a variety of subsurface conditions. However, the results of this simulation indicate that interfacial concentrations will not be at equilibrium if the vapor is advected. Note that for this simulation with a stagnant vapor phase the interfacial concentrations only achieve 95 percent of equilibrium over the time simulated.

6 CONCLUSIONS AND RECOMMENDATIONS

6.1 CONCLUSIONS

The conclusions that can be made from this study are:

- A lab methodology has been developed to measure the mass transfer coefficients of VOC's under conditions approximating those in the subsurface;
- Two computer codes have been developed that can be used to analyze the data generated with the lab methodology;
- The optimal values for mass transfer coefficient determined by the two computer codes were found to agree within 11 percent;
- The liquid-phase mass transfer coefficient for toluene in water under conditions approximating those in the subsurface was measured and found to increase by one order of magnitude for a two order of magnitude increase in pore velocity;
- A simulation of toluene transport in the subsurface under ambient conditions indicates that interfacial vapor concentrations may be within 95 percent of equilibrium for points within 5 to 6 times-of travel from the source, but that significant portions of a contaminant plume may not be near equilibrium; and
- The toluene mass transfer coefficients measured are small enough that the saturated-unsaturated interface may not be near equilibrium under most conditions encountered during enhanced volatilization or pump and purge remediation.

6.2 RECOMMENDATIONS

The following recommendations for further research are made:

- The lab methodology developed in this study should be used to generate similar data on a number of VOC's and for different porous media sizes;
- The data for various VOC's and media sizes should be correlated using dimensional analysis, and the exponents on the dimensionless groups should be determined by either optimizing all the exponents to fit the data or by forcing the exponent on diffusivity to conform to a theoretical value and optimizing the remaining exponents to fit the data;
- The use of oxygen, or a compound with approximately the same mass transfer coefficient as oxygen, should be studied to develop a method for determining the transverse dispersivity in-situ; and
- The two-dimensional Galerkin finite element code developed for this study should be used to simulate subsurface conditions during enhanced volatilization and pump and purge remediation to determine conditions under which the interfacial equilibrium assumption is not valid.

7 APPENDIX A

- NOTATION
- REFERENCES

7.1 NOTATION

C_c = concentration in CS_2 extractions, (M/L^3)
C_{he} = concentration in hexane extraction of aqueous effluent, (M/L^3)
C_{hi} = concentration in hexane extraction of aqueous influent, (M/L^3)
C_l = liquid-phase concentration in saturated domain, (M/L^3)
C_{lb} = bulk liquid-phase concentration, (M/L^3)
C_l^* = liquid concentration in equilibrium with vapor phase, (M/L^3)
$C_{l,int}^*$ = interfacial liquid concentration in equil. with vapor, (M/L^3)
C_l^u = liquid-phase concentration in unsaturated domain, (M/L^3)
C_v = vapor-phase concentration in unsaturated domain, (M/L^3)
C_{vb} = bulk vapor-phase concentration, (M/L^3)
C_v^* = vapor concentration in equilibrium with liquid phase, (M/L^3)
$C_{v,int}^*$ = interfacial vapor concentration in equil. with liquid, (M/L^3)
d_p = particle diameter, (L)
D_{ai}^f = diffusivity of component a in the film in phase i, (L^2/t)
D, D_v, D_l = molecular diffusivity, (L^2/t)
$\mathbf{D}_h$ = hydrodynamic dispersion tensor, (L^2/t)
D_l = longitudinal dispersion coefficient, (L^2/t)
D_t = transverse dispersion coefficient, (L^2/t)
g = gravitational constant, (L/t^2)
H_c = Henry's constant, (dimensionless)
J_i^A = advective mass flux of contaminant in i-direction, ($M/L^2 \cdot t$)
J_i^D = total dispersive mass flux of contaminant in i-direction, ($M/L^2 \cdot t$)
J_i^T = total mass flux of contaminant in i-direction, ($M/L^2 \cdot t$)
$\mathbf{J}_{sat}^{lp}|_i nt$ = mass flux of contaminant in liquid at interface, ($M/L^2 \cdot t$)
$\mathbf{J}_{uns}^{vp}|_i nt$ = mass flux of contaminant in vapor at interface, ($M/L^2 \cdot t$)
J_l = mass flux into liquid based on k_l and bulk concentrations, ($M/L^2 \cdot t$)
J_v = mass flux into vapor based on k_v and bulk concentrations, ($M/L^2 \cdot t$)
k_l = liquid-phase mass transfer coefficient, (L/t)
k_l^i = liquid-phase mass transfer coefficient for compound i, (L/t)
$k_l^{O_2}$ = liquid-phase mass transfer coefficient for oxygen, (L/t)
k_{rf} = first-order reaction rate at fast sites on solid phase, (t^{-1})
k_{rl} = first-order reaction rate in liquid phase, (t^{-1})

k_{rs} = first-order reaction rate at slow sites on solid phase, (t^{-1})
k_s = liquid-solid mass transfer rate constant at the slow sites, (t^{-1})
k_v = vapor-phase mass transfer coefficient, (L/t)
k_v^i = vapor-phase mass transfer coefficient for compound i, (L/t)
$k_v^{H_2O}$ = vapor-phase mass transfer coefficient for water, (L/t)
K = hydraulic conductivity in one dimension, (L/t)
K = hydraulic conductivity tensor, (L/t)
K_{cf} = equilibrium constant for sorption at fast sites, (L^3/M)
K_{cs} = equilibrium constant for sorption at slow sites, (L^3/M)
K_l = overall mass transfer coefficient based on liquid phase, (L/t)
K_v = overall mass transfer coefficient based on vapor phase, (L/t)
$K_l a$ = overall mass transfer rate constant based on liquid phase, (t^{-1})
$K_v a$ = overall mass transfer rate constant based on vapor phase, (t^{-1})
l_i = film thickness for phase i, (L)
L = contact length for penetration theory, (L)
m = max number of variables that combine w/o forming a dimensionless group
$\dot{m}_l$ = mass transfer rate based on liquid analyses, (M/t)
$\dot{m}_v$ = mass transfer rate based on vapor analyses, (M/t)
M_{CO_2} = molecular weight of CO_2, (M/m)
M_{H_2O} = molecular weight of H_2O, (M/m)
M_i = molecular weight of compound i, (M/m)
N_x, N_y, N_z = mass flux of water in principal directions, ($M/L^2 \cdot t$)
n = porosity of a porous media, (dimensionless)
n_s = porosity in the saturated domain, (dimensionless)
n_u = porosity in the unsaturated domain, (dimensionless)
p = number of dimensionless groups possible w/ Buckingham-π method
p_v = vapor pressure of a pure compound, (F/L^2)
q_s = total solid-phase concentration in saturated domain, (dimensionless)
q_{fs} = solid-phase fast site concentration in saturated domain (dimensionless)
q_{ss} = solid-phase slow site concentration in saturated domain (dimensionless)
q_u = total solid-phase concentration in unsaturated domain, (dimensionless)
q_{fu} = solid-phase fast site concentration in unsaturated domain (dimensionless)
q_{su} = solid-phase slow site concentration in unsaturated domain (dimensionless)
q_i = specific discharge in the i-direction, (L/t)
R = universal gas constant, ($F \cdot L/m \cdot T$)
S = solubility of a VOC in water, (M/L^3)

S_s = specific storage coefficient, (L^{-1})

S_w^o = degree of water saturation in unsaturated media, (dimensionless)

t = time, (t)

t_v = period of time GAC sample vial was exposed to vapor effluent, (t)

Δt = increment of time, (t)

v_{ave} = average velocity in a parabolic flow field (laminar flow), (L/t)

v_{max} = maximum velocity in a parabolic flow field (laminar flow), (L/t)

v_x, v_y, v_z = pore velocity in principal directions, (L/t)

$v, v_p, \bar{v}$ = average pore velocity, (L/t)

$\vec{v}$ = pore velocity vector, (L/t)

V_c = volume of CS_2 used for GAC extractions, (L^3)

V_h = volume of hexane used for hexane-water extractions, (L^3)

$\dot{V}_l$ = volumetric water flow rate through column, (L^3/t)

V_w = volume of water used for hexane-water extractions, (L^3)

x, y, z = principal directions in rectangular coordinates, (L)

$\Delta x, \Delta y, \Delta z$ = incremental lengths in the principal directions, (L)

α_l = longitudinal dispersivity, (L)

α_t = transverse dispersivity, (L)

β = exponent on diffusivity in mass transfer coefficient correlations, (dimensionless)

Δ = incremental operator, (dimensionless)

ϵ_l = overall recovery of toluene: liquid-phase analyses, (dimensionless)

ϵ_v = overall recovery of toluene: vapor-phase analyses, (dimensionless)

η = number of variables used in Buckingham-π method

θ = dimensionless time, t/χ, (dimensionless)

θ_e = dimensionless time to equilibrium interfacial conditions, (dimensionless)

θ_{ss} = dimensionless time to steady-state for a conservative tracer, (dimensionless)

Θ = average residence time of fluid in the mass transfer region, (t)

κ_m = compressibility of soil matrix, ($L \cdot t^2/M$)

κ_w = compressibility of water, ($L \cdot t^2/M$)

μ = liquid-phase viscosity, ($M/L \cdot t$)

ρ = density, (M/L^3)

ρ_b = bulk density of soil matrix, (M/L^3)

ρ_l = liquid-phase density, (M/L^3)

τ = porous media tortuousity, $0 < \tau \leq 1.0$, (dimensionless)

ϕ = piezometric head, (L)

χ = distance from contaminant source expressed as time of travel, x/v_p, (t)

∇ = gradient operator for more than one dimension, (L^{-1})

7.2 REFERENCES

Aksoy, M. 1988. *Benzene Carcinogenicity.* CRC Press. Boca Raton, FL.

Albin, G.W., and G.C. Holdren. 1985. Removal of Organics from Water in an Aeration Basin – A Mathematical Model. Water Research, 19(3), 363–371.

Atlas, E., R. Foster, and C.S. Giam. 1982. Air-Sea Exchange of High Molecular Weight Organic Pollutants: Laboratory Studies. Env. Sci. and Tech., 16(5), 283–286.

Bear, J. 1979. *Hydraulics of Groundwater.* McGraw-Hill, New York, NY.

Bird, R.B., W.E. Stewart, and E.N. Lightfoot. 1960. The Equations of Change for Isothermal Systems. *Transport Phenomena.* 71–111. John Wiley & Sons, New York, NY.

Cameron, D.R., and A. Klute. 1977. Convective-Dispersive Solute Transport with a Combined Equilibrium and Kinetic Adsorption Model. Water Resources Research. 13, 183–88.

Cardner, D.V., and J.D. Hellums. 1967. Simultaneous Heat and Mass Transfer in Laminar Free Convection with a Moving Interface. Ind. Eng. Chem. Fund., 6(3), 376–380.

Chin, D.A. 1986. Estimation of Dispersion Coefficients in Porous Media. J. Hydraulic Eng., 112(7), 591–607.

Cohen, Y., W. Cocchio, and D. Mackay. 1978. Laboratory Study of Liquid-Phase Controlled Volatilization Rates in Presence of Wind Waves. Env. Sci. and Tech., 12(5), 553–558.

Crank, J. 1985. *The Mathematics of Diffusion.* Oxford University Press, New York, NY.

Crow, W.L., E.P. Anderson, and E.M. Minugh. 1987. Subsurface Venting of Vapors Emanating from Hydrocarbon Product on Ground Water. Groundwater Mon. Rev., Winter 1987, 51–57.

Cussler, E.L. 1984. *Diffusion: Mass Transfer in Fluid Systems.* Cambridge University Press. New York, NY.

Danckwerts, P.V. 1951. Significance of Liquid-Film Coefficients in Gas Absorption. Ind. Eng. Chem., 43(6), 1460–1467.

Deacon, E.L. 1977. Gas Transfer to and Across an Air-Water Interface. Tellus, 29(4), 363–374.

Dilling, W.L., N.B. Tefertiller, and G.J. Kallos. 1975. Evaporation Rates and Reactivities of Methylene Chloride, Chloroform, 1,1,1-Trichloroethane, Trichloroethylene, Tetrachloroethylene,and Other Chlorinated Compounds in Dilute Aqueous Solutions. Env. Sci. and Tech., 9(9), 833–838.

Dilling, W.L. 1977. Interphase Transfer Processes. II. Evaporation Rates of Chloro Methanes, Ethanes, Ethylenes, Propanes, and Propylenes from Dilute Aqueous Solutions: Comparisons with Theoretical Predictions. Env. Sci. and Tech., 11(4), 405–409.

Fair, J.R., D.E. Steinmeyer, W.R. Penney, and J.A. Brink. 1973. Gas-Liquid Contacting: Packed Columns. *Chemical Engineers' Handbook. 5th ed.* ed R.H. Perry and C.H. Chilton. McGraw-Hill, New York, NY.

Fuller, E.N., P.D. Schettler, and J.C. Giddings. 1966. A New Method for Prediction of Binary Gas-Phase Diffusion Coefficients. Ind. Eng. Chem., 58(5), 19–27.

Gibbs, R.K., and D.M. Himmelblau. 1963. Effect of Concentration on the Gas-Liquid Mass Transfer Coefficient. Ind. Eng. Chem. Fund., 2(1), 55–61.

Glotfelty, D.E., and C.J. Schomburg. 1989. Volatilization of Pesticides From Soil. *Reactions and Movement of Organic Chemicals in Soils.* Soil Science Society of America Special Publication Number 22. ed B.L. Sawhney and K. Brown. American Society of Agronomy, Inc., Madison, WI, pp 181–207.

Gowda, T.P.H., and J.D. Lock. 1985. Volatilization Rates of Organic Chemicals of Public Health Concern. J. Env. Eng., 111(6), 755–776.

Hayduk, W., and H. Laudie. 1974. Prediction of Diffusion Coefficients for Nonelectrolytes in Dilute Aqueous Solutions. AIChE J., 20(3), 611–615.

Holmén, K., and P. Liss. 1984. Models for Air-Water Gas Transfer: An Experimental Investigation. Tellus, 36B(2), 92–100.

Hutzler, N.J., J.S. Gierke, and L.C. Krause. 1989. Movement of Volatile Organic Chemicals in Soil. *Reactions and Movement of Organic Chemicals in Soils.* Soil Science Society of America Special Publication Number 22. ed B.L. Sawhney and K. Brown. American Society of Agronomy, Inc., Madison, WI, pp 373–403.

Huyakorn, P.S., and G.F. Pinder. 1983. *Computational Methods in Subsurface Flow.* Academic Press, Inc.

Kaczmar, S.W., F.M. D'Itri, and M.J. Zabik. 1984. Volatilization of Selected Haloforms from Aqueous Environments. Env. Tox. Chem., 3, 31–35.

Kahaner, D., C. Moler, and S. Nash. 1988. *Numerical Methods and Software.* Prentice Hall.

King, C.J. 1964. The Additivity of Individual Phase Resistances in Mass Transfer Operations. AIChE J., 10(5), 671–677.

Kozinski, A.A., and C.J. King. 1966. The Influence of Diffusivity on Liquid Phase Mass Transfer to the Free Interface in a Stirred Vessel. AIChE J., 12(1), 109–116.

Lamont, J.C., and D.S. Scott. 1970. An Eddy Cell Model of Mass Transfer into the Surface of a Turbulent Liquid. AIChE J., 16(4), 513–519.

Leighton, D.T., Jr., and J.M. Calo. 1981. Distribution Coefficients of Chlorinated Hydrocarbons in Dilute Air-Water Systems for Groundwater Contamination Applications. J. Chem. Eng. Data, 26(4), 382–385.

Levich, V.G. 1962. *Physicochemical Hydrodynamics.* Prentice-Hall, Inc., Englewood Cliffs, NJ.

Lewis, W.K., and W.E. Whitman. 1924. Principles of Gas Absorption. Ind. Eng. Chem., 16, 1215–1220.

Liss, P.S., and P.G. Slater. 1974. Flux of Gases Across the Air-Sea Interface. Nature, 247, Jan 25, 1974, 181–184.

Lugg, G.A. 1968. Diffusion Coefficients of Some Organic and Other Vapors in Air. Anal. Chem., 40(7), 1072–1077.

Lyman, W.J., W.F. Reehl, and D.H. Rosenblatt. 1982. *Handbook of Chemical Property Estimation Methods: Environmental Behavior of Organic Compounds.* McGraw-Hill Book Company, New York, NY.

Mackay, D., and A.W. Wolkoff. 1973. Rate of Evaporation of Low-Solubility Contaminants from Water Bodies to Atmosphere. Env. Sci. and Tech., 7(7), 611–614.

Mackay, D., and P.J. Leinonen. 1975. Rate of Evaporation of Low-Solubility Contaminants from Water Bodies to Atmosphere. Env. Sci. and Tech., 9(13), 1178–1180.

Mackay, D., and A.T.K. Yeun. 1983. Mass Transfer Coefficient Correlations for Volatilization of Organic Solutes from Water. Env. Sci. and Tech., 17(4), 211–217.

Maddox, R.N. 1973. Gas Absorption. *Chemical Engineers' Handbook. 5th ed.* ed R.H. Perry and C.H. Chilton. McGraw-Hill, New York, NY.

Marchello, J.M., and H.L. Toor. 1963. A mixing Model for Transfer Near a Boundary. Ind. Eng. Chem. Fund., 2(1), 8–12.

Marsily, G. de. 1986. *Quantitative Hydrogeology: Groundwater Hydrology for Engineers.* Academic Press, New York, NY.

Matter-Muller, C., W. Gujer, and W. Giger. 1981. Transfer of Volatile Substances from Water to the Atmosphere. Water Research, 15(11), 1271–1279. McCabe, W.L.,

and J.C. Smith. 1976. *Unit Operations of Chemical Engineering, 3rd ed.*. McGraw-Hill Book Company, New York, NY.

Munz, C., and P.V. Roberts. 1989. Gas- and Liquid-Phase Mass Transfer Resistances of Organic Compounds During Mechanical Surface Aeration. Water Research, 23(5), 589–601.

NIOSH. 1984. *NIOSH Manual of Analytical Methods, 3rd ed.* Method Number 1501. National Institute for Occupational Safety and Health. Cincinnati, OH, Feb. 1984.

O'Connor, D.J. 1983. Wind Effects on Gas-Liquid Transfer Coefficients. J. Env. Eng., 109(3), 731–752.

Perlmutter, D.D. 1961. Surface-Renewal models in Mass Transfer. Chem. Eng. Sci., 16, (3&4), 287–296.

Pfeffer, R. 1964. Heat and Mass Transport in Multiparticle Systems. Ind. Eng Chem. Fund., 3(4), 380–383.

Poirier-McNeill, M.M. 1989. *Mass Transfer From Non-Aqueous Phase Liquids to the Aqueous Phase in Groundwater Systems*. M.S.E.E. Thesis, University of North Carolina at Chapel Hill, Chapel Hill, NC.

Rathbun, R.E., D.J. Shultz, and D.W. Stephens. 1975. *Preliminary Experiments with a Modified Tracer Technique for Measuring Stream Reaeration Coefficients.* USGS Open-File Report 75–256. United States Government Printing Office, Washington, D.C., 1975.

Rathbun, R.E., and R.S. Grant. 1978. *Comparison of the Radioactive and Modified Techniques for Measurement of Stream Reaeration Coefficients.* USGS Open-File Report 78–68. United States Government Printing Office, Washington, D.C., 1978.

Rathbun, R.E., and D.Y. Tai. 1981. Technique for Determining the Volatilization Coefficients of Priority Pollutants in Streams. Water Research, 15, 243–250.

Rathbun, R.E., and D.Y. Tai. 1982. Volatilization of Organic Compounds from Streams. J. Env. Eng. Div., ASCE, 108(EE5), 973–989.

Rathbun, R.E., and D.Y. Tai. 1983. Gas-Film Coefficients for Streams. J. Env. Eng., 109(5), 1111–1127.

Rathbun, R.E., and D.Y. Tai. 1984. Volatilization of Chlorinated Hydrocarbons from Water. *Gas Transfer at Water Surfaces.* ed. W. Brutsaert, and G.H. Jirka. D. Reidel Publishing Co., Boston, MA.

Rathbun, R.E., and D.Y. Tai. 1986. *Gas-Film Coefficients for the Volatilization of Ketones from Water.* USGS Water-Supply Paper 2286. United States Government Printing Office, Washington, D.C., 1986.

Rathbun, R.E., and D.Y. Tai. 1988. *Application of the Two-Film Model to the Volatilization of Acetone and t-Butyl Alcohol from Water as a Function of Temperature.* USGS Water-Supply Paper 2318. United States Government Printing Office, Washington, D.C., 1988.

Rathbun, R.E., and D.Y. Tai. 1988. *Volatilization of Benzene and Eight Alkyl-Substituted Compounds from Water.* USGS Water-Supply Paper 2342. United States Government Printing Office, Washington, D.C., 1988.

Roberts, P.V., and P.G. Dändliker. 1983. Mass Transfer of Volatile Organic Contaminants from Aqueous Solution to the Atmosphere during Surface Aeration. Env. Sci. and Tech., 17(8), 484–489.

Roberts, P.V., C. Munz, and P. Dändliker. 1984. Modeling Volatile Organic Solute Removal by Surface and Bubble Aeration. J. WPCF, 56(2), 157–163.

Ronen, D., M. Magaritz, N. Paldor, and Y. Bachmat. 1986. The Behavior of Groundwater in the Vicinity of the Water Table Evidenced by Specific Discharge Profiles. Water Resources Research, 22(8), 1217–1224.

Sideman, S. 1966. The Equivalence of the Penetration and Potential Flow Theories. Ind. Eng. Chem., 58(2), 54–58.

Silberberg, I.H. 1973. Dimensional Analysis. *Chemical Engineers' Handbook. 5th ed.* ed R.H. Perry and C.H. Chilton. 2-81–2-85. McGraw-Hill, New York, NY.

Sleep, B.E., and J.F. Sykes. 1989. Modeling the Transport of Volatile Organics in Variably Saturated Media. Water Resources Research, 25(1), 81– 92.

Smith, J.H., D.C. Bomberger, Jr., and D. Haynes. 1980. Prediction of the Volatilization Rates of High-Volatility Chemicals from Natural Water Bodies. Env. Sci. and Tech., 14(11), 1332–1337

Smith, J.H., D.C. Bomberger, Jr., and D. Haynes. 1981. Volatilization Rates of Intermediate and Low Volatility Chemicals from Water. Chemosphere, 10(3), 281–289.

Tsivoglou, E.C. 1967. *Tracer Measurement of Stream Reaeration.* Federal Water Pollution Control Admin., Div. of Tech. Services, US Dept. of Interior, Washington, D.C.

Weber, W.J., Jr., and C.T Miller. 1988. Modeling the Sorption of Hydrophobic Contaminants by Aquifer Materials—I: Rates and Equilibria. Water Resources Research. 22(4), 457–464.

White, L.D., D.G. Taylor, P.A. Mauer, and R.E. Kupel. 1970. A Convenient Optimized Method for the Analysis of Selected Solvent Vapors in the Industrial Atmosphere. Am. Ind. Hygiene Ass. J., 31, March-April, 225–232.

Wilke, C.R., and P. Chang. 1955. Correlation of Diffusion Coefficients in Dilute Solution. AIChE J., 1, 264–270.

Wilke, C.R., and C.Y. Lee. 1955. Estimation of Diffusion Coefficients for Gases and Vapors. Ind. Eng. Chem., 47(6), 1253–1257.

Wolff, C.J.M., and H.B. van der Heijde. 1982. A model to Asses the Rate of Evaporation of Chemical Compounds from Surface Waters. Chemosphere, 11(2), 103–117.

8 APPENDIX B

- **ANALYTICAL SOLUTION**
- **NUMERICAL SOLUTION**

8.1 ANALYTICAL SOLUTION

The analytical solution was for diffusion in one dimension in a finite domain with mass transfer limitation at one boundary and no flow at the other boundary.

GOVERNING EQUATION: the diffusion equation in one dimension.

$$\frac{\partial C}{\partial t} = D\frac{\partial^2 C}{\partial x^2} \tag{8-1}$$

where C is concentration, D is diffusivity, x is position, and t is time.

BOUNDARY CONDITIONS:

$$\frac{\partial C}{\partial x} = 0 \quad , \qquad \text{for} \quad x = 0 \tag{8-2}$$

$$-D\frac{\partial C}{\partial x} = K_l(C_e - C_i) \quad , \qquad \text{for} \quad x = l \tag{8-3}$$

where K_l is the overall mass transfer coefficient, C_e is the concentration that would exist in the medium at the interface if it were in equilibrium with the exterior phase, C_i is the concentration in the medium at the interface, and l is the location of the interface.

INITIAL CONDITION:

$$C = C_0 \quad , \qquad \text{for} \quad 0 \le x \le l \tag{8-4}$$

SOLUTION: (from Crank, 1975)

$$\frac{C - C_e}{C_0 - C_e} = 1 - \sum_{n=1}^{\infty} \frac{2L\cos(\beta_n x/l)\exp(-\beta_n^2 Dt/l^2)}{(\beta_n^2 + L^2 + L)\cos\beta_n} \tag{8-5}$$

$$\beta \tan\beta = L \tag{8-6}$$

$$L = \frac{lK_1}{D} \tag{8-7}$$

8.2 NUMERICAL SOLUTION

The saturated domain had two degrees of freedom, and the unsaturated domain had three degrees of freedom. To minimize computational burden, the governing equations were modified to reduce the degrees of freedom to one for each domain. This was done by resolving the temporal derivatives by a finite difference approximation prior to applying the Galerkin finite element approximation for the spatial derivatives.

8.2.1 SATURATED DOMAIN

The liquid-phase governing equation was

$$R_f \frac{\partial C_l}{\partial t} = -\vec{v} \cdot \nabla C_l + \nabla \cdot (\mathbf{D}_h \nabla C_l) - k_{rl} C_l - \frac{\rho_b}{n} k_{rs} K_{cf} C_l - k_s \frac{\rho_b}{n} (K_{cs} C_l - q_{ss}) \tag{8-8}$$

Sorption on the solid phase was modeled as a two-site mechanism. The total solid-phase concentration was

$$q_s = q_{ss} + q_{fs} \tag{8-9}$$

where the concentration at the fast sites was calculated, once the liquid-phase concentration was known, by

$$q_{fs} = K_{cf} C_l \tag{8-10}$$

The solid phase concentration at the slow sites could have been determined by solving

$$\frac{dq_{ss}}{dt} = k_s(K_{cs}C_l - q_{ss}) - k_{rs}q_{ss} \qquad (8\text{–}11)$$

simultaneously with the liquid-phase equation, equation (8–8) . Instead, the problem was reduced to one degree of freedom. To do this, a finite difference approximation was applied to the temporal derivative of equation (8–11)

$$\frac{q_{ss}^{l+1} - q_{ss}^{l}}{\Delta t} = k_s K_{cs} C_l^{l+1} - (k_s + k_{rs}) q_{ss}^{l+1} \qquad (8\text{–}12)$$

where the superscripts l and $l+1$ denote the previous and present time steps. Solving equation (8–12) for the present time step yielded

$$q_{ss}^{l+1} = \frac{q_{ss}^{l}}{1 + \Delta t(k_s + k_{rs})} + \left(\frac{\Delta t k_s K_{cs}}{1 + \Delta t(k_s + k_{rs})}\right) C_l^{l+1} \qquad (8\text{–}13)$$

The temporal derivative in the liquid phase equation ((8–8)) was approximated by finite difference, then equation (8–13) was substituted for the q_{ss}^{l+1} term. This yielded an expression for the liquid that depended on the previous and present liquid-phase concentrations and on the previous solid-phase concentration.

8.2.2 UNSATURATED DOMAIN

As in the saturated domain, the total solid phase concentration was the sum of the fast and slow site concentrations

$$q_u = q_{fu} + q_{su} \qquad (8\text{–}14)$$

The governing equation for the slow sites was

$$\frac{dq_{su}}{dt} = k_s(K_{cs}C_{lu} - q_{su}) - k_{rs}q_{su} \qquad (8\text{–}15)$$

The temporal derivative was expressed as a finite difference by

$$\frac{q_{su}^{l+1} - q_{su}^{l}}{\Delta t} = k_s K_{cs} C_{lu}^{l+1} - (k_s + k_{rs}) q_{su}^{l+1} \tag{8–16}$$

and the expression was solved for q_{su}^{l+1}. The liquid-phase equation in the unsaturated zone was

$$\begin{aligned} R_f \frac{\partial C_{lu}}{\partial t} = & - k_{rl} C_{lu} + \left(\frac{1 - S_w^\circ}{S_w^\circ} \right) K_l a (C_v - H_c C_{lu}) \\ & - \left(\frac{\rho_b}{n S_w^\circ} \right) k_s (K_{cs} C_{lu} - q_{su}) - \frac{\rho_b}{n S_w^\circ} k_{rf} K_{cf} C_{lu} \end{aligned} \tag{8–17}$$

Once again, the temporal derivative of equation (8–17) was resolved by finite difference and the equation for q_{su}^{l+1} was substituted into the finite difference expression. Then, the liquid-phase equation was solved for the present time step, C_{lu}^{l+1}. Finally, the governing equation for the vapor phase

$$\frac{\partial C_v}{\partial t} = -\vec{v_v} \cdot \nabla C_v + \nabla \cdot (\mathbf{D}_h^u \nabla C_v) - K_l a (C_v - H_c C_{lu}) \tag{8–18}$$

was treated similarly, and the result was an expression for the vapor-phase concentration as a function of the present and previous vapor concentrations and the previous solid and liquid concentrations.

8.2.3 VALIDATION OF THE CODE

The numerical code was validated for advection and dispersion in the saturated liquid and unsaturated vapor phases, and for fast and slow sorption on the solid phase in both domains. In addition, the liquid-vapor interphase mass transfer within the saturated domain was validated. None of the validation results for these processes are presented here.

The code was also validated for interactions at the saturated-unsaturated interface using the analytical solution presented in the previous section. This was done by imposing a constant, uniform boundary condition at the interface. Two figures for the validation of this interphase mass transfer are presented. For both figures the initial concentration throughout the phase was 1.0 and the mass transfer coefficient was 1.0×10^{-3} cm/s. Figure 8–1 is a validation for mass transfer from the vapor phase into a liquid phase with an equilibrium concentration of 0.50 and a vapor-phase transverse dispersion coefficient of 2.5×10^{-4} cm^2/s. Figure 8–2 is a validation for mass transfer from the liquid into the vapor with a vapor concentration of 0.0 and a liquid-phase transverse dispersion coefficient of 2.5×10^{-5} cm^2/s.

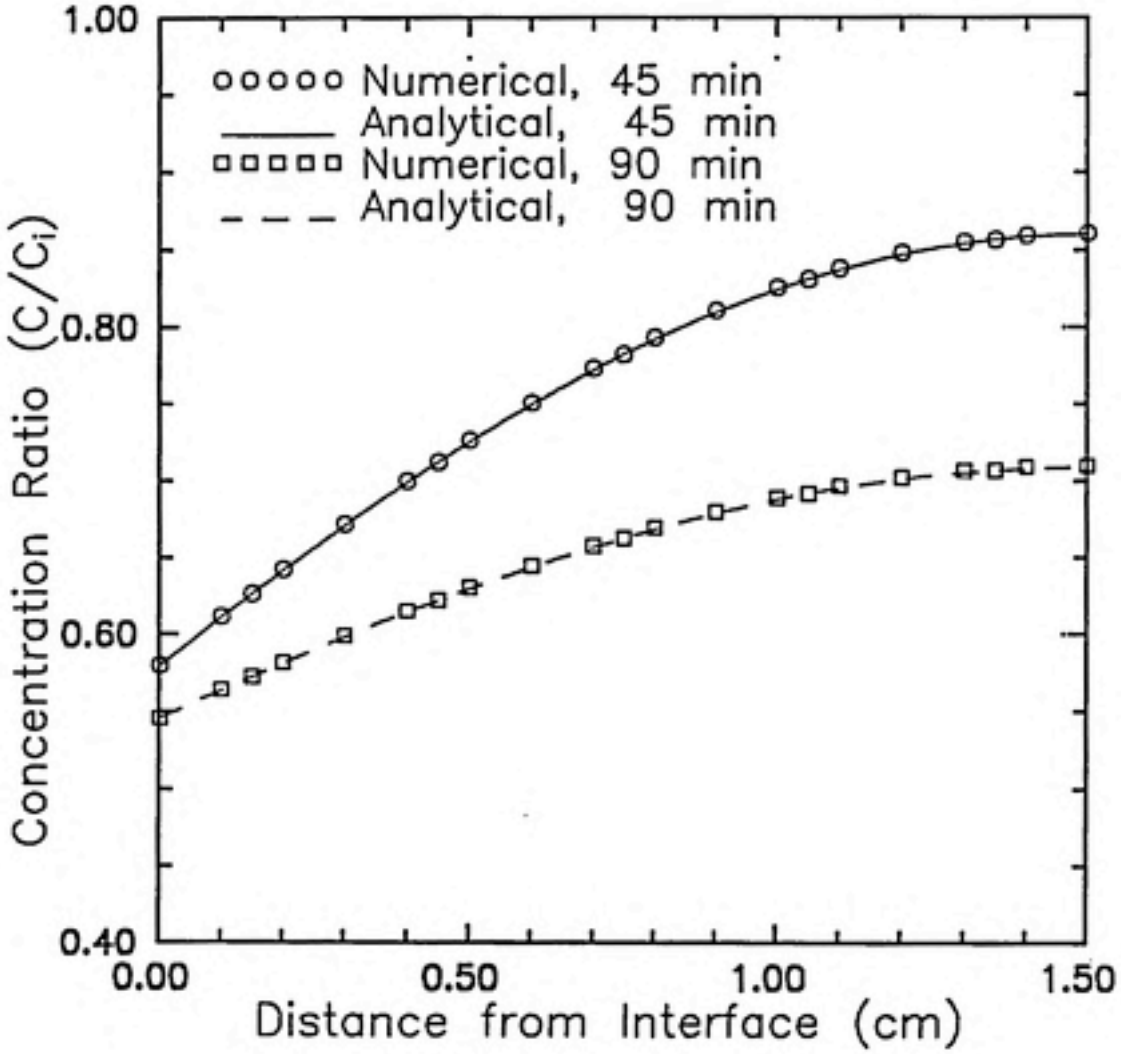

Figure 8–1. Validation of the Numerical Code for Mass Transfer

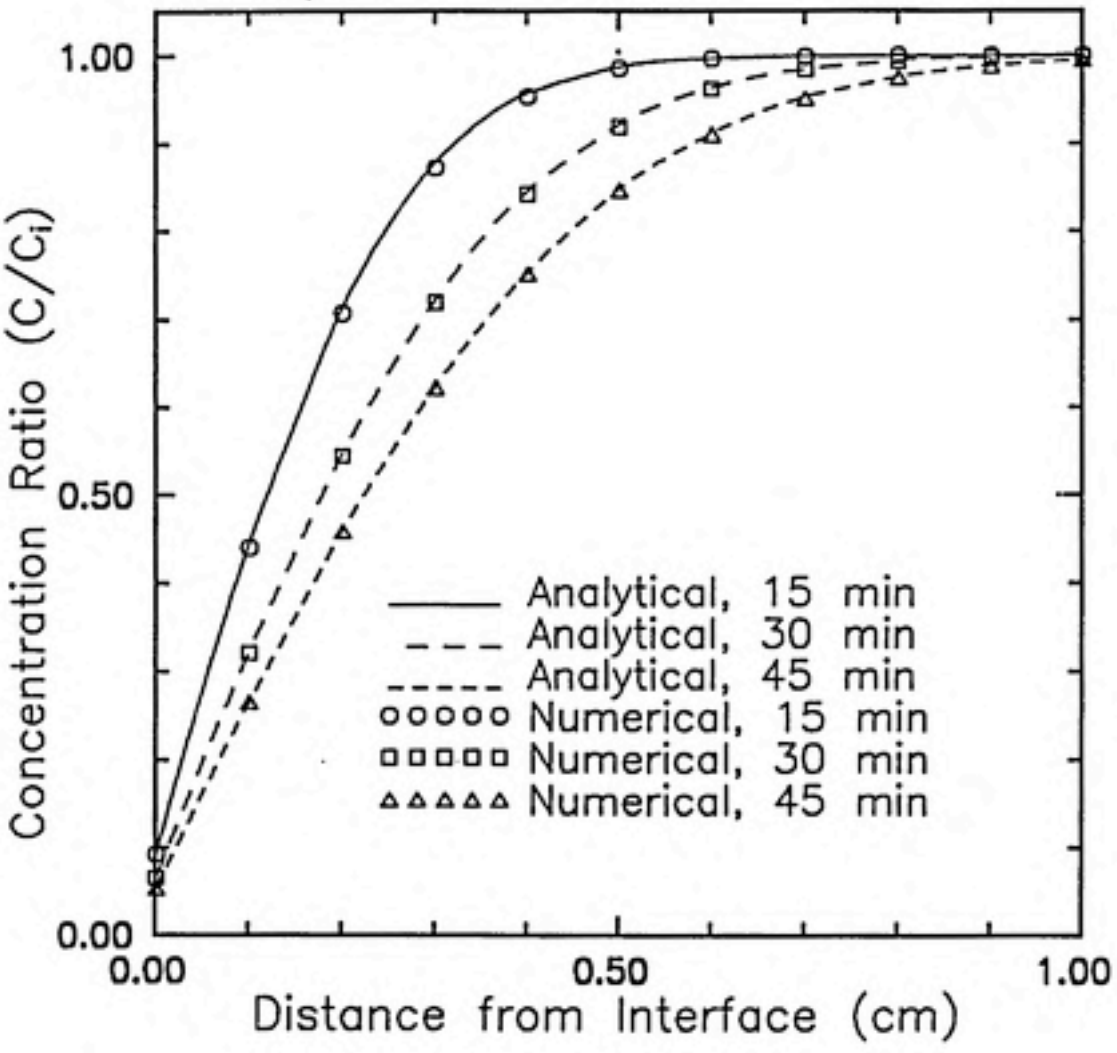

Figure 8–2. Validation of the Numerical Code for Mass Transfer